POLYMER MEMBRANE BASED OPTICAL AND ELECTROCHEMICAL ANION/POLYANION SENSORS

by

Lin Wang

A dissertation submitted in partial fulfillment
of the requirements for the degree of
Doctor of Philosophy
(Chemistry)
in The University of Michigan
2009

Doctoral Committee:

Professor Mark E. Meyerhoff, Chair
Professor Dimitri N. Coucouvanis
Associate Professor Joerg Lahann
Assistant Professor Mi Hee Lim

To my mother and father

ACKNOWLEDGEMENTS

I would like to take this opportunity to thank all the people who helped me during my graduate studies. Special thanks go to my advisor, Dr. Mark E. Meyerhoff, who continuously guided and encouraged me throughout my five years of research and who had always been patient and supportive when I have had difficulties. His enthusiasm for science shines a light for me when I feel confused and will always inspire me in my future career. I would also like to thank Dr. Dimitri N. Coucouvanis, Dr. Joerg Lahann and Dr. Mi Hee Lim for serving as my committee members and for their challenging questions and valuable discussions and suggestions.

I would like to give my deep thanks to my colleagues and collaborators. Thanks to Dr. Jeremy Mitchell-Koch who was my mentor when I started in Dr. Meyerhoff's lab as a rotation student; thanks to Dr. Youngjea Kang and Dr. Mariusz Pietrzak for their help and discussion in the electrochemistry area; thanks to Dr. Zhengrong Zhou and Dr. Sang-yeul Hwang for their help and discussions in organic synthesis; thanks to Dr. Stacey Buchanan for her help on the work related to polyanion sensors; thanks to Dr. Łukasz Górski and Dr. Elżbieta Malinowska at Warsaw University of Technology for their excellent communications and collaborations in studying the water layer formation on the coated wire nitrite selective electrodes; thanks to Dr. Yiduo Wu, Fenghua Zhang and Jun Yang for their precious discussions on the daily research questions that I came up with. I feel so lucky to have worked in Dr. Meyerhoff's lab, and I will never forget the experience of

working together with all the current and past group members: Dr. Dongxuan Shen, Dr. Kebede Gemene, Biyun Wu, Qinyi Yan, Laura Zimmerman, Natalie Walker, Dr. Kun Liu, Bo Peng, Wenyi Cai, Teng Xue, and Dr. Jason Bennet. Thank you all for the help and support. I also want to thank my dear friends in Ann Arbor and in China for the enjoyable moments we shared and the persistent support you provided throughout my graduate studies.

Finally, I would like to sincerely thank my dearest mom, Shaorong Cui, and dad, Jianzhong Wang, for their love and support, although they know nothing about chemistry. I would have given up a hundred times without my mom's constant encouragement. She teaches me to be brave when facing frustrations and gives me the courage to move on. All she gave will be beneficial throughout my life no matter where I am and what I am doing.

TABLE OF CONTENTS

LIST OF FIGURES

Figure

LIST OF TABLES

Table

LIST OF ABBREVIATIONS

AIBN	2,2'-Azobisisobutyronitrile
Al(III)(MOTPP)Cl	Chloro(5-(4-methacryloyloxyphenyl)-10,15,20-triphenyl porphyrinato)aluminum(III)
Al(III)OEP	Chloro-aluminum(III)-octaethylporphyrin
Al(III)TPP	Chloro-aluminum(III)-tetraphenylporphyrin
BSA fraction V	Bovine albumin fraction V
CE	Capillary electrophoresis
CH_2Cl_2	Methylene chloride
CIs	Confidence intervals
Co(III)TPP	Acetato-cobalt(III)-tetraphenylporphyrin
CS	Chondroitin sulfate
CWEs	Coated wire electrodes
DCC	1,3-Dicyclocarbodiimide
DFP	Diisopropyl fluorophosphate
DMA	*n*-Decyl methacrylate
DMAP	4-(Dimethylamino) pyridine
DMF	N,N-dimethylformamide
DOS	Dioctylsebacate

DS	Dextran sulfate
FDA	Food and Drug Administration
GPM	Gas permeable membrane
HF	Hydrofluoric acid
HNO_2	Nitrous acid
HOTPP	5-4(Hydroxyphenyl)-10-15-20-triphenylporphyrin
H_2O_2	Hydrogen peroxide
HPLC	High performance liquid chromatography
IR	Infrared
ISEs	Ion-selective electrodes
KTFPB	Potassium tetrakis[3,5-bis(trifluoromethyl)phenyl]borate
MALDI-TOF	Matrix assisted laser desorption ionization-time of flight
MES	4-Morpholinoethanesulfonic acid
MMA	Methyl methacrylate
MOTPP	5-(4-Methacryloyloxyphenyl)-10,15,20-triphenylporphyrin
NED	*N*-(1-naphthyl)ethylenediamine dihydrochloride
NMR	Nuclear magnetic resonance
NO	Nitric oxide
NPOE	*o*-Nitrophenyl octyl ether
OSCS	Oversulfated chondroitin sulfate
PBS	Phosphate-buffered saline

PTFE	Polytetrafluoroethylene
PVC	Poly(vinyl chloride)
SEM	Scanning electron microscope
TDMA	Tridodecylmethylammonium
THF	Tetrahydrofuran
USP	U.S. Pharmacopeia

CHAPTER 1

INTRODUCTION

1.1. Ion Selective Electrodes and Optodes

1.1.1 Ion Selective Electrodes

Ion selective electrodes (ISEs) are among the most frequently used sensing devices in laboratory analysis, as well as in industrial processes, clinical measurements, and environmental monitoring.[1, 2] There are three main types of membrane materials used to prepare ISEs. The first type is glass membranes made from cation-exchange type of glass (silicate of chalcogenide) which are commonly used for preparation of pH electrodes.[3] Another type is crystalline membranes made from mono- or poly-crystallites of a single substance, an example of which is the fluoride selective electrode based on LaF_3 single crystals.[4] Lastly, membranes can be made of organic polymers containing a specific ion-exchange or ionophore species which are the most widely employed ISEs. An example of this last type is the potassium selective electrode based on valinomycin as a neutral carrier potassium complexing agent.[5]

Organic polymer membrane type cation and anion ISEs appeared almost at the same time. In 1967 Pedersen reported the complexation of alkali metal cations by

crown ethers,[6] and in 1968 Park and Simmons reported the first synthetic receptor for inorganic anions.[7] However, since then, cation ISEs developed much more rapidly and effectively than the anion ISEs due to the intrinsic differences between anions and cations.[8, 9] Anions are relatively larger and therefore require organic membrane receptors with a much larger binding sites. Secondly anions are more strongly hydrated than cations of equal size. Finally, many anions exist in a narrow pH range, owing to protonation equilibria that affect their size and charge.

The principles of ISEs operation are well understood. Figure 1.1 shows a general measurement set-up of an ISE based cell. The cell potential can be described as the sum of the phase boundary potentials of the system as:

$$E_{cell} = K + E_{sample/mem} + E_{mem/int.soln} \qquad \text{(Eq. 1.1)}$$

where K is a constant and $E_{mem/sample}$ and $E_{mem/int.soln}$ can be expressed as:

$$E_{sample/mem} = \frac{RT}{zF} \ln k_I + \frac{RT}{zF} \ln \frac{a_{sample}}{a_{mem}} \qquad \text{(Eq. 1.2)}$$

$$E_{mem/int.soln} = \frac{RT}{zF} \ln k'_I + \frac{RT}{zF} \ln \frac{a_{mem}}{a_{int.soln}} \qquad \text{(Eq. 1.3)}$$

where R is the gas constant, T is the absolute temperature, z is the charge of the target ion, F is the Faraday constant, and a is the activity of the target ion in the sample, membrane and internal solution phase respectively. k_I and k'_I are functions of the relative free energies of solvation in the sample, the membrane, and the internal solution phase ($k_I = \exp(\{\mu^0(sample) - \mu^0(mem)\}/RT)$, $k'_I = \exp(\{\mu^0(mem) - \mu^0(int.soln)\}/RT)$, where $\mu^0(sample)$, $\mu^0(mem)$, and $\mu^0(int.soln)$ are the chemical standard potentials of the ion I in the respective phase). The theoretical value of a

Nernstian slope can be calculated to be 59.2/z mV per decade at 298 K.

By adding lipophilic anion-exchanger (i.e., tetraalkyl quaternary ammonium salt, see Figure 1.2 and Figure 1.3) to the organic membrane phase, E_{cell} in Eq. 1.1 can be further simplified to a function only related to a_{sample}. If the organic phase is doped with a fixed concentration of lipophilic anion-exchanger sites, the concentration of counter ions is equal to that of the lipophilic anion-exchanger in the organic phase regardless of the concentration change in the aqueous phase. Therefore, the a_{mem} in Eq. 1.2 and Eq. 1.3 are constant, and Eq. 1.1 can be simplified to the very well known Nernst Equation:

$$E_{cell} = K' + \frac{RT}{zF} \ln a_{aq} \qquad \text{(Eq. 1.4)}$$

where the constant $K' = K - \frac{RT}{zF} \ln a_{int.soln} + \frac{RT}{zF} \ln k_I k'_I$

Since there are no specific interactions between the anion-exchanger and target anions, potentiometric selectivity coefficients of such membrane electrodes are related to the ability of the anion to partition from the aqueous phase into the organic phase. Therefore, these anion-exchanger-based electrodes are known to exhibit the so-called Hofmeister selectivity pattern[10] (see Eq. 1.5) and follow the Nikolskii Eiseman equation[11] (see Eq. 1.6)

$ClO_4^- > SCN^- \approx I^- > Sal^- > NO_3^- > Br^- > NO_2^- \approx Cl^- >> HCO_3^- > H_2PO_4^- \approx F^- \approx SO_4^{2-}$ (Eq. 1.5)

$$E_{cell} = K' + \frac{RT}{zF} \ln[a_{X(sample)} + \sum_J k_{X,Y}^{pot} a_Y^{z_X/z_Y}] \qquad \text{(Eq. 1. 6)}$$

where the change in EMF relates not only to the target ion activity ($a_{X(sample)}$), but

also to the interference ion activity (a_Y), the corresponding selectivity coefficient ($k^{pot}_{X,Y}$), and the charges of the primary and interference ions (z_X and z_Y). The potentiometric selectivity coefficient, $k^{pot}_{X,Y}$, is determined by the partition process and is expressed as:

$$\ln k^{pot}_{X,Y} = \ln \frac{k_Y}{k_X} \qquad \text{(Eq. 1.7)}$$

where k_X and k_Y are the partition coefficients of the primary and interferent anions (X and Y).

The desirable values for $k^{pot}_{X,Y}$ should be very small. However, by using ionophores (see Figure 1.3) that possess strong and reversible interactions with target anions, a non-Hofmeister anion selectivity patterns can be realized, and the $k^{pot}_{X,Y}$ value in Eq. 1.6 is modified to:

$$\ln k^{pot}_{X,Y} = \ln \frac{k_Y}{k_X} + \ln \frac{\beta_Y}{\beta_X} \qquad \text{(Eq. 1.8)}$$

where the selectivity coefficient is decided not only by the single ion partition coefficients (k_X and k_Y), but also by the binding interactions between the ionophore and the target anion (β values). Strong binding between the ionophore and the target ion implies very large value of β_X, which can compensate for the possibly small value of k_X in the partition process and consequently give a desired low value for the selectivity coefficient.

1.1.2 Coated Wire Ion Selective Electrodes

Conventional ISE configurations are inconvenient and unnecessarily expensive,

owing to their large size and internal filling solutions; therefore, miniaturization of ISEs has become a growing trend in the field of electrochemical sensors.[12, 13] The disadvantages of conventional type ISEs can be overcome by the development of coated wire electrodes (CWEs) or solid-state devices. A needle-type CWE was the first type of miniaturized electrodes, and was intended for intracellular measurements.[14, 15] In CWEs, the organic polymeric ion selective membranes are deposited directly on a conductive electrode material by very simple dip coating method. The electrode material could be either a metal wire, a graphite rod or a graphite paste.[16, 17] Removal of the inner filling solution brings numerous advantages to the ISEs. Besides their small size, low cost, mechanical flexibility, and simple construction, the CWEs have response characteristics equal to and occasionally better than the conventional type ISEs. In many cases, the selectivity and detection limit of the CWEs are significantly improved compared to a conventional ISEs with internal solutions.[15, 18] This is because the leaching of primary ion from the internal solution is prevented in the CWE configuration.

However, a main disadvantage of the CWEs is the unstable potential that develops at the interface of the organic ion selective sensing membrane and the conducting substrate.[19] The formation of an aqueous layer, which serves as a pseudo internal electrolyte between the polymeric membrane and solid conductor, has been considered as one of the possible reasons for this problem.[20] Since the composition of this aqueous layer is not controllable, the cell constant (EMF) changes are in an unpredicted manner. Another factor that contributes to the instability of the CWEs

is the poorly defined charge transfer at the blocked interface between the ion-sensitive membrane, with ionic conductivity, and the conducting substrate, with electronic conductivity (e.g., no defined redox reactions).

A variety of approaches have been reported in attempt to improve the stability of CWEs. One effective approach is employing intermediate layers which translate the ionic response of the sensing membrane into a stable electronic signal by better poising the phase boundary potential between the polymeric membrane and solid conductor. The intermediate layers can be hydrogels,[21, 22] conducting polymers,[22] redox-active monolayers,[23-26] or the recently reported three dimensionally ordered macroporous carbon electrodes.[27] Another approach to improve the stability of CWEs is incorporating certain additives into the polymeric membrane so that the charge transfer between the sensing membrane and the solid conductor is facilitated. Lipophilic silver complexes,[28] as well as conducting polymers[29] possessing ion-electron conductivity, have been used for this purpose.

1.1.3 Ion Selective Optodes

The ion selective optodes described in this work focus on optical sensors based on bulk extraction equilibria from aqueous phase into a hydrophobic polymeric membrane.[1, 30] Besides the ionophore, the ion selective optode also contains a chromoionophore or fluoroionophore in the polymeric membrane which can change the optical properties of the polymer. Chromoionophores are usually lipophilic pH indicators that transfer the binding of the target ion to the ionophore into an optical

signal. Chromoionophores are classified as either neutral or charged chromoionophores, depending on their electrical charge.[31] The neutral chromoionophores are positively charged in their protonated form and neutral in their deprotonated form, while charged chromoionophores are neutral in their protonated form and negatively charged in their deprotonated form. Figure 1.4 gives examples of the response mechanism of two anion optical sensors that employ an anion ionophore (L) and a chromoionophore pH indicator in the same film.[32] The selectivity of these optodes is determined by both the stability constant of the ionophore with the target ion and the pKa of the chromoionophore.[1, 31] Figure 1.5 gives the pKa values of several commonly used chromoionophores in poly(vinyl chloride) (PVC) membranes with different plasticizers.

Compared with the potentiometric sensors, these optical sensors have many advantages, such as lower detection limit, higher sensitivity and versatile sensor design. However, since the sensing films are quite thin (5 – 10 μm) most of the optodes still suffer from relatively short life time, which can be alleviated by using more lipophilic membrane components or by immobilizing the chromoionophore and/or ionophore to a polymer backbone.[33]

1.2. Metalloporphyrins Used as Ionophores in Anion Selective Sensors

1.2.1 Metalloporphyrins as Ionophores in Anion Selective Electrodes

The very first articles reporting the application of metalloporphyrins as

ionophores to prepare anion-selective polymeric membrane based electrodes were published in the middle 1980s.[34] Since then, various metalloporphyrins have been tested as potential ionophores for anions. The specific nature of the metal cation present in the metalloporphyrin structure governs the selectivity of membranes doped with these ionophores. Table 1.1 illustrates the application of several metalloporphyrins toward the detection of different anions. As can be seen, Mn(III) porphyrins exhibit preference for Cl^- and SCN^-;[35, 36] oxo-bridged iron(III) porphyrins show an improved selectivity for SCN^-;[37] Sn(IV) porphyrins are strongly selective for salicylate;[38] MoO(III) porphyrins respond to OH^- with an almost Nernstian slope;[39] In(III) porphyrins display an enhanced and super-Nernstian response to Cl^-;[40] Co(III) porphyrins[35, 36, 41, 42] and the recently reported Rh(III) porphyrins[43] show strong affinity to NO_2^-. Using Ga(III) porphyrins,[44] Zr(IV) porphyrins[45] and Al(III) porphyrins[46], it is possible to develop polymeric membrane based ISEs which can achieve fluoride selectivity approaching that exhibited by the solid-state LaF_3-based fluoride ISE.

It has been reported previously that incorporating lipophilic anionic or cationic sites in the polymeric membranes, in addition to a given ionophore species, can improve the selectivity of the ISEs by controlling the ratio of free ionophore to complexed ionophore in the membrane phase.[47] Knowledge of the working mechanism (neutral carrier ionophores versus charged carrier ionophores) is critical toward this purpose. Indeed, membranes doped with ionophores that function as charged carriers (see Figure 1.6) require lipophilic anionic additives (e.g.,

tetraphenylborate derivatives), while in the case of ionophores that serve as neutral carriers (see Figure 1.6), cationic additives (tetraalkylammonium salts) are needed.

1.2.2 Dimer-monomer Equilibrium of Metalloporphyrins

Previous studies have reported that the main limitations of the existing polymeric membranes doped with metalloporphyrins are super-Nernstian slopes (greater than -59/z mV per decade), long response time, slow recovery, as well as short lifetime for the ISEs. These behaviors have been ascribed to a dimer-monomer equilibrium of the metalloporphyrin species within the polymeric membranes of the sensors when in contact with an aqueous test solution containing target anions.[44]

The dimer-monomer equilibrium has been successfully applied to devise optical sensors that can respond in real-time to variations in analyte levels in both aqueous and gas phases.[48] For example, lipophilic anionic sites in the form of tetraphenylborate derivatives are usually added to membranes, and stabilize the positively charged hydroxide bridged dimeric species formed by two metalloporphyrins. This process can occur in the absence of appreciable levels of target anions in a bathing aqueous test solution. By adding anions that can strongly ligate to the metalloporphyrin metal center to the test solutions, the dimers within the organic membrane are converted to monomers which gives a corresponding shift in the Soret band as detected by UV/visible spectra of the polymeric films. The crystal structures of μ-hydroxy-bridged dimers of In(III) and Ga(III) porphyrins

confirm the dimer structures.[48] Formation constants for Reaction 1.1, where $M[OEP]^{+}_{org}$ is the metallo-octaethyl porphyrin in the organic membrane phase, have been found to be on the order of 10^{16} L/mol which explains why hydroxide ion-bridged dimers ($(M[OEP])_2OH^{+}_{org}$) are formed in the membranes even when the bathing sample buffer has a pH of 5.5 or lower.

$$2M[OEP]^{+}_{org} + OH^{-} \leftrightarrow (M[OEP])_2OH^{+}_{org} \qquad \text{(Reaction 1.1)}$$

UV/visible spectroscopy data with organic phase solutions or polymeric films containing Al(III) porphyrins show large changes in the Soret band upon addition of fluoride ions.[49, 50] However, in this case, the Al(III) porphyrins exist as monomers initially, and dimers are formed after the addition of fluoride as described in Reaction 1.2.[50]

$$2M^{+}_{aq} + 2F^{-}_{aq} + 2Al[OEP]TFPB_{org} \leftrightarrow (Al[OEP]F)_{2(org)} + 2MTFPB_{org} \qquad \text{(Reaction 1.2)}$$

where TFPB stands for tetrakis[bis-(3,5-trifluoromethyl)phenyl]borate, Al[OEP] is chloro-aluminum(III)-octaethylporphyrin and M is cation from the analyte solution. The obtained crystal structure of bis-(μ-fluoro) dimer of Sc(III) porphyrin[51] confirms this dimerization process. These inherent changes in the spectral properties can be used for optical fluoride sensing.

Although beneficial in designing ion selective optodes, dimer formation in the polymer films needs to be eliminated in the case of electrochemical sensors due to the disadvantages described earlier in this section. There are two possible approaches to eliminate the dimer formations. One is using a picket fence porphyrin as the ligand to prevent the dimer formation by steric hindrance.[46] The other is covalent attachment

of the porphyrins to polymer backbones.[52]

1.3. Polymer Membrane Based Potentiometric Polyanion Sensors

ISEs based on polymeric membranes are routinely used in clinical tests to measure ions such as Na^+, K^+, Ca^{2+} in blood.[53, 54] There has also been interests in developing similar sensors that are suitable for the direct detection of larger biomolecules. These molecules include polyions, such as negatively charged polysaccharides which are widely used as anticoagulants (e.g., heparin), DNA, polyphosphates, and protamine used as an antidote for heparin (see Figure 1.7). Initially, the application of ISEs to detect these large polyion species seemed to be impossible. Based on Eq. 1.4, it can be expected that for polyions like heparin, which has an average negative charge of about 70 per molecule, the slope value obtained will be very small, smaller than 1 mV per decade, which is analytically useless. However, it was first reported in 1992 that a large and reproducible EMF response toward polyanionic species (see Figure 1.8) such as heparin, can be achieved if ISEs were appropriately formulated and operated under non-equilibrium conditions.[55] Later, the system was extended to the measurement of polycationic species, such as protamine.[56]

As introduced previously, an ISE doped with anion-exchanger such as quaternary ammonium salt exhibits the so-called Hofmeister selectivity pattern governed by the extraction process of the anions from aqueous phase to membrane phase. However, when the target anions are polyanion species, the anion-exchanger can form

cooperative ion-pairs with the polyanion in the membrane phase. An extraction process can be described by the following equation:

$$zS^{+}(org) + zCl^{-}(org) + Poly^{z-}(aq) = zCl^{-}(aq) + PolyS_{z}(org) \quad \text{(Eq. 1.9)}$$

where S is the anion exchanger, $Poly^{z-}(aq)$ is the polyanion with charge z. The equilibrium constant of the above process is:

$$K = \frac{PolyS_{z}(org)}{Poly^{z-}(aq)[S^{+}(org)]^{z}}[\frac{Cl^{-}(aq)}{Cl^{-}(org)}]^{z} \quad \text{(Eq. 1.10)}$$

The ion-pair formation constant between the polyanion and the anion exchanger can be written as:

$$\beta = \frac{PolyS_{z}(org)}{Poly^{z-}(org)[S^{+}(org)]^{z}} \quad \text{(Eq. 1.11)}$$

Therefore, Eq. 1.10 can be further written as:

$$K = \frac{\beta Poly^{z-}(org)}{Poly^{z-}(aq)}[\frac{Cl^{-}(aq)}{Cl^{-}(org)}]^{z} = \beta\frac{k_{poly}}{(k_{Cl})^{z}} \quad \text{(Eq. 1.12)}$$

where k_{poly} and k_{Cl} are partition coefficient of the polyanion and chloride. In practical use of such type of polyanion sensor, the membrane has contacted a high concentration of chloride before the addition of polyanion, therefore, the outer phase boundary potential of the membrane is determined by the chloride concentration in the sample solution and in the membrane:

$$E_{Cl} = E^{0} - \frac{RT}{F}\ln\frac{a_{Cl^{-}}(aq)}{a_{Cl^{-}}(org)} \quad \text{(Eq. 1.13)}$$

where $a_{Cl^{-}}(org)$ is determined by the concentration of cationic site in the anion exchanger S and any possible anionic site $R^{-}(org)$ in the membrane in a way of $a_{Cl^{-}}(org) = S_{z}(org) - R^{-}(org)$. After the addition of polyanion, the phase boundary

potential at the sample/membrane interface can be expressed by combining Eq. 1.12 and Eq. 1.13:

$$E_{poly} = E^0 - \frac{RT}{zF}\ln\frac{k_{poly}}{(k_{Cl})^z}\frac{Poly^{z-}(aq)}{Poly^{z-}(org)} \quad \text{(Eq. 1.14)}$$

The potential change ΔEMF is (subtract Eq. 1.13 from Eq. 1.14 and consider $a_{Cl^-}(org) = S_z(org) - R^-(org)$):

$$\Delta EMF = \frac{RT}{F}\ln\frac{a_{Cl^-}(aq)}{S_z(org) - R^-} - \frac{RT}{zF}\ln\frac{k_{poly}}{(k_{Cl})^z}\frac{Poly^{z-}(aq)}{Poly^{z-}(org)} \quad \text{(Eq. 1.15)}$$

When all the chloride ions at the outermost surface of the polymer membrane are replaced by polyanions during the extraction process, a maximum ΔEMF is obtained. Under such conditions, $zPoly^{z-}(org) = S_z(org) - R^-(org)$, and the total mass of anion exchanger is $S_T = S_z(org) + zPolyS_z(org)$. Since the interaction between the polyanion and anion exchanger is so strong, we can assume the free polyanion in the membrane phase is negligible, and $S_z(org) = R^-(org)$. Then $Poly^{z-}(org)$ can be written as:

$$Poly^{z-}(org) = \frac{S_T - R^-(org)}{zR^-(org)^z\beta} \quad \text{(Eq. 1.16)}$$

Finally the maximum ΔEMF is derived as:

$$\Delta EMF = \frac{RT}{F}\ln\frac{a_{Cl^-}(aq)}{R^-(org)[S_T - R^-(org)]} - \frac{RT}{zF}\ln\frac{k_{poly}}{(k_{Cl})^z}\frac{zPoly^{z-}(aq)}{S_T - R^-(org)} \quad \text{(Eq. 1.17)}$$

Dictated by Eq. 1.17, the maximum ΔEMF is described as the true equilibrium response in Figure 1.8, and is related to the chloride concentration in the sample solution, the total concentration of anion exchanger, the possible anionic sites in the polymer membrane, the partition of the polyanion compared with that of chloride and,

more importantly, the ion pair formation constant β. It has been reported that the structure of the anion exchanger and the charge density of the polyanion which can affect β in terms of steric hindrance and electrostatic interaction both have influence on the maximum ΔEMF.[57]

Polymer membrane potentiometric polyanion sensors provide a very rapid, simple and inexpensive way to detect polyanion species. Since their invention about twenty years ago, they have been used in various applications,[58] such as in potentiometric titrations to determine the concentrations of polyionic drugs (including heparin and protamine), in the development of electrochemical enzyme assays, and in monitoring levels of specific enzyme inhibitors. Further applications of polyanion sensors are explored in the dissertation work (see below).

1.4. Polymer Membrane Based Potentiometric Gas Sensors

Over the past three decades, potentiometric sensors for monitoring gases have developed rapidly. Various types of potentiometric sensors have been introduced for the detection of oxygen,[59] carbon dioxide,[60] sulfur oxides,[61] nitrogen oxides,[62] ammonia,[63] etc. Particularly, measurements of some of these gases in biological samples[64, 65](e.g., whole blood) have been a very attractive application of these potentiometric gas sensors.

The first potentiometric sensor design for carbon dioxide determination in blood was introduced by Severinghaus and Bradley in 1958.[60] In their design, the analyte gases diffuse into a thin layer of electrolyte through a gas permeable membrane.

The thin layer of inner electrolyte contacts a glass membrane pH electrode as well as a bulk volume of the same electrolyte, where the reference electrode is placed. An equilibrium reaction between the analyte gases and water exists in this thin electrolyte layer. The pH electrode measures the equilibrium pH when the partial pressure of gas is equal on both sides of the gas permeable membrane. There are certain limitations in this design, such as the slow response and long recovery time at low gas concentrations, poor selectivity over other acidic or basic gases which can diffuse through the gas permeable membrane and change the pH in the electrolyte layer, high detection limits, and difficulties in miniaturization.

The development of the ionophores in polymer membrane ISEs makes it possible for the development of a novel type of gas sensing systems. A miniaturized ammonia gas sensor employing an internal polymer membrane ammonium probe based on nonactin, an ammonium ion ionophore, was introduced in 1980 (see Figure 1.9).[63] This new design of gas sensors offers many advantages over the traditional pH electrode based gas sensors, including improved detection limit and selectivity. Later, this design of gas sensors has been applied in the detection of many other gases such as SO_2, NO_x, and CO_2 using the sulfite,[66] nitrate,[67] and carbonate[68] ionophores as the active components of the inner ISEs.

1.5. Statement of Research

The primary purpose of this dissertation research is the development, the fundamental mechanistic study, and the application of polymeric membrane based

ion selective electrodes and optodes employing metalloporphyrin species as ionophores. Efforts were also undertaken to explore the application of a previously reported polyanion potentiometric sensor[57] in determining the presence as well as quantifying a high charge density polyanion contaminant (oversulfated chondroitin sulfate (OSCS)) in biomedical heparin preparations.

Chapter 2 describes the verification of fluoride bridged dimer formation through a newly synthesized Al(III) protoporphyrin diester derivative. To eliminate such unwanted dimer formation in potentiometric measurements, a methacrylate copolymer with covalently attached Al(III) porphyrin has been synthesized and characterized. The performances of the ISEs and optodes employing this material were evaluated.

Chapter 3 describes an optimized coated wire ISE system based on a Co(III) porphyrin for the detection of nitrite ion. The analytical performance of the CWEs was assessed. Specifically, a main disadvantage of CWEs system, the water layer formation between the sensing membrane and the solid conductor, was addressed. Methods to prolong the electrode lifetime were examined. An optical sensor utilizing Co(III) porphyrin and a chromoionophore was introduced for nitrite detection with good sensitivity.

Chapter 4 describes a new application of a previously reported potentiometric polyanion sensor. The polyanion sensors were used to detect a high charge density polyanion, specifically, OSCS, in biomedical heparin preparations related to a recently reported contaminated heparin issue.[69, 70] Quantification of the OSCS was

also achieved by both the potentiometric method and a nuclear magnetic resonance (NMR) method.[69, 70]

Chapter 5 describes an unusual observation of using Co(III) porphyrin, a nitrite ionophore, in polymer membrane for the detection of nitric oxide (NO) gas. The mechanism for the enhanced sensitivity of such electrodes toward NO over nitrite is explained.

Chapter 6 summarizes this dissertation work and suggests future research directions.

Finally, it should be noted that this dissertation is prepared on the basis of multiple manuscripts. Chapter 2, Chapter 3 and Chapter 4 are adapted from either published articles or manuscripts to be submitted for publication. The synthesis, characterization and application of polymethacrylate with covalently attached Al(III) porphyrins described in Chapter 2 has been published as a full paper in *Analytica Chimica Acta* (2008).[71] The study on the influence of inner transducer properties on EMF response and stability of coated wire anion-selective membrane electrodes based on metalloporphyrin ionophores described in Chapter 3 was a collaboration with Malinowska's lab at Warsaw University of Technology and was published as a full paper in *Journal Solid State Electrochemistry* (2009).[72] Detection of the high charge density polyanion contaminants in biomedical heparin preparation using a polyanion sensor, as reported in Chapter 4, was published as a correspondence in *Analytical Chemistry* (2008).[73] A manuscript on the quantification of such high charge density contaminants has been prepared and recently submitted for publication in

Electroanalysis. A collaboration work with Dr. Simonian at Auburn University to detect diisopropyl fluorophosphate (DFP) using optical fluoride sensor has been prepared and submitted for publication in *Analytica Chimica Acta*.

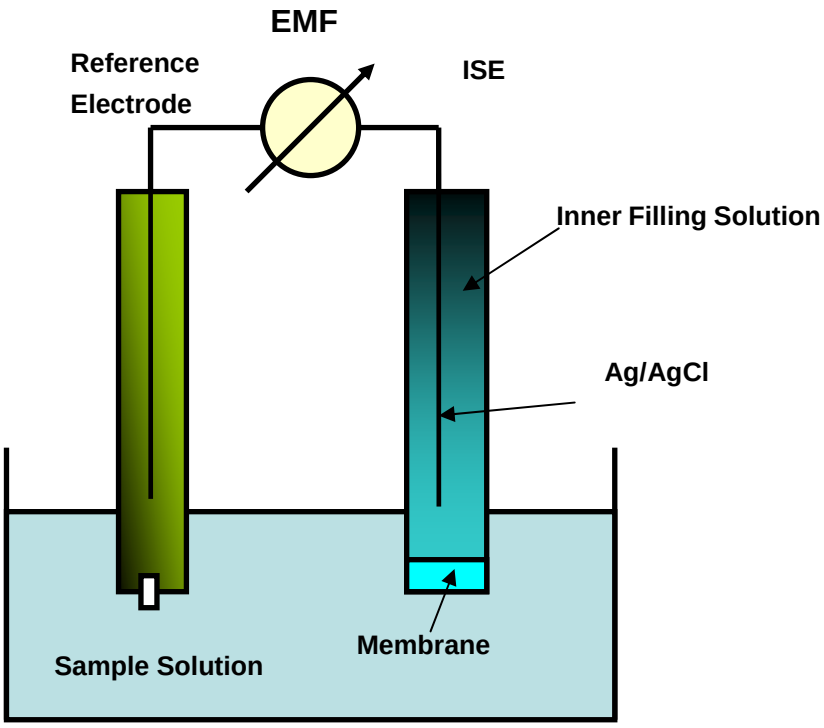

Figure 1.1. Schematic diagram of an ISE measurement.

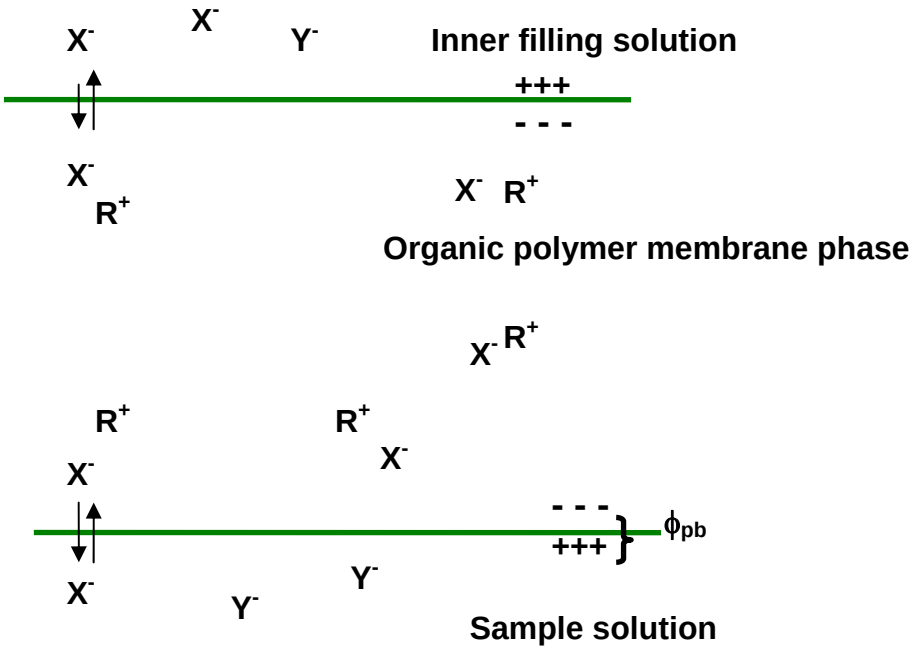

Figure 1.2. ISEs based on anion exchanger; X^- is the target anion, Y^- is the interference anion, and R^+ represents the lipophilic anion exchangers (i.e., R^+ = quaternary ammonium ion).

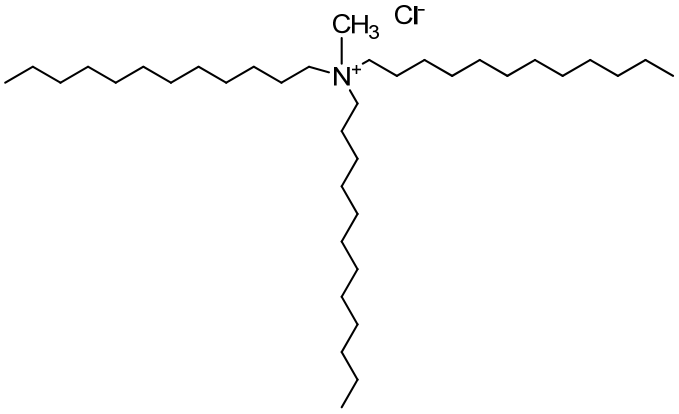

Tridodecylmethylammonium chloride (TDMA)

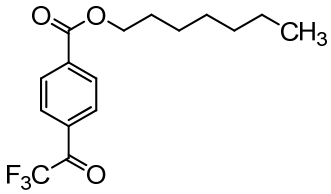

Carbonate ionophore I

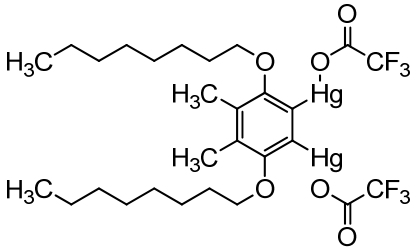

Chloride ionophore II

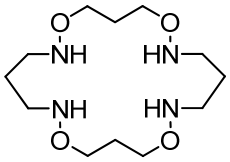

Nitrate ionophore II

Figure 1.3. Chemical structures of a quaternary ammonium salt (TDMA) and several anion ionophores.

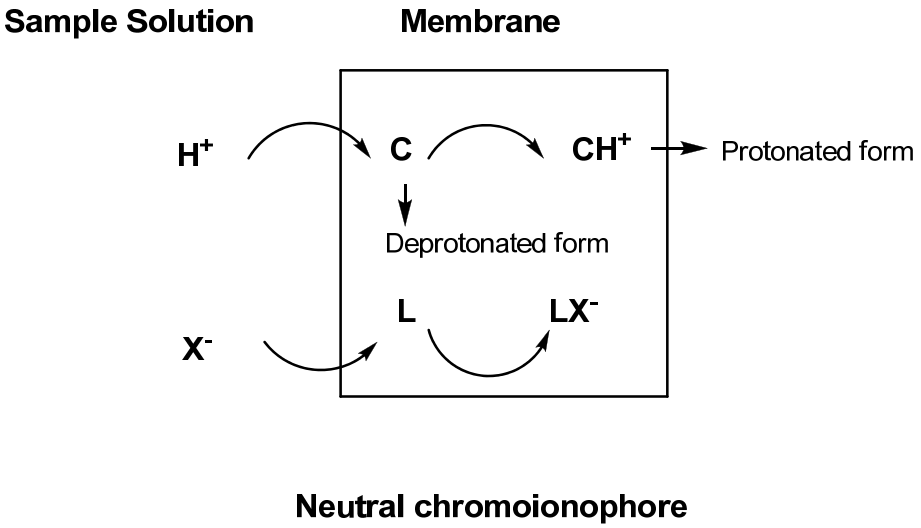

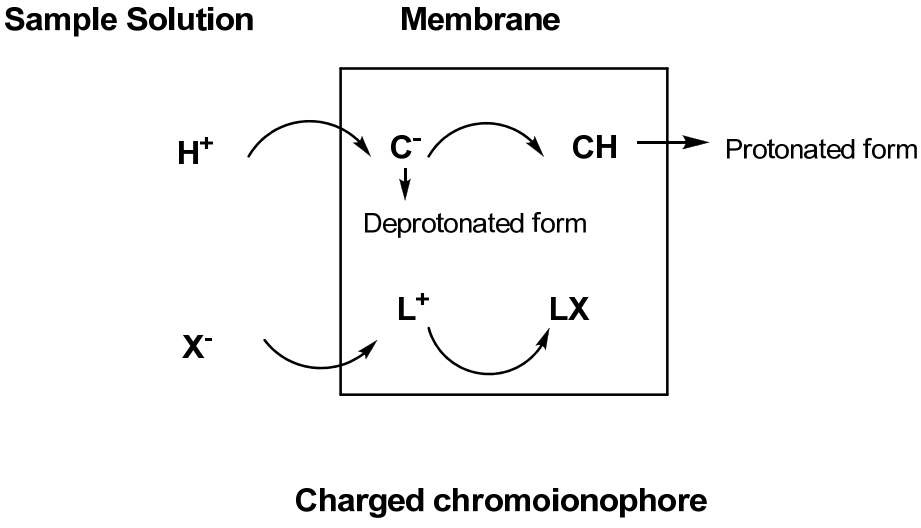

Figure 1.4. Response mechanism of anion optical sensors when using neutral and charged chromoionophores. C and CH represent the corresponding protonated/deprotonated forms of the chromoionophore, L is the anion ionophore added together with the chromoionophore in the membrane phase, X^- is the target anion.

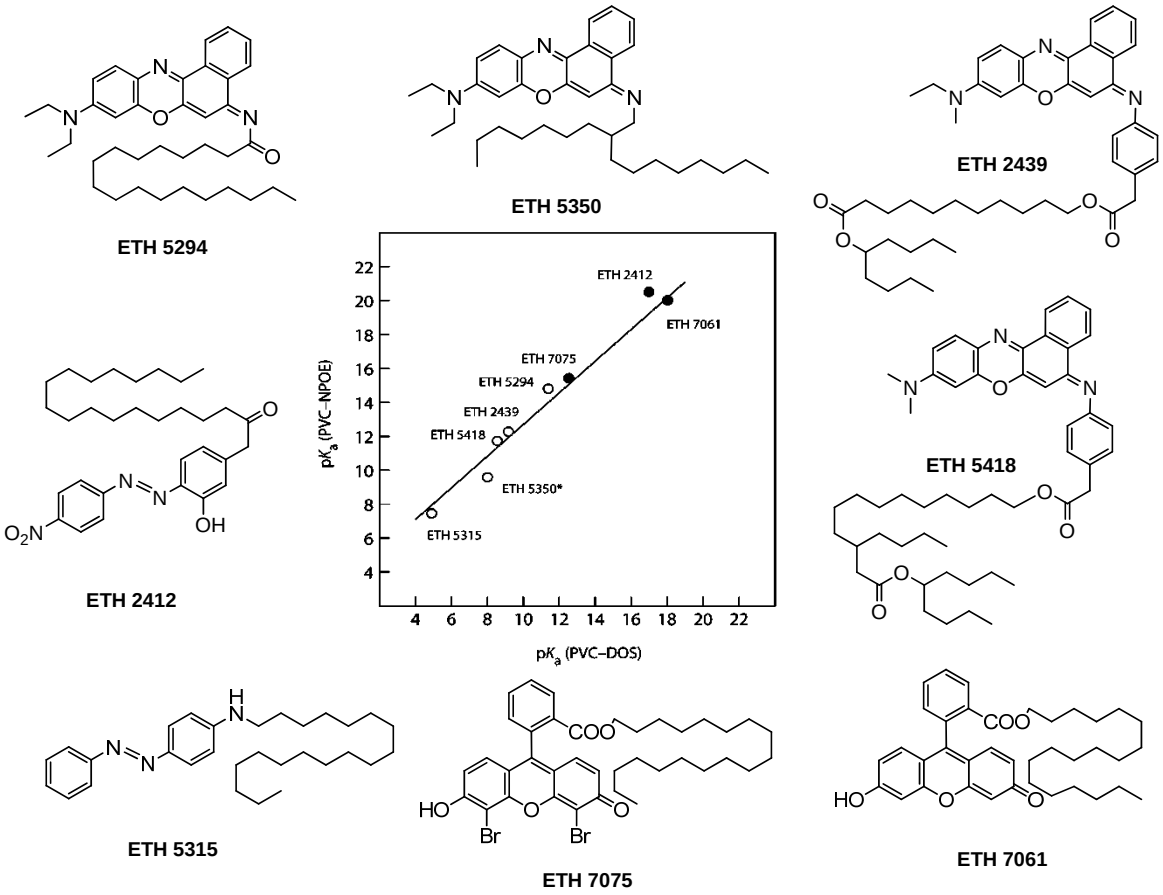

Figure 1.5. pKa values of eight chromoionophores in polar PVC/o-nitrophenyl octyl ether (NPOE) membrane and non-polar PVC/dioctylsebacate (DOS) membranes.

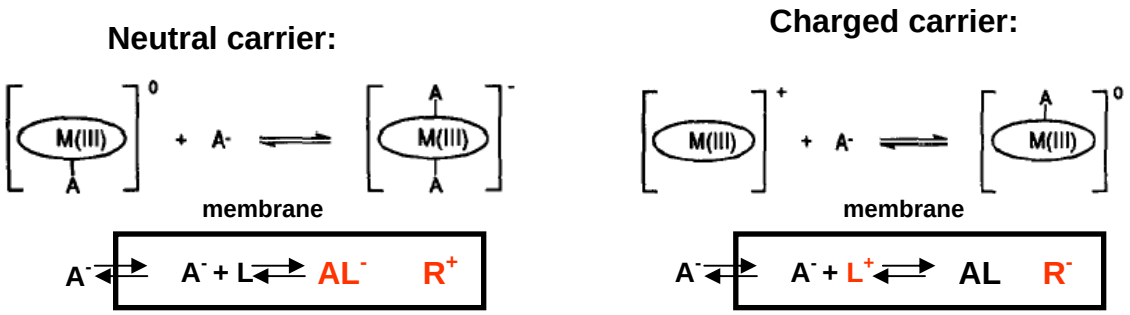

Figure1.6. Schematic representation of neutral and charged carrier mechanisms with ionic additives in the membrane phase. The boxes designate the organic phase, A^- is the target anion, L is the ionophore and R^-/R^+ are the lipophilic ionic additive incorporated in each carrier type.

Heparin

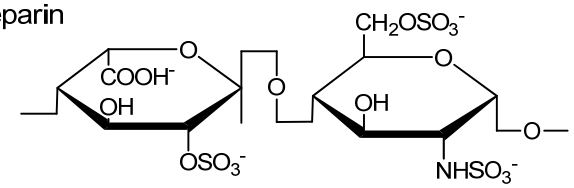

I-Caragreenan

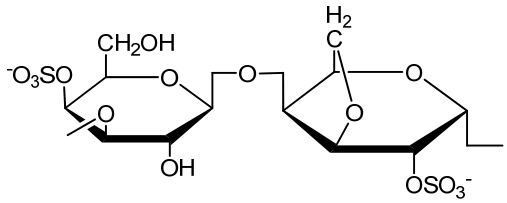

DNA

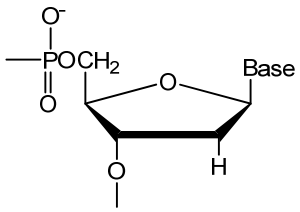

Polyphosphate

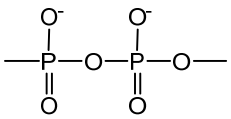

Protamine

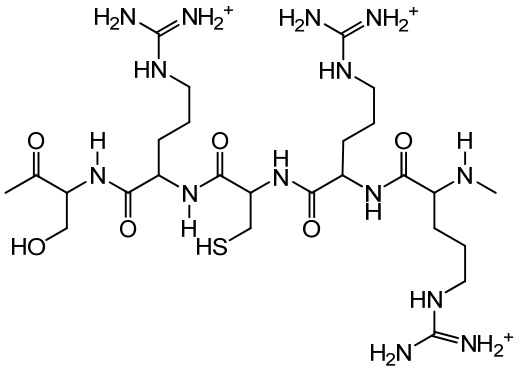

Figure 1.7. Repeating subunit structures of important polyionic species. A segment of the amino sequence is given for protamine.

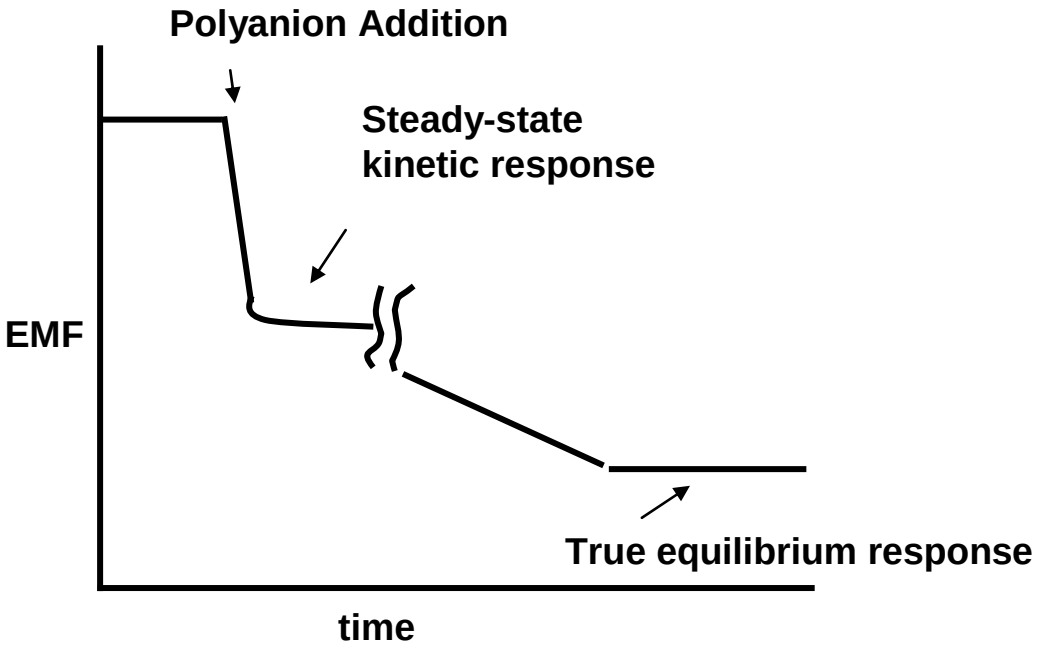

Figure 1.8. Time profile of EMF response of polyanion sensor to given test polyanion.

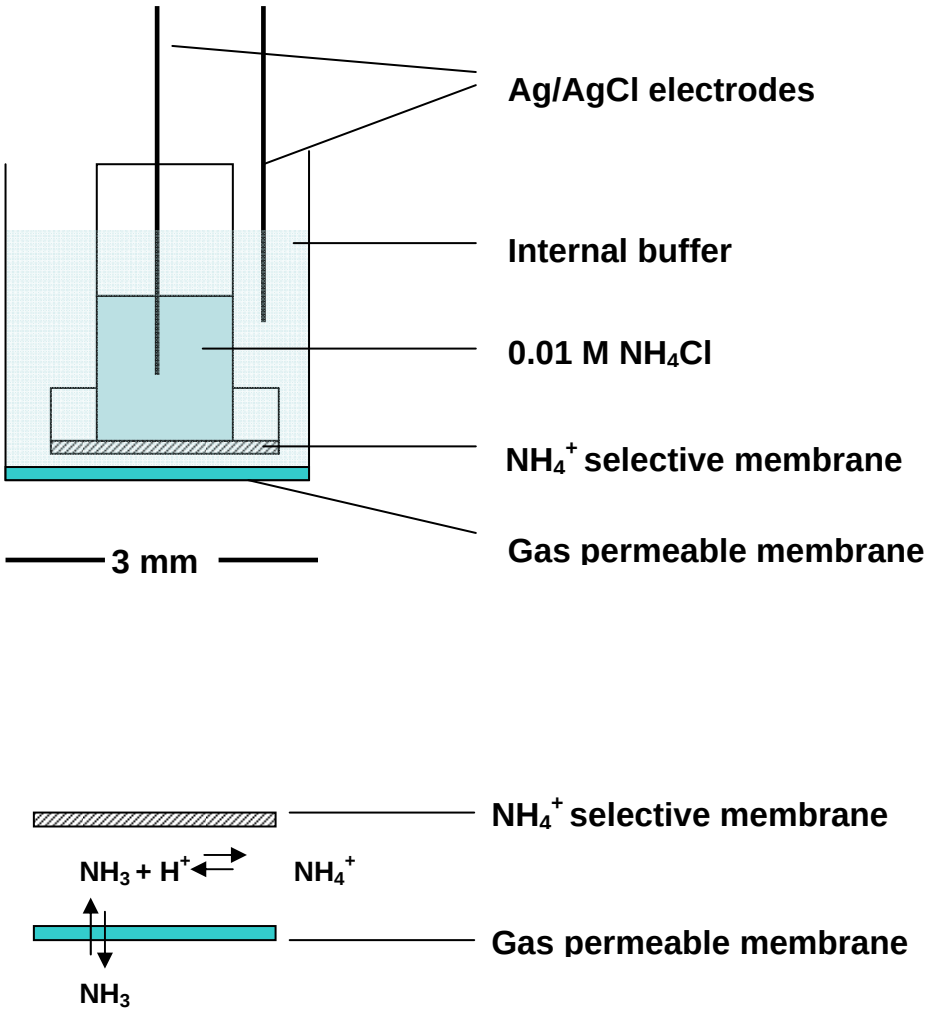

Figure 1.9. Schematic diagram of the miniature ammonium gas sensor.

Table 1.1. Influence of the metal center of porphyrins on the sensor selectivity[9]

Metal center	*Detected anion*
Mn^{3+}	Cl^-
	SCN-
Fe^{3+}	SCN^-
Co^{3+}	NO_2^-
	SCN^-
MoO^{3+}	OH^-
In^{3+}	Cl^-
	NO_2^-
Sn^{4+}	$Salicylate^-$

1.6. References

(1) Bakker, E.; Buhlmann, P.; Pretsch, E. *Chem. Rev.* **1997**, *97*, 3083-3132.
(2) Buhlmann, P.; Pretsch, E.; Bakker, E. *Chem. Rev.* **1998**, *98*, 1593-1687.
(3) Nikolskii, B. P.; Belyustin, A. A. *J Anal Chem USSR* **1980**, *35*, 1435-1451.
(4) Frant, M. S.; Ross, J. W. *Science* **1966**, *154*, 1553-1555.
(5) Frant, M. S.; Ross, J. W. *Science* **1970**, *167*, 987-&.
(6) Pedersen, C. J. *J. Am. Chem. Soc.* **1967**, *89*, 7017-&.
(7) Park, C. H.; Simmons, H. E. *J. Am. Chem. Soc.* **1968**, *90*, 2431-&.
(8) Biachi, A.; Bowman-James, K.; Garcia-Espana, E. *Supramolecular Chemistry of Anions*; Wiley-VCH: New York, 1997.
(9) Antonisse, M. M. G.; Reinhoudt, D. N. *Electroanalysis* **1999**, *11*, 1035-1048.
(10) Hofmeister, F. *Arch. Exp. Pathol. Pharmakol* **1888**, *24*, 247.
(11) Umezawa, Y. *Handbook of Ion-Selective Electrodes: Selectivity Coefficients*; CRC Press: Roca Raton,FL, 1990.
(12) Trebbe, U.; Niggemann, M.; Cammann, K.; Fiaccabrino, G. C.; Koudelka-Hep, M.; Dzyadevich, S.; Shulga, O. *Fresenius J. Anal. Chem.* **2001**, *371*, 734-739.
(13) Nagy, G.; Nagy, L. *Anal. Lett.* **2007**, *40*, 3-38.
(14) Cattrall, R. W.; Freiser, H. *Anal. Chem.* **1971**, *43*, 1905-1906.
(15) James, H.; Freiser, H.; Carmack, G. *Anal. Chem.* **1972**, *44*, 856-857.
(16) Ruzicka, J.; Tjell, J. C.; Lamm, C. G. *Anal. Chim. Acta* **1972**, *62*, 15-28.
(17) Kalcher, K.; Kauffmann, J. M.; Wang, J.; Svancara, I.; Vytras, K.; Neuhold, C.; Yang, Z. *Electroanalysis* **1995**, *7*, 5-22.
(18) James, H. J.; Carmack, G. P.; Freiser, H. *Anal. Chem.* **1972**, *44*, 853-855.
(19) Buck RP, F. H. *Ion Selective Electrodes in Analytical Chemistry. vol. 1.*; Plenum: New York, 1978.
(20) Hauser, P. C.; Chiang, D. W. L.; Wright, G. A. *Anal. Chim. Acta* **1995**, *302*, 241-248.
(21) Dybko, A.; Zachara, J.; Golimowski, J.; Wroblewski, W. *Anal. Chim. Acta* **2003**, *485*, 103-109.
(22) Gyurcsanyi, R. E.; Rangisetty, N.; Clifton, S.; Pendley, B. D.; Lindner, E. *Talanta* **2004**, *63*, 89-99.
(23) Fibbioli, M.; Morf, W. E.; Badertscher, M.; de Rooij, N. F.; Pretsch, E. *Electroanalysis* **2000**, *12*, 1286-1292.
(24) Grygolowicz-Pawlak, E.; Wygladacz, K.; Sek, S.; Bilewicz, R.; Brzozka, Z.; Malinowska, E. *Sens. Actuator B-Chem.* **2005**, *111*, 310-316.
(25) Grygolowicz-Pawlak, E.; Plachecka, K.; Brzozka, Z.; Malinowska, E. *Sens. Actuator B-Chem.* **2007**, *123*, 480-487.
(26) Gorski, L.; Grygolowicz-Pawlak, E.; Rudzka, A.; Plachecka, K.; Malinowska, E. *Chem. Anal.* **2006**, *51*, 909-921.
(27) Lai, C.-Z.; Fierke, M. A.; Stein, A.; Buhlmann, P. *Anal. Chem.* **2007**, *79*, 4621-4626.
(28) Liu, D.; Meruva, R. K.; Brown, R. B.; Meyerhoff, M. E. *Anal. Chim. Acta*

1996, *321*, 173-183.
(29) Zachara, J. E.; Toczylowska, R.; Pokrop, R.; Zagorska, M.; Dybko, A.; Wroblewski, W. *Sens. Actuator B-Chem.* **2004**, *101*, 207-212.
(30) Seiler, K.; Simon, W. *Sens. Actuator B-Chem.* **1992**, *6*, 295-298.
(31) Bakker, E.; Simon, W. *Anal. Chem.* **1992**, *64*, 1805-1812.
(32) Qin, Y.; Bakker, E. *Talanta* **2002**, *58*, 909-918.
(33) Rosatzin, T.; Holy, P.; Seiler, K.; Rusterholz, B.; Simon, W. *Anal. Chem.* **1992**, *64*, 2029-2035.
(34) Chang, Q.; Meyerhoff, M. E. *Anal. Chim. Acta* **1986**, *186*, 81-90.
(35) Ammann, D.; Huser, M.; Krautler, B.; Rusterholz, B.; Schulthess, P.; Lindemann, B.; Halder, E.; Simon, W. *Helv. Chim. Acta* **1986**, *69*, 849-854.
(36) Huser, M.; Morf, W. E.; Fluri, K.; Seiler, K.; Schulthess, P.; Simon, W. *Helv. Chim. Acta* **1990**, *73*, 1481-1496.
(37) Gao, D.; Li, J. Z.; Yu, R. Q.; Zheng, G. D. *Anal. Chem.* **1994**, *66*, 2245-2249.
(38) Chaniotakis, N. A.; Park, S. B.; Meyerhoff, M. E. *Anal. Chem.* **1989**, *61*, 566-570.
(39) Abe, H.; Kokufuta, E. *Bull. Chem. Soc. Jpn.* **1990**, *63*, 1360-1364.
(40) Park, S. B.; Matuszewski, W.; Meyerhoff, M. E.; Liu, Y. H.; Kadish, K. M. *Electroanalysis* **1991**, *3*, 909-916.
(41) Li, X. Z.; Harrison, D. J. *Anal. Chem.* **1991**, *63*, 2168-2174.
(42) Shamsipur, M.; Javanbakht, M.; Hassaninejad, A. R.; Sharghi, H.; Ganjali, M. R.; Mousavi, M. F. *Electroanalysis* **2003**, *15*, 1251-1259.
(43) Pietrzak, M.; Meyerhoff, M. E. *Anal. Chem.* **2009**, *81*, 3637-3644.
(44) Steinle, E. D.; Amemiya, S.; Buhlmann, P.; Meyerhoff, M. E. *Anal. Chem.* **2000**, *72*, 5766-5773.
(45) Malinowska, E.; Gorski, L.; Meyerhoff, M. E. *Anal. Chim. Acta.* **2002**, *468*, 133-141.
(46) Mitchell-Koch, Jeremy T.; Pietrzak, M.; Malinowska, E.; Meyerhoff, Mark E. *Electroanalysis* **2006**, *18*, 551-557.
(47) Bakker, E.; Malinowska, E.; Schiller, R. D.; Meyerhoff, M. E. *Talanta* **1994**, *41*, 881-890.
(48) Parzuchowski, P. G.; Kampf, J. W.; Rozniecka, E.; Kondratenko, Y.; Malinowska, E.; Meyerhoff, M. E. *Inorg. Chim. Acta* **2003**, *355*, 302-313.
(49) Badr, I. H. A.; Meyerhoff, M. E. *J. Am. Chem. Soc.* **2005**, *127*, 5318-5319.
(50) Badr, I. H. A.; Meyerhoff, M. E. *Anal. Chem.* **2005**, *77*, 6719-6728.
(51) Kang, Y.; Kampf, J. W.; Meyerhoff, M. E. *Anal. Chim. Acta.* **2007**, *598*, 295-303.
(52) Qin, Y.; Bakker, E. *Anal. Chem.* **2004**, *76*, 4379-4386.
(53) Khalil, S. A. H.; Moody, G. J.; Thomas, J. D. R. *Anal. Lett.* **1986**, *19*, 1809-1830.
(54) Anker, P.; Wieland, E.; Ammann, D.; Dohner, R. E.; Asper, R.; Simon, W. *Anal. Chem.* **1981**, *53*, 1970-1974.
(55) Ma, S. C.; Yang, V. C.; Meyerhoff, M. E. *Anal. Chem.* **1992**, *64*, 694-697.
(56) Ramamurthy, N.; Baliga, N.; Wahr, J. A.; Schaller, U.; Yang, V. C.;

Meyerhoff, M. E. *Clin. Chem.* **1998**, *44*, 606-613.
(57) Fu, B.; Bakker, E.; Yang, V. C.; Meyerhoff, M. E. *Macromolecules* **1995**, *28*, 5834-5840.
(58) Dai, S.; Esson, J. M.; Lutze, O.; Ramamurthy, N.; Yang, V. C.; Meyerhoff, M. E. *J. Pharm. Biomed. Anal.* **1999**, *19*, 1-14.
(59) Kuwata, S.; Miura, N.; Yamazoe, N.; Seiyama, T. *Denki Kagaku* **1983**, *51*, 947-948.
(60) Severinghaus, J. W.; Bradley, A. F. *J. Appl. Physiol.* **1958**, *13*, 515-520.
(61) Fligier, J.; Czichon, P.; Gregorowicz, Z. *Chem. Anal.* **1978**, *23*, 119-126.
(62) Rao, N.; Vandenbleek, C. M.; Schoonman, J. *Solid State Ion.* **1992**, *52*, 339-346.
(63) Meyerhoff, M. E. *Anal. Chem.* **1980**, *52*, 1532-1534.
(64) Arquint, P.; Vandenberg, A.; Vanderschoot, B. H.; Derooij, N. F.; Buhler, H.; Morf, W. E.; Durselen, L. F. J. *Sens. Actuator B-Chem.* **1993**, *13*, 340-344.
(65) Meruva, R. K.; Meyerhoff, M. E. *Anal. Chim. Acta* **1997**, *341*, 187-194.
(66) Pranitis, D. M.; Meyerhoff, M. E. *Anal. Chim. Acta* **1989**, *217*, 123-133.
(67) Martin, G. B.; Meyerhoff, M. E. *Anal. Chim. Acta* **1986**, *186*, 71-80.
(68) Greenberg, J. A.; Meyerhoff, M. E. *Anal. Chim. Acta* **1982**, *141*, 57-64.
(69) Guerrini, M.; Beccati, D.; Shriver, Z.; Naggi, A.; Viswanathan, K.; Bisio, A.; Capila, I.; Lansing, J. C.; Guglieri, S.; Fraser, B.; Al-Hakim, A.; Gunay, N. S.; Zhang, Z. Q.; Robinson, L.; Buhse, L.; Nasr, M.; Woodcock, J.; Langer, R.; Venkataraman, G.; Linhardt, R. J.; Casu, B.; Torri, G.; Sasisekharan, R. *Nat. Biotechnol.* **2008**, *26*, 669-675.
(70) Kishimoto, T. K.; Viswanathan, K.; Ganguly, T.; Elankumaran, S.; Smith, S.; Pelzer, K.; Lansing, J. C.; Sriranganathan, N.; Zhao, G. L.; Galcheva-Gargova, Z.; Al-Hakim, A.; Bailey, G. S.; Fraser, B.; Roy, S.; Rogers-Cotrone, T.; Buhse, L.; Whary, M.; Fox, J.; Nasr, M.; Dal Pan, G. J.; Shriver, Z.; Langer, R. S.; Venkataraman, G.; Austen, K. F.; Woodcock, J.; Sasisekharan, R. *N. Engl. J. Med.* **2008**, *358*, 2457-2467.
(71) Wang, L.; Meyerhoff, M. E. *Anal. Chim. Acta* **2008**, *611*, 97-102.
(72) Gorski, L.; Matusevich, A.; Pietrzak, M.; Wang, L.; Meyerhoff, M. E.; Malinowska, E. *J. Solid State Electrochem.* **2009**, *13*, 157-164.
(73) Wang, L.; Buchanan, S.; Meyerhoff, M. E. *Anal. Chem.* **2008**, *80*, 9845-9847.

CHAPTER 2

FLUORIDE SELECTIVE SENSORS BASED ON POLYMETHACRYLATE POLYMERS WITH APPENDED ALUMINUM(III) TETRAPHENYLPORPHYRINS

2.1. Introduction

The development of inexpensive fluoride sensors to potentially replace the classical single-crystal LaF_3-based ion-selective electrode (ISE)[1-4], is an area of great interest owing to the many real-world applications for such devices. Fluoride ion is added intentionally to drinking water and dental hygiene products for the purpose of reducing the frequency of dental caries, and fluoride levels in municipal water supplies and in these dental products need to be tightly controlled. Fluoride is also present in certain vegetables due to the use of a variety of pesticides that contain fluorine/fluoride. Further, a good fluoride sensor can be utilized as a detector for developing simple bioanalytical systems to quantitate glucose, cholesterol and a host of other clinically relevant species by employing a coupled enzymatic reaction to liberate fluoride from fluorophenol substrates via a peroxidase catalyzed reaction.[5-7]

Polymeric membrane/film type electrochemical and optical anion sensors would provide an attractive alterative to the classical LaF_3-based ISE. However, as described in Chapter 1, selectivity coefficients of the anion-selective electrodes and

optodes based on dissociated anion-exchangers, are related to the ability of the anion to partition from the aqueous phase into the organic phase since specific interactions between the anion-exchanger and target anions do not exist. Therefore, these anion-exchanger-based electrodes are known to exhibit the so-called Hofmeister selectivity pattern (see Eq. 1.4)[10] where fluoride yields the least response since it has the most negative Gibbs free energy of hydration ($\triangle G_{hyd}^{298}(F^-)$ = -104.3 ± 0.7 kcal/mol).[11]

It has been reported recently that by using certain metalloporphyrin species as ionophores (e.g., Ga(III)-porphyrins,[12] Zr(IV)-porphyrins,[1] or Al(III)-porphyrins[4]), it is possible to develop polymeric membrane/film based ISEs that achieve fluoride selectivity approaching that exhibited by the solid-state fluoride ISE. However, at present, there are certain limitations to these sensors, such as super-Nernstian responses, long response time, short use-life and a higher than desired detection limits. These issues must be resolved before practical applications of these devices can be fully realized. Such problematic behaviors have been ascribed to the occurrence of dimer-monomer equilibria of the metalloporphyrin species within the polymeric membrane phase of the sensors when they are in contact with an aqueous test solution containing the target anion.[12] However, by taking advantage of this equilibrium process, polymeric film type optical sensors can be designed that exhibit excellent fluoride response. Indeed, it was shown recently that an chloro-aluminum(III)-octaethylporphyrin (Al(III)OEP) based fluoride optical sensor yields a detection limit even lower than that of the classical solid-state fluoride ISE

but with comparable selectivity.[2, 3]

There are two approaches to possibly eliminate the dimer formation of metalloporphyrin ionophores, which is desired for the fabrication of ideally functioning membrane electrodes. One means is to utilize picket-fence porphyrin structures as the ligand to prepare the Al(III) ionophores,[4] so that dimer formation can be prevented via steric hindrance. The other approach involves covalently attaching the Al(III) porphyrins to a polymer backbone. The latter method has been studied by a number of research groups.[13-16] As reported by Qin and Bakker,[17] dimer formation for a chloride ion selective In(III) porphyrin system was eliminated by modifying the metalloporphyrin with a methacrylate functionality to allow attachment within polymethacrylate polymer, and use of that polymer as a macromolecular ionophore agent in conventional PVC membranes. Herein, we report a similar effort to attach chloro-aluminum(III)-tetraphenylporphyrin (Al(III)TPP) to polymethacrylate polymers. We further examine the behavior of both potentiometric membrane electrodes and optical sensing polymeric films that are formulated with this new macromolecular ionophore. It will be shown that while excellent fluoride selectivity is maintained, and longer operational lifetimes can be achieved, the Al(III)TPP attached to the polymethacrylate can still undergo dimer formation in the presence of fluoride ion in the bathing solution. Hence, both electrochemical and optical sensors prepared from this new material show analytical behavior quite similar to those reported for the free Al(III)TPP ligand, but with enhanced use-life.

2.2. Experimental Section

2.2.1. Materials

Protoporphyrin IX, 1-hydroxybenzotriazole, 4-(dimethylamino) pyridine (DMAP), 1,3-dicyclocarbodiimide (DCC), 1-dodecanol, tetrabutyl ammonium fluoride, 4-hydroxybenzaldehyde, benzaldehyde, pyrrole, propionic acid, acetic acid, methacryloyl chloride, and triethylamine were all purchased from Aldrich (Milwaukee, WI). The monomer *n*-decyl methacrylate (DMA), 99%, was obtained from Polysciences, Inc. (Warrington, PA). The monomers methyl methacrylate (MMA), 99.5% and the polymerization initiator 2,2'-azobisisobutyronitrile, 98% (AIBN), were obtained from Aldrich. Inhibitors were removed from the monomers by prior distillation. AIBN was re-crystallized from warm methanol prior to use. Potassium tetrakis[3,5-bis(trifluoromethyl)phenyl]borate (KTFPB), o-nitrophenyl octyl ether (NPOE), high molecular weight poly(vinyl chloride)(PVC) and ETH 7075 were purchased from Fluka (Milwaukee, WI). All salts were obtained from Aldrich and aqueous solutions of them were prepared by dissolving the appropriate sodium salts in Millipore purified water (18MΩ cm). All solvents, including chloroform, methylene chloride (CH_2Cl_2), methanol and tetrahydrofuran (THF) and the silica gel used for chromatography were obtained from Fisher Scientific (Pittsburgh, PA).

2.2.2 Synthesis and Dimerization of a Lipophilic Al(III) Protoporphyrin IX Diester Derivative

A protoporphyrin IX bis-dodecyl diester (see Figure 2.1) was prepared and characterized as reported previously by Ford.[18] One mmol protoporphyrin IX was dissolved in 50 mL of dry distilled THF. Two mmol of 1-hydroxybenzotriazole and 0.1 mmol of 4-(dimethylamino) pyridine (DMAP) were added. The solution was placed in an ice bath at 0 °C, and 2 mmol of 1,3-dicyclocarbodiimide (DCC) was added slowly to the flask. The mixture was stirred for approximately 10 min before 2.006 mmol of 1-dodecanol was added dropwise via syringe. The reaction was stirred in the ice bath for about 3 h, allowed to come to room temperature, and continuously stirred overnight. The reaction products were first filtered, and the residuals were washed with THF to remove any remaining products of the DCC coupling reaction. THF was then evaporated, and the remaining solid was washed with cold chloroform, which will dissolve the protoporphyrin diester derivative and leave the urea byproducts as solid. After evaporation of the chloroform, the product was purified by column chromatography (silica gel) using chloroform as the solvent. Final products were characterized by mass spectrometry, yielding the desired molecular weight peak at m/z = 899.2. Metallization of this protoporphyrin IX bis-dodecyl diester was conducted as described in the literature.[19, 20] The aluminum(III) protoporphyrin IX bis-dodecyl diester (see Figure 2.1) was characterized by mass spectrometry showing the desired molecular weight peak at m/z = 955.1, as well as UV/visible spectrometry.

Fluoride dimer of the above Al(III) protoporphyrin IX derivative was synthesized

by dissolving the porphyrin in chloroform and shaking the organic layer with 1 M hydrofluoric acid (HF) solution (pH = 3, adjusted by sodium hydroxide) or by adding different amount of tetrabutyl ammonium fluoride solid. No hydrolysis was observed under the acidic environment (pH = 3) over 24 hours. The chloroform was evaporated after the extraction, and the products were analyzed by a micromass tofspec-2E matrix assisted, laser-desorption time-of-flight mass spectrometer (MALDI-TOF MS).

2.2.3. Syntheses of Polymerizable Al(III)-Porphyrin Complex

5-4(Hydroxyphenyl)-10-15-20-triphenylporphyrin (HOTPP) was prepared as reported elsewhere.[21, 22] The procedure used to synthesize the aluminum complexes Al(III)(HOTPP)Cl was analogous to that also described in the literature.[19, 20] The chloro(5-(4-methacryloyloxyphenyl)-10,15,20-triphenylporphyrinato)aluminum(III) (Al(III)(MOTPP)Cl) (see Figure 2.2) was prepared by the procedure reported by Qin and coworkers.[17] The crude product was purified by flash chromatography on silica using CH_2Cl_2 as the solvent. Final products were characterized by mass spectrometry, yielding the desired molecular weight peak at m/z = 755.2.

2.2.4. Synthesis and Characterization of Polymeric Ionophore

The methacrylate copolymer was synthesized via a thermally initiated free radical solution polymerization. Five weight percent of the Al(III)(MOTPP)Cl (50

mg) species, 0.78 g of MMA, and 0.20 g of DMA were dissolved in anhydrous ethyl acetate. The solution was purged with nitrogen for 30 min before 6 mg of AIBN was added. The homogeneous solution was stirred at a temperature of 90 °C, and the reaction was maintained for 18 h. After this time, the solvent was evaporated and the polymer was re-dissolved in 2 mL of THF. Aliquots of polymer solution were added dropwise to 100 mL of methanol under vigorous stirring. The precipitate was collected and washed thoroughly with methanol to ensure the complete removal of any free porphyrin. The polymer was then dried under vacuum.

2.2.5. ISE membrane Formulation and EMF Measurements

The ISE membranes used for potentiometric measurements consisted of 1 wt% (20 wt% of copolymer) of the macromolecular Al(III) porphyrin ionophore and various quantities of anionic additive salt (KTFPB), 66 wt% of NPOE plasticizer, and 33 wt% PVC. All components (total mass 200 mg) were dissolved in 2 - 3 mL of freshly distilled THF, and the cocktails were poured into a 25 mm-id glass ring affixed to a glass microscope slide. The solvent was allowed to evaporate overnight, yielding a transparent colored film. Disks with 8 mm diameter were cut from the parent membrane and mounted in electrode bodies (Oesch Sensor Technology, Sargans, Switzerland). An internal filling solution composed of 0.01 M NaCl or 0.01 M NaCl and 0.01 M NaF was used. These same solutions were also employed as conditioning solutions for the ISEs prior to fluoride calibration measurements.

The sample buffer employed in this study was 0.05 M glycine, adjusted to pH 3.0 with phosphoric acid (gly/phos buffer). All analyte solutions were prepared from sodium salts of various anions dissolved in the buffer. Since at pH=3.0, ca. 60% of all fluoride present in solution is protonated (HF) and is not detected by the electrode, all calibration curves were plotted by using total fluoride concentrations in the test buffer solution (i.e, $[F^-]$ + [HF]), instead of free activity of fluoride. Data presented in the figures were normalized in order to make the starting EMF values of all electrodes equal to zero.

2.2.6. Optical Measurements

The optical sensing films either have exactly the same composition as the ISE membranes or contained 25.8 mmol/kg (40 wt% copolymer) ionophore, 100 mol% ETH7075, NPOE plasticizer, and PVC (2:1 mass ratio). All the components (total mass 100 mg) were dissolved in distilled THF to give a 2 mL cocktail. The films were then prepared by a spin-coating device (model SCS-G3-8 obtained from Cookson Electronics; Providence, RI) on a square-shaped quartz plate 35 mm in length. The rotation speed was 600 rpm, while 100 μL of the polymer film cocktail was injected onto the rotating glass plate each time to spin for 5 seconds. The films were dried in air before use and were stored in the dark when they were not used for measurements. For further optical measurements, the quartz plate coated with the deposited film was mounted in a custom-built spectrophotometer flow cell similar to that described elsewhere.[23] The flow cell was mounted into a Perkin-Elmer

double-beam UV/visible spectrophotometer (model Lambda 35; Boston, MA). The 0.05M gly/phos buffer (pH = 3) was allowed to flow for 30 min at a flow rate of 1.4 mL/min to precondition the films, using a Gilson Minipuls-3 peristaltic pump (Middleton, WI). The response of the optical sensing film toward different anions was recorded by adding respective aliquots of the test solution to a stirred reservoir containing 50 mL of buffer. The resulting buffered salt solution was pumped through the cell and recirculated into the buffer reservoir. The spectra of the films were recorded in the range between 360 nm to 630 nm when equilibrium was reached. To correct for the background absorbance, the absorbance measured at 630 nm was subtracted from the absorbance values at the wavelengths of interest. Total fluoride ion concentration was used instead of fluoride activity in all experiments.

2.3. Results and Discussion

2.3.1. Verification of the Fluoride Bridged Dimer Formation in the Synthesized Al(III) Protoporphyrin IX Diester Derivative

Recently, an X-ray structure of the bis-fluoro bridged Sc(III)-porphyrin dimer was successfully obtained to show the dimer formation when metalloporphyrin contacted fluoride source.[24] Unfortunately, using the same procedure, the crystalline product obtained by shaking Al(III)OEP with HF solution can not be fully identified by X-ray crystallography. Some sandwich structures with one bridging ligand and outermost two axial ligands were obtained. However, the ligands are ambiguous

between fluoride and H_2O due to the deficiency of X-ray crystallography in discriminating oxygen and fluorine atoms. No crystal can be obtained by using the synthesized Al(III) protoporphyrin IX diester derivative either, due to its viscous physical property at room temperature. However, one advantage of the synthesized Al(III) protoporphyrin IX diester derivative is that its fluoride bridged dimer can survive at relatively low concentrations in organic solvent compared with the fluoride bridged dimer of Al(III)OEP. Therefore, it is possible to study its dimeric structures by using mass spectrometry. Figures 2.3 and 2.4 show the results obtained from MALDI-TOF mass spectrometry when the synthesized Al(III) protoporphyrin IX diester derivative contacts different types of fluoride sources. When shaken with HF, the product is a mixture of fluoride monomer, mono- and bis- fluoride bridged dimer, and even some fluoride bridged trimer (see Figure 2.3). However, when the fluoride source is changed to tetrabutyl ammonium fluoride solid, no matter what ratios of synthesized Al(III) protoporphyrin IX diester derivative to tetrabutyl ammonium fluoride were use, only one dimeric structure with single fluoride bridge together with some fluoride monomeric structure can be observed. Figure 2.4 shows the synthesized Al(III) protoporphyrin IX diester derivative and tetrabutyl ammonium fluoride ratio of 2:1 which gives the largest dimer to monomer ratio in the mass spectrum.

2.3.2. Characterization of Polymethacrylate with Covalently Linked Al(III)TPP

The copolymer with covalently linked Al(III) tetraphenyl porphyrin (Al(III)TPP) ionophore (see Figure 2.2) was characterized by ^{1}H-NMR, where low intensity resonances from protons on the porphyrin phenyl rings were observed due to the presence of a nearby quadruple nuclei (Al(III)). Therefore, to determine the amount of Al(III) porphyrin complex in the copolymer, UV/visible spectroscopy was employed. Based on using pure Al(III)TPP as a standard, the concentration of the grafted aluminum porphyrin on the polymer backbone was estimated to be 64.7 mmol/kg. The molecular weight of the copolymer was determined by gel permeation chromatography with stabilized THF as the carrier solvent and polystyrene as a standard. The respective peak, number and weight molecular averages were determined as Mp = 29,411, Mn = 20,919, and Mw = 42,214. Moreover, the amount of Al(III) porphyrin attached could be changed by altering the ratio of starting monomers. Reduced amount of Al(III)(MOTPP)Cl results in a lower value of attached Al(III) porphyrin, which possibly will increase the distance between two Al(III) porphyrin molecules in the polymer chain. **A** different ratio of MMA and DMA monomer was also tried in the polymerization. Employing a MMA:DMA ratio of 1:2, the resulting membrane did not exhibit as good selectivity as the current results obtained from MMA and DMA at a ratio of 1:4. If more DMA was used, a very viscous polymer was obtained which was not compatible with the other membrane components (i.e., PVC and NPOE). The synthesized PDMA/PMMA copolymer with Al(III) covalently attached was indeed tested directly as a sensing film without adding any PVC. Unfortunately, such films were too

brittle/fragile and could not be peeled off from the glass slide on which they were cast. The mechanical properties of the films were not appropriate for the use as a membrane for preparation of ion selective electrodes.

2.3.3. Potentiometric Response Characteristics of ISEs Formulated with Covalently Attached Al(III)TPP

Although Al(III)OEP has been used as a highly selective fluoride ionophore in optical sensing films,[2, 3] when free Al(III) porphyrins (including Al(III)TPP) have been utilized in polymer membranes for potentiometric sensing of fluoride, the response toward fluoride was found to be quite slow, and super-Nernstian response with slopes greater than -100 mV/decade was observed.[4] The undesirable behavior of such ISE membranes was attributed to the aforementioned dimer-monomer equilibrium within the polymeric film when the film contacted fluoride ion.[4] It was anticipated here that use of the new macromolecular ionophore would overcome these problems. Initial efforts to prepare films directly with only the new copolymer with covalently linked Al(III)TPP species yielded brittle membranes that did not have adequate mechanical properties to be used to construct ion selective electrodes (see 2.3.2). Therefore, the new methacrylate copolymer with covalently attached Al(III)TPP was mixed with appropriate amounts of KTFPB, PVC and NPOE to yield a dark purple transparent film. Preliminary testing suggested that optimal potentiometric fluoride selectivity and response can be achieved by adding 50 mol% KTFPB (relative to Al(III)TPP content in the copolymer) to the membrane

formulation (data for other KTFPB levels not shown here.). Indeed, potentiometric response and selectivity of a PVC/NPOE membrane containing 20 wt% methacrylate copolymer with the covalently attached Al(III) porphyrin and 50 mol% of KTFPB were tested using two different internal filling solutions (with and without fluoride added). Membrane electrodes with 10 mM NaCl only as the inner filling solution (and conditioned in this solution as well) display near-Nernstian fluoride response (-62.0 mV/decade in range of 10^{-4} – 10^{-2} M total fluoride) (see Figure 2.5) and maintain a high degree of potentiometric selectivity toward fluoride ion. Only salicylate is a significant interference, with a potentiometric selectivity of the membrane for fluoride relative to salicylate, $K^{pot}_{F/Sal} = 0.1$. In contrast, membrane electrodes with fluoride added to the inner solution (at 0.01 M) and preconditioned in this solution and then washed thoroughly with test buffer, display a sub-Nernstian fluoride response (-33.2 mV/decade) in the range of 10^{-5}M – 10^{-2} M (data not shown here). Such behavior is quite similar to membrane electrodes formulated with free Al(III) porphyrins (Al(III)OEP or Al(III)TPP) as ionophores as reported previously,[4] where it was found that employing fluoride within the internal solution decreases the observed slope value of the fluoride calibration curve. Such behavior in the presence of high fluoride may indicate a dimer-monomer equilibrium when the membranes are in prolonged contact with fluoride ion.[4] Indeed, it has been suggested previously that Al(III) porphyrins can interact with fluoride ion and potentially form dimeric species in which one or two fluoride ions are bridging ligands.[2-4] Further examination of the sensing membranes used in this work by UV/visible absorption

spectroscopy could confirm whether such chemistry is occurring in the films that are also formulated with the new polymethacrylate copolymer possessing the immobilized Al(III)TPP species.

Figure 2.6 illustrates the UV/visible spectra of a polymer film prepared using exactly the same composition as the membrane employed in the potentiometric measurements reported in Figure 2.5. The film was initially equilibrated in 0.05 M gly/phos buffer (pH = 3.0), and the Soret absorbance band was observed at 421 nm (dashed line in Figure 2.6). After the film was equilibrated with solutions containing increasing concentrations of fluoride by using a flow cell system to pump the solution over the film,[2, 3] the absorbance at 421 nm decreases with a concomitant appearance and increase of a new band at 404 nm. Previous studies have attributed such a hypsochromic shift in the Soret band to formation of a dimeric metalloporphyrins in polymer phase (compared to monomers). The spectral data shown in Figure 2.6 therefore clearly indicates the likely formation of a fluoride-bridged dimeric species between Al(III)TPP species covalently linked to the polymethacrylate polymer, with about 33% of the initial monomeric Al(III)TPP species dimerized at a fluoride level of 0.1 M. Such fluoride induced dimer formation was also shown recently to occur within polymeric films formulated with free Sc(III)-porphyrins as ionophores, and an X-ray structure of the bis-fluoro bridge Sc(III)-porphyrin dimer was obtained to support the occurrence of this process.[24] The observation of dimer formation for the polymer linked Al(III)TPP species is somewhat surprising since similar polymers with covalently linked In(III)TPP were

found previously not to form hydroxide ion bridged dimers when used to prepare chloride ion-selective sensing membranes.[17] One possible explanation may be a more favorable conditional equilibrium constant for fluoride induced dimer formation in the case of the Al(III)TPP species vs. the dimer formation constant for In(III)TPP with hydroxide when examined under relatively low pH conditions (pH = 5.5).[17] Since in the case of the In(III) porphyrins, hydroxide dimers are broken to monomers by the addition of low levels of chloride to the bathing solution, the binding constant for dimer formation at pH = 5.5 is probably not as strong as the formation constant for forming bis-fluoro bridged dimers as one increases fluoride ion in the bathing solution. In addition, since multiple Al(III)TPP structures exist on a single polymeric chain, a cooperative type of stacking between porphyrins on adjacent chains is possible, which further increases the apparent equilibrium constant for fluoride bridging induced dimer formation for the polymer with the Al(III)TPP structure attached.

Although the covalent attachment method cannot eliminate the dimer formation completely, it gives the ISE membrane a longer operational lifetime. Compared with free Al(III) porphyrins, Al(III)TPP, Al(III)OEP and Al(III) picket fence porphyrin,[4] the slope of fluoride calibration curve of the covalently attached Al(III) porphyrin system did not change dramatically over two weeks (22% loss in the slope value of fluoride calibration curve of the covalently attached Al(III) porphyrin system in two weeks compared with the 33% loss in the slope value of fluoride calibration curve of the unattached Al(III)TPP system in only one week) (see Figure 2.7),

although a decrease in the slope value of the calibration curve could be observed with a longer time period (one month). Furthermore, no phase separation of copolymer with covalently linked Al(TPP) species and the PVC was observed. Membranes having the same composition as employed for potentiometric measurements were immersed in 0.01 M NaCl as well as 0.01 M NaCl and NaF buffer solutions (pH = 3.0 phosphate/glycine) for one week. Microscopic examination of such membranes revealed no obvious phase separation or clear islands of different polymeric materials within the membranes for one week, however, islands were observed one month after immersing the membrane in the 0.01 M NaCl as well as 0.01 M NaCl and NaF buffer solutions (pH = 3.0 phosphate/glycine). Those membranes showing the islands were re-dissolved, however, the mass spectra did not suggest any peaks related to the detachment of Al(III) porphyrin, which means hydrolysis and crystallization of the detached Al(III) porphyrin are not the sources for the islands. Phase separation or the crystallization of the methacrylate copolymer might contribute to the change of the membrane.[25]

2.3.4. Optical Response Characteristics of Membranes Formulated with Covalently Attached Al(III) Porphyrin Together with ETH7075

As mentioned above, optical fluoride sensors that take advantage of the dimer-monomer equilibrium between Al(III)OEP have been reported in literature.[13, 14] The optical sensing film uses the principles of anion/proton co-extraction chemistry to achieve an optical response. The lipophilic pH chromoionophore translates the

binding of the fluoride ion to the Al(III) porphyrin as an optical signal, allowing optical measurement at a higher wavelength range than for the porphyrin species itself. In addition, there is evidence to suggest that the pH chromoionophore can also interact with certain porphyrins via a π-π interaction, potentially weakening the dimer formation constant to a point where reversibility in dimer formation is possible.[3] When a buffer solution (0.05 M gly/phos, pH 3.0) without fluoride flows over the film, the deprotonated form of the indicator dye (C^-) (λ_{max} = 530 nm) is the predominant absorbance band observed in the wavelength range of 450-550 nm. As fluoride is added to the buffer, the deprotonated form of the indicator decreases, and the protonated form (CH) increases in absorbance (λ_{max} = 470 nm) (see Figure 2.8).

A film with the new methacrylate copolymer possessing covalently attached Al(III) porphyrin and 100% mole of ETH-7075 relative to the Al(III)TPP species present in the polymer phase exhibits very good selectivity toward fluoride ion in such an optical sensing configuration (see Figure 2.9). Selectivity is similar to that observed with the electrochemical sensor described above. The response is reversible and the detection limit (ca. 10 μM) is comparable with previous studies with free Al(III)TPP as ionophore for optical fluoride measurements, but not as good when free Al(III)OEP is employed to fabricate optical sensors for fluoride (0.1 μM).[2] While we observed the expected absorbance change in the deprotonated form of the chromoionophore, a change in the Soret band absorbance of Al(III) porphyrin could also be observed which indicates some dimer formation during the process; however, the dimer formation in this material is not as strong as the dimer formation in the

Al(III)OEP system.[2, 3]

2.4. Summary

Dimeric structures were verified by mass spectrometry when Al(III) porphyrins contact fluoride. To eliminate such dimer formation in the potentiometric measurements, a methacrylate copolymer with covalently attached Al(III) porphyrins has been synthesized and characterized. Although a portion of the Al(III) porphyrins appended to the polymer structure still form dimeric species in the presence of fluoride, sensors prepared with membranes doped with the polymethacrylate copolymer exhibit a longer operational lifetime (vs. sensors fabricated with free Al(III)TPP). When used in an optical sensor configuration, the sensing films prepared with the newly synthesized material yield comparable fluoride responses to those obtained with the corresponding free Al(III)TPP species.

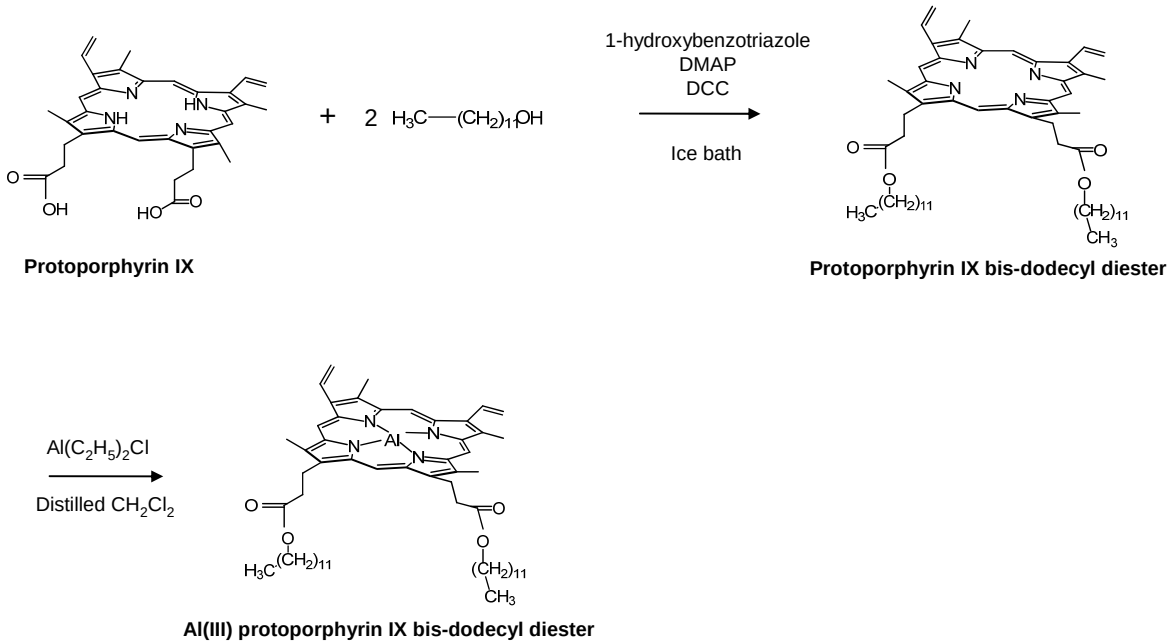

Figure 2.1. Synthetic procedure of the Al(III) protoporphyrin IX bis-dodecyl diester.

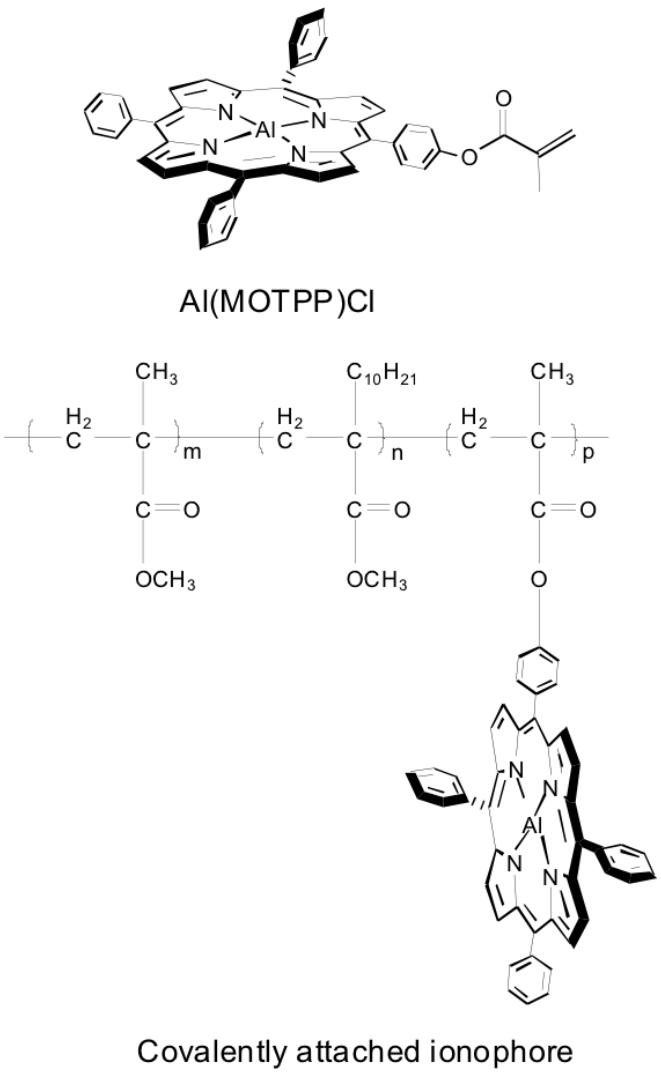

Figure 2.2. Structure of Al(MOTPP)Cl and the methacrylate copolymer with covalently attached Al(III) porphyrin.

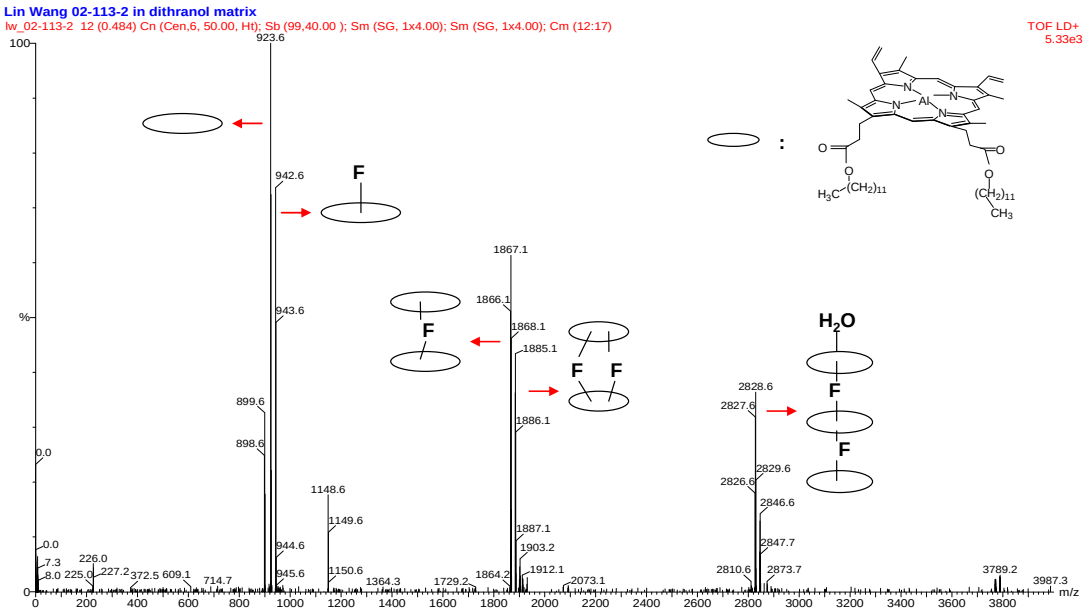

Figure 2.3. Mass spectrum of the products from the reaction of synthesized Al(III) protoporphyrin IX diester derivative and 1 M HF solution.

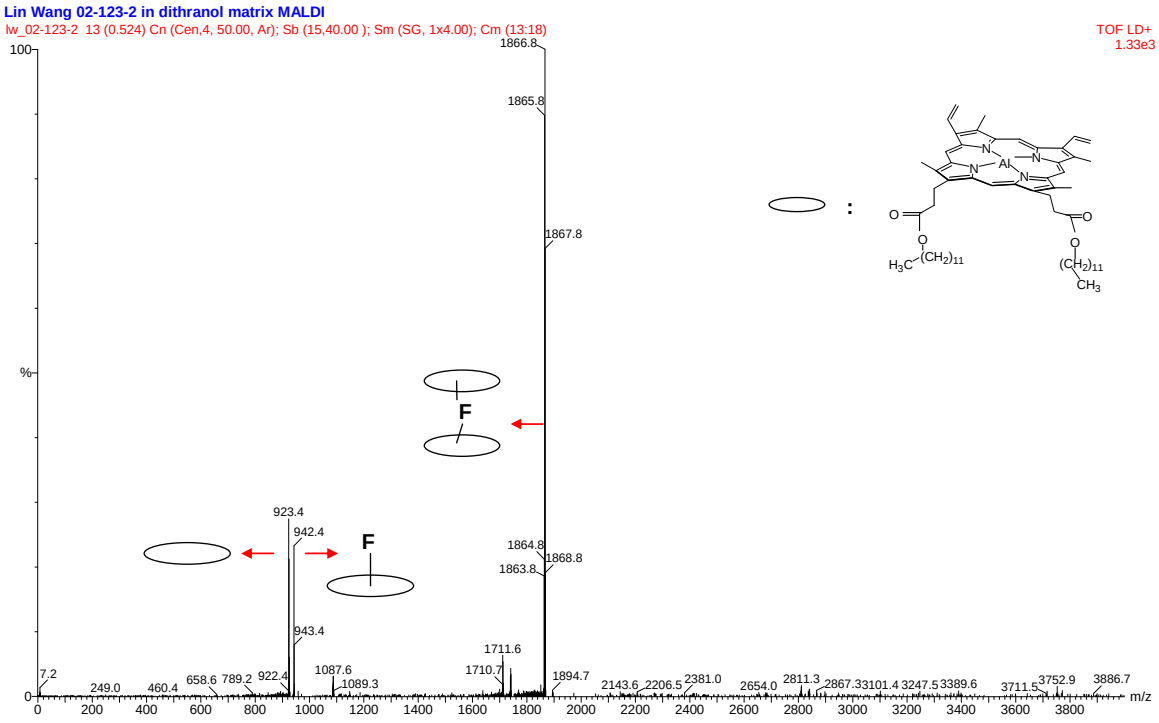

Figure 2.4. Mass spectrum of the products from the reaction of synthesized Al(III) protoporphyrin IX diester derivative and tetrabutyl ammonium fluoride solid.

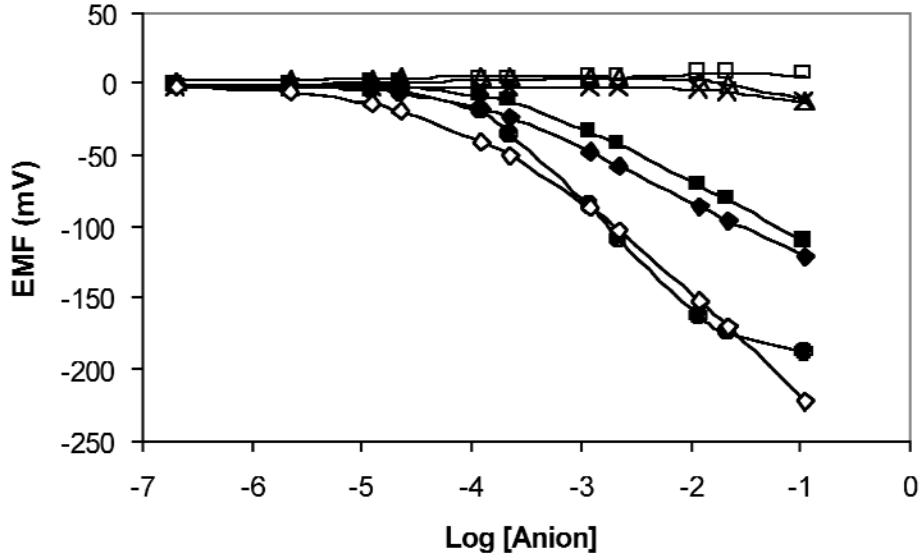

Figure 2.5. Potentiometric anion response for electrodes containing 20 wt% methacrylate copolymer with covalently attached Al(III) porphyrin and 50 mol% KTFPB (relative to Al(III) porphyrin) in PVC/NPOE membrane; (●) F, (■) SCN^-, (◆) ClO_4^-, (×) Br^-, (△) NO_3^-, (□) Cl^-, (◇) Sal^-. Response obtained in pH = 3.0 gly/phos buffer. Internal solution: 0.01 M NaCl in pH = 3.0 gly/phos buffer.

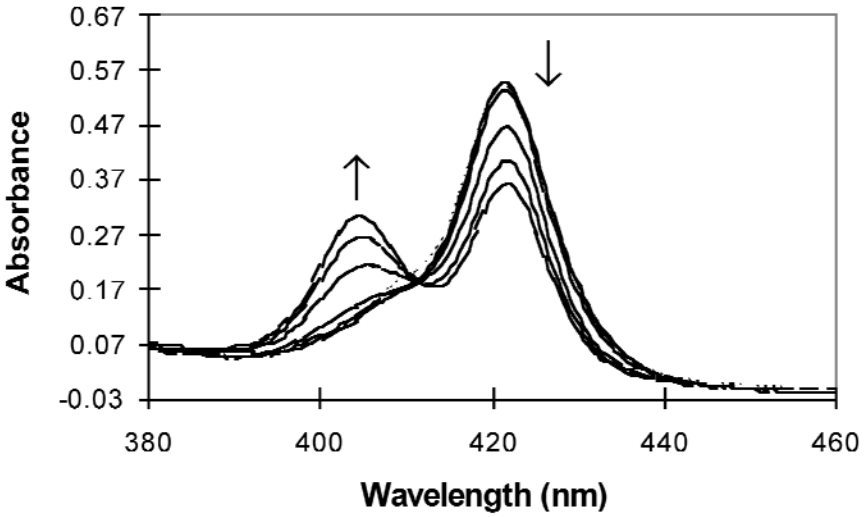

Figure 2.6. UV/visible spectra of a membrane containing methacrylate copolymer with covalently attached Al(III) porphyrin and 50 mol% KTFPB (relative to Al(III) porphyrin) upon increasing the bathing concentration of fluoride. (---) initial spectrum equilibrated in gly/phos buffer, pH 3.0. Concentration of fluoride increased from zero to 100 mM, increasing 10 fold each spectrum.

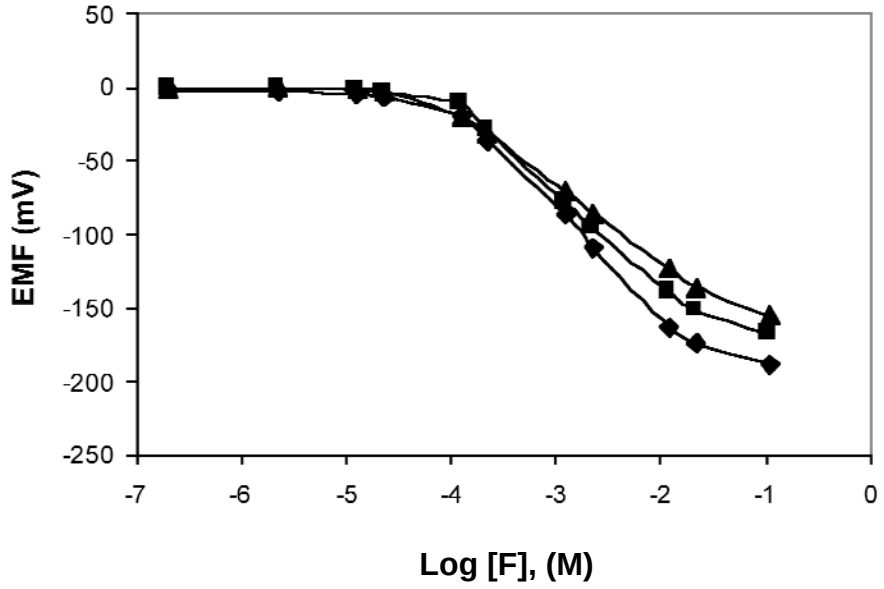

Figure 2.7. Response of membrane electrodes containing 20% methacrylate copolymer with covalently attached Al(III) porphyrin and 50 mol% KTFPB (relative to Al(III) porphyrin) toward fluoride ion as a function of time; (◆) the first day, (■) after one week, (▲) after two weeks.

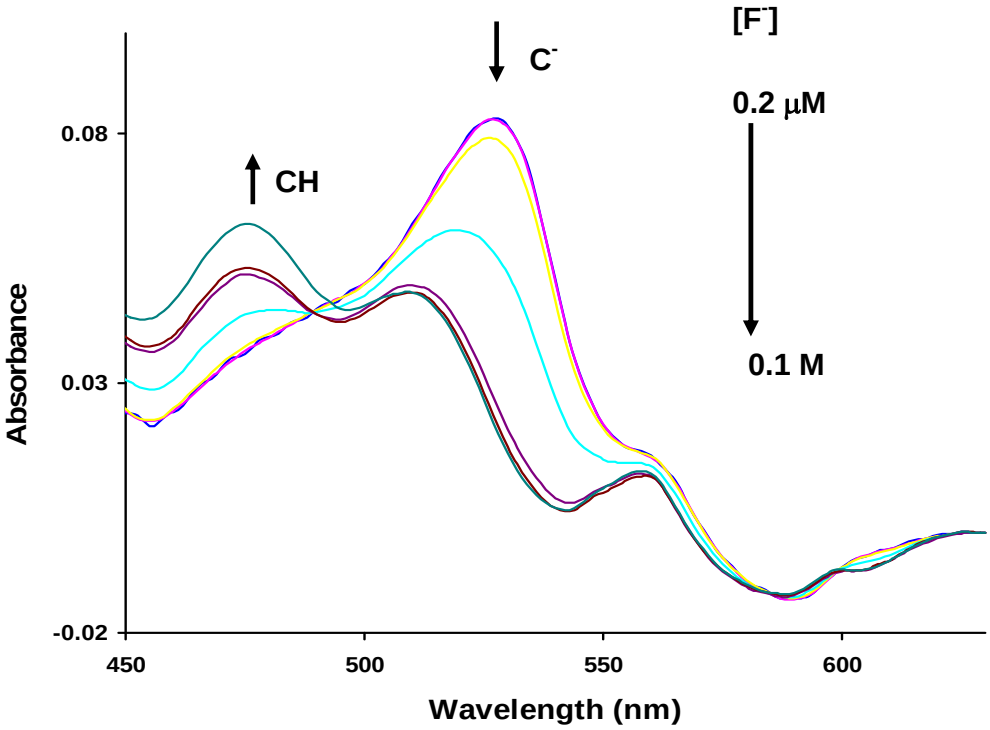

Figure 2.8. Spectral change of Al(III) polymethacrylate copolymer-ETH7075 based fluoride optical sensor prepared using PVC/NPOE when exposed to different concentrations of fluoride ion: 0.2 μM, 2.2μM, 22μM, 0.2 mM, 2.2 mM, 21.3 mM, and 0.1 M

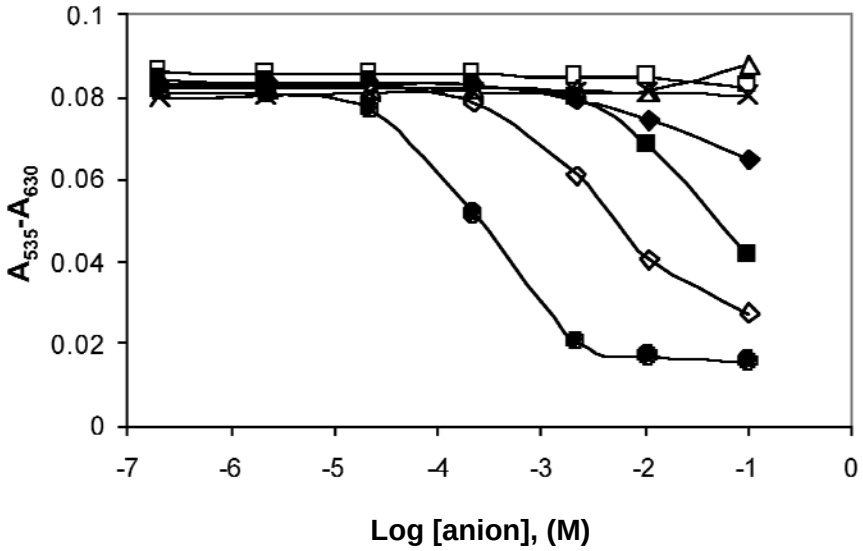

Figure 2.9. Optical response at 535 nm (background absorbance subtracted) of methacrylate copolymer with covalently attached Al(III) porphyrin in PVC/NPOE film containing 100 mol% ETH7075 toward different anions; (●) F, (■) SCN^-, (◆) ClO_4^-, (×) Br^-, (△) NO_3^-, (□) Cl^-, (◇) Sal^-. Response obtained in pH = 3.0 gly/phos buffer.

2.5. References

(1) Malinowska, E.; Gorski, L.; Meyerhoff, M. E. *Anal. Chim. Acta.* **2002**, *468*, 133-141.
(2) Badr, I. H. A.; Meyerhoff, M. E. *J. Am. Chem. Soc.* **2005**, *127*, 5318-5319.
(3) Badr, I. H. A.; Meyerhoff, M. E. *Anal. Chem.* **2005**, *77*, 6719-6728.
(4) Mitchell-Koch, Jeremy T.; Pietrzak, M.; Malinowska, E.; Meyerhoff, Mark E. *Electroanalysis* **2006**, *18*, 551-557.
(5) Hughes, G. M. K.; Saunders, B. C. *Chem. Ind* **1954**, 1265.
(6) Siddiqi, I. W. *Clin. Chem.* **1982**, *28*, 1962-1067.
(7) Abd-Rabboh, H. S. M.; Meyerhoff, M. E. *Talanta* **2007**, *72*, 1129-1133.
(8) Wegmann, D. W., H.; Ammann, D.; Morf, W. E.; Pretsch, E.; Sugahara, K.; Simon, W. *Mikrochim. Acta (Wien)* **1984**, 1-16.
(9) Ozawa, S.; Miyagi, H.; Shibata, Y.; Oki, N.; Kunitake, T.; Keller, W. E. *Anal. Chem.* **1996**, *68*, 4149-4152.
(10) Hofmeister, F. *Arch. Exp. Pathol. Pharmakol* **1888**, *24*, 247.
(11) Zhan, C.-G.; Dixon, D. A. *J. Phys. Chem. A* **2004**, *108*, 2020-2029.
(12) Steinle, E. D.; Amemiya, S.; Buhlmann, P.; Meyerhoff, M. E. *Anal. Chem.* **2000**, *72*, 5766-5773.
(13) Heng, L. Y.; Hall, E. A. H. *Anal. Chem.* **2000**, *72*, 42-51.
(14) Lee Yook Heng, E. A. H. H. *Electroanalysis* **2000**, *12*, 178-186.
(15) Malinowska, E.; Gawart, L.; Parzuchowski, P.; Rokicki, G.; Brzozka, Z. *Anal. Chim. Acta.* **2000**, *421*, 93-101.
(16) Qin, Y., Peper, S, Bakker,E *Electroanalysis* **2002**, *14*, 1375-1381.
(17) Qin, Y.; Bakker, E. *Anal. Chem.* **2004**, *76*, 4379-4386.
(18) Conrado, C. L.; Wecksler, S.; Egler, C.; Magde, D.; Ford, P. C. *Inorg. Chem.* **2004**, *43*, 5543-5549.
(19) Aida, T.; Inoue, S. *J. Am. Chem. Soc.* **1983**, *105*, 1304.
(20) Aida, T.; Wada, K.; Inoue, S. *Macromolecules;* **1987**, *20*, 237.
(21) Kamachi, M. A., H.; Nozakura, S. *J. Polym. Sci. Polym. Lett. Ed.* **1983**, *21*, 693.
(22) Coutant, D. E.; Clarke, S. A.; Francis, A. H.; Meyerhoff, M. E. *J. Chromatogr. A* **1998**, *824*, 147-157.
(23) Badr, I. H. A.; Meyerhoff, M. E. *Anal. Chim. Acta.* **2005**, *553*, 169-176.
(24) Kang, Y.; Kampf, J. W.; Meyerhoff, M. E. *Anal. Chim. Acta.* **2007**, *598*, 295-303.
(25) Brinkhuis, R. H. G.; Schouten, A. J. *Macromolecules* **1992**, *25*, 2725-2731.

CHAPTER 3

NITRITE SELECTIVE SENSORS BASED ON COBALT(III) PORPHYRINS

3.1. Introduction

Nitrite is known to be ubiquitous within environmental, food, industrial and physiological samples.[1-3] Moreover, detection of nitrite within physiological samples (e.g., blood) is attracting great interest since nitrite can function as a marker of nitric oxide (NO) production in vivo.[4, 5] NO is known to be an important molecule with many metabolic functions, including the regulation of vascular tone, inhibition of platelet aggregation, serving as a neurotransmitter, exhibiting cytotoxic effects, inhibiting thrombosis, and exhibiting anti-inflammatory properties.[6-8] Therefore, the measurement of nitrite may be useful as a reliable indicator of NO production by the enzyme nitric oxide synthase (NOS) in the human body.

Optically, nitrite is detected using a complex Griess assay method.[9, 10] Electrochemically, benzylbis(triphenylphosphine) palladium(II)[11] and uranyl salophen[12] have been reported as nitrite selective ionophores in membrane electrodes. Co(III) complexes such as Co(III)-cyanocobyrinate,[13-15] Co(III)-phthalocyanine,[16] Co(III)-tetraphenylporphyrin derivatives,[17] and recently reported Rh(III) complexes[18] have also been suggested as nitrite ionophores for preparing polymeric membrane

based ion selective electrodes (ISEs). When determining nitrite in a real sample, the greatest interference come from lipophilic anions such as thiocyanate, salicylate and perchlorate.[19] The selectivity of anion-responsive liquid-membranes (either potentiometric or optical) could be enhanced by various methods,[20] including using appropriate membranes that can prevent ionic interferences from reaching the sensing membrane. In this case, nitrite can be converted to NO_x (g) via acidification of the sample, and then allowing this gas to pass through a gas permeable membrane to reach the inner nitrite sensor. Therefore, our primary concern in this chapter is to design nitrite sensors with relatively low detection limits rather than to achieve absolute selectivity. In this attempt, acetato-cobalt(III)-tetraphenylporphyrin (Co(III)TPP), a reported neutral carrier ionophore,[21] was chosen as the nitrite selective reagent due to its simplicity of preparation and relatively good performance toward nitrite detection.

Coated wire electrodes (CWEs) have been reported to have lower detection limits and better selectivity than the conventional type of ISEs with internal solutions.[22, 23] Besides, CWEs are inexpensive, mechanically flexible, and very simple to construct. More importantly, CWEs can easily be miniaturized for possible future clinical measurements or in vivo sensing. However, the main disadvantage of CWEs is the unstable potential that develops at the interface of the ion selective sensing membrane and the conducting substrate, which seriously affects the lifetime of the electrodes.[24] In collaboration with Dr. Malinowska's group at Warsaw University of Technology, various lipophilic intermediate layers have been tested to prevent the water layer

formation between the ion sensing membrane and the graphite conducting substrate.[25] Another factor that accounts for the short lifetime of those Co(III) porphyrin based nitrite selective electrodes is the crystallization process of Co(III) porphyrin in the polymeric membranes. Small crystals in the membrane can be observed even if the membrane is stored in the ambient environment without contacting nitrite solutions. Inspired by the prolonged life time of electrodes through covalent attachment of an ionophore onto a polymer backbone in Chapter 2, herein Co(III) porphyrins are similarly attached to a polymethacrylate structure, and the performance of electrodes employing this macromolecular nitrite ionophore is also assessed.

An optical sensing system employing the principle of anion/proton co-extraction chemistry[26] (see Reaction 3.1) is also examined here to develop an optical nitrite sensor, using thin olymer films containing an Co(III) porphyrin ionophore and a proton chromoionophore, in accordance with the following reaction:

$$L + C + H^+(a) + X^-(a) \leftrightarrow [LX]^-[CH]^+ \qquad \text{(Reaction 3.1)}$$

where X^- is the analyte anion (e.g., nitrite), C is the proton chromoionophore (e.g., chromoionophore I in the deprotonated form), and L is a neutral carrier ionophore (e.g., Co(III) porphyrin). The chromoionophore transfers the binding of nitrite with the ionophore into an optical signal. The optimized optical sensor employing Co(III)TPP and chromoionophore I exhibited reasonably good selectivity toward nitrite with a detection limit of approximately 1 μM. The response is fast and reversible. These results are promising for future use of the sensor in measuring nitrite levels in physiological samples by using a gas permeable membrane and

acidification of the sample to further enhance selectivity.

3.2. Experimental Section

3.2.1. Materials

4-Hydroxybenzaldehyde, benzaldehyde, pyrrole, propionic acid, methacryloyl chloride, triethylamine and cobalt(II) acetate tetrahydrate were all purchased from Aldrich (Milwaukee, WI). The monomer *n*-decyl methacrylate (DMA), 99%, was obtained from Polysciences, Inc. (Warrington, PA). The monomers methyl methacrylate (MMA), 99.5% and the polymerization initiator 2,2'-azobisisobutyronitrile, 98% (AIBN), were obtained from Aldrich. Inhibitors were removed from the monomers by prior distillation. AIBN was re-crystallized from warm methanol prior to use. Tridodecylmethylammonium chloride (TDMA), o-nitrophenyl octyl ether (NPOE), high molecular weight poly(vinyl chloride)(PVC) and chromoionophore I, II, III and VII were purchased from Fluka (Milwaukee, WI). All salts were obtained from Aldrich, and aqueous solutions of them were prepared by dissolving the appropriate sodium salts in Millipore purified water (18 MΩ cm). All solvents, including chloroform, methylene chloride (CH_2Cl_2), methanol, tetrahydrofuran (THF), N,N-dimethylformamide (DMF) and the silica gel used for chromatography were obtained from Fisher Scientific (Pittsburgh, PA). The graphite rod, heat shrink tubing and mineral oil were purchased from Aldrich. The graphite

powder, Tygon tubing and copper wire were obtained from Fisher Scientific.

3.2.2. Synthesis of Co(III)TPP and Polymeric Material with Covalently Attached Co(III) Porphyrin

The Co(III)TPP was prepared according to previous procudures.[27, 28] 5-4(Hydroxyphenyl)-10-15-20-triphenylporphyrin (HOTPP) was prepared as reported elsewhere.[29, 30] The crude product was purified by flash chromatography on silica using CH_2Cl_2 as the solvent. Final products were characterized by mass spectrometry, yielding the desired molecular weight peak at m/z = 631.6. The 5-(4-methacryloyloxyphenyl)-10,15,20-triphenylporphyrin (MOTPP) was prepared by the procedure reported by Qin and coworkers.[31] The crude product was purified by flash chromatography on silica using CH_2Cl_2 as the solvent. Final products showed desired molecular weight peak at m/z = 699.1. The methacrylate copolymer was synthesized via a thermally initiated free radical solution polymerization, similar to the procedure described in Chapter 2, using DMA, MMA and the synthesized MOTPP. The resulting polymer was dissolved in DMF and refluxed with Co(II) acetate for 10 min.[27, 28] After this time, DMF was evaporated, and the polymer was re-dissolved in 2 mL of THF and precipitated in methanol. The precipitate was collected and washed thoroughly with methanol to ensure the complete removal of any free porphyrin. The polymer was then dried under vacuum. UV/visible spectroscopy was employed to determine the amount of Co(III) porphyrin complex in the copolymer. Based on using pure Co(III)TPP as a standard, the concentration of the grafted cobalt porphyrin

on the polymer backbone was estimated to be 40.0 mmol/kg.

3.2.3. Fabrication of Coated Wire Type Electrode and EMF Measurements

Graphite rod electrodes (see Figure 3.1) were prepared by using a heat shrink tubing as an insulator, leaving 5 mm at one end for the ion selective membrane coating. The graphite rods were sonicated in acetone, then in water, and dried in air before use. Graphite paste electrodes were prepared in Tygon tubing (ca. 1 in. long, 1/16 i.d., 1/8 o.d.), cut to 5 cm in length. A copper wire, 1.3 mm diameter, was inserted into these tubes, forming a 5 mm deep cavity at one end, while the other end of copper wire was soldered to a flexible wire with a connection plug. The carbon paste was then placed into the created cavity polished to form a flat electrode surface. Graphite paste was prepared by grinding the mixture of 75 wt% graphite powder and 25 wt% mineral oil in a mortar.

The ISE membranes used for potentiometric measurements consisted of 1 wt% Co(III)TPP or copolymer calculated to contain the same amount of Co(III)TPP, various quantities of cationic additive salt (TDMA), 66 wt% NPOE, and 33 wt% PVC. All components (total mass 200 mg) were dissolved in 1.5 mL of freshly distilled THF. Graphite rod and graphite paste electrodes were prepared by dipping the electrodes into the cocktail solution for different times, leaving 10 min between each dipping to allow for solvent evaporation. The electrodes were allowed to stabilize overnight. After dipping 10 times, the thickness of the resulting membrane was 150 μm as measured by scanning electron microscope (SEM). The sample buffer

employed in this study was 0.05 M 4-morpholinoethanesulfonic acid (MES), adjusted to pH 4.8 with sodium hydroxide. All analyte solutions were prepared from sodium salts of various anions dissolved in MES buffer. A solution of 0.01 M $NaNO_2$ was employed as the conditioning solution for the CWEs prior to nitrite calibration measurements. Between measurements on the life time of the electrodes, electrodes were stored in 0.01 M $NaNO_2$. Data presented in the figures were normalized in order to make the starting EMF values of all electrodes equal to zero. Selectivity coefficients were calculated by the separate solution method[32] using EMF values measured in 0.1 M salt solutions and theoretical slope values.

In the study of the aqueous layer formation, sensors coated with plasticized PVC membranes were initially conditioned in 0.01 M $NaNO_2$ solution overnight. Then, the solution was changed between 0.1 M NaCl (interfering anion solution) and 0.1 M $NaNO_2$ solutions with time intervals sufficient to observe the EMF stability or to see a definite tendency of the EMF instability and the general trend of its behavior. The observed dynamic EMF response was analyzed in terms of potential drifts upon replacing the primary ions by interfering ions that indicate the presence of an aqueous film between the sensing membrane and the solid-contact.[33]

3.2.4. Optical Measurements

The optical sensing films contained 72 mmol/kg Co(III)TPP, 100 mol% chromoionophores, plasticizer NPOE, and PVC (2:1 mass ratio). All the components (total mass 100 mg) were dissolved in distilled THF to give a 1 mL

cocktail. The films were then made by a spin-coating device (model SCS-G3-8 obtained from Cookson Electronics; Providence, RI) on a square-shaped quartz plate of 35 mm in length. The rotation speed was 1000 rpm, and 100 μL of the polymer film cocktail was injected onto the rotating glass plate with a spin time of 20 seconds. The films were dried in air for at least 1 h before using and were prepared freshly each time. The flow cell setup and the experimental procedure were the same as described in Chapter 2 using 0.05 M MES buffer, pH = 4.5. The spectra of the films were recorded in the range between 360 nm to 800 nm when equilibria were reached. To correct for the background absorbance, the absorbance measured at 800 nm were subtracted from the absorbance values at the wavelengths of interest.

3.3. Results and Discussion

3.3.1. Potentiometric Response Characteristics of an Optimized Coated Wire Electrode System Using Co(III) Porphyrin as Ionophore

It has been reported previously that incorporating lipophilic anionic or cationic sites in the polymeric membrane electrodes based on metalloporphyrins can improve the selectivity of the ISEs by controlling the ratio of free ionophore to complexed ionophore in the membrane phase.[34] In an attempt to optimize the selectivity of coated wire type electrodes, different amounts of TDMA were added into the membranes. A CWE with three layers of coating was initially examined. As seen in Figure 3.2, 25 mol% of TDMA to the incorporated Co(III)TPP exhibits the best selectivity and a

Nernstian response toward nitrite.

The thickness of the membrane may also affect the performance of the CWEs. Therefore, CWEs with three coating layers and ten coating layers were compared. Although both of them show Nernstian responses, as shown in Table 3.1, the selectivity coefficients of thinner membranes are statistically different from those of thicker membranes. This might be due to thin water layers more easily formed between the sensing membranes and electrode substrates when the sensors were prepared with the thinner membranes. Although the electrodes were placed in buffer for 1 h between the measurements of primary and interference anions, the transmembrane ion fluxes from inner solution to outer and vice versa[33] may still significantly change the composition of the water layer giving inaccurate selectivity coefficients. CWEs with more lipophilic inner conductive electrode substrates to eliminate the water layer formation will be discussed later. Sensitivity of the ISEs is slightly improved by using CWEs compared to using the conventional type ISEs with inner filling solutions since the leaching of the internal solutions is prevented. CWEs with three coating layers and ten coating layers have detection limit of 2.3 x 10^{-6} M and 5.3 x 10^{-6} M, respectively, compared to that of the conventional type ISE's of 5.5 x 10^{-6} M (see Figure 3.3). However, one major disadvantage of this CWE type nitrite sensor is the short lifetime in terms of the slope for the nitrite calibration curve. CWEs with three layer coatings lost 33% of this slope value in seven days, and CWEs with ten layers coating lost 16% of the Nernstian slope in two weeks. Efforts to prolong the operational life time of CWEs are discussed below.

3.3.2. Water Layer Formation on Coated Wire Electrodes

It has been reported previously that there is an aqueous layer between the membrane and electrode solid support which behaves as a pseudo electrolyte with an extremely small volume and uncontrollable composition. Therefore, this aqueous layer may greatly influence the response parameters of a solid-contact ISE electrode, hindering the examination of unbiased membrane performance.[33] By using materials which can potentially provide an unfavorable environment for the aqueous layer formation, the drift of the CWEs can be decreased. A procedure described by Fibbioli et al.[33] was employed by varying the sample solution between primary and interference anions and observing the degree of drift of the sensor for such changes caused by the transmembrane ion fluxes. As shown in Figure 3.4, among the explored electrodes, the effect of the water layer on the EMF drift was strongest in the case of a graphite rod electrode. However, no aqueous layer was observed (little drift after changing solution composition) for electrodes prepared with graphite paste using mineral oil, which can be attributed to higher lipophilicity of this conducting support. The general form of the time response curse was quite reproducible for each type of the electrodes, but the time for EMF stabilization and the value of drift varied even during one experiment, which shows unpredictability and instability of the water layer composition.

The selectivity coefficients of CWEs employing graphite paste as the electrode substrate with different membrane thicknesses were compared. As it can be seen in Table 3.2, the difference in selectivity coefficients for CWEs with different

membranes thicknesses is reduced by using mineral oil graphite paste as the electrode substrate to prevent the aqueous layer formation. However, in this case the calibration curve toward nitrite is super-Nernstian (-86 mV/decade) due to some unknown active ingredients in the mineral oil; therefore, the selectivity coefficients should be treated as approximate values.

3.3.3. Characterization and Potentiometric Response Characteristics of Polymethacrylate with Covalently Linked Co(III)TPP

Another factor that contributes to the short life time (in terms of the decrease in the slope value of the nitrite calibration curve) of these Co(III)TPP based CWEs is the crystallization of the ionophore. Crystals of the ionophore can be observed after ten days even for the membrane stored in the ambient laboratory environment. Based on the previous study showing that the covalent attachment of Al(III) porphyrins can improve electrode lifetime, the Co(III) porphyrin was attached to a similar polymethacrylate copolymer. Conventional type ISEs with internal solutions employing covalently attached Co(III) porphyrin and free Co(III)TPP were examined. Although the electrodes using covalently attached Co(III) showed detection limits one magnitude higher then electrodes using unattached Co(III)TPP, the operational life time was increased dramatically from 4-7 days to over one month (see Table 3.3).

3.3.5. Optical Response Characteristics of Membranes Formulated with Co(III) Porphyrin Together with ETH5294

As mentioned previously, optical sensors can take advantage of the principles of

anion/proton co-extraction chemistry to achieve an optical response. The lipophilic pH chromoionophore translates the binding of the nitrite ion to the Co(III) porphyrin into an optical signal, allowing optical measurement at a higher wavelength range. Co(III) porphyrins are neutral carrier ionophores, therefore, a neutral carrier mechanism chromoionophore is needed when designing the optical sensor (see Figure 1.4). When nitrite binds with the chromoionophore, the deprotonated form (C) decreases in absorbance and the protonated form (CH^+) increases in absorbance. For this purpose, four different neutral carrier type chromoionophores (chromoionophore I, II, III, VII) with different pKa values were tested (see Figure 3.5). Among them, chromoionophore I showed the maximum absorbance change at the same nitrite concentration and therefore was chosen as the chromoionophore to be doped within the polymeric membrane. The absorbance maximum of the deprotonated form of chromoionophore I is at $\lambda =$ 547 nm. The optimal pH of the flow cell system was also tested. As shown in Reaction 3.1, a lower pH can facilitate the extraction of nitrite into the polymer membrane. However, very low pH solutions (i.e., pH = 3.0) are not appropriate since the pKa of nitrous acid (HNO_2) is 3.29, and HNO_2 can easily decompose and release NO_x gas. A solution with pH = 4.5 yields the most sensitive nitrite response with ca. 6% of the nitrite present in solution in the protonated form (HNO_2).

Figure 3.6 shows absorption spectra change with increasing nitrite concentration. It can be observed that as the nitrite concentration was increased, the Soret band of the Co(III)TPP shifted to a higher wavelength which is due to the ligand change from

single nitrite to two nitrites. At the same time, the deprotonated form of the chromoionophore decreased when more nitrite was extracted into the membrane, and the protonated form of the chromoionophore increased (expected based on Reaction 3.1). As shown in Figure 3.7, the nitrite response can be observed at a nitrite concentration as low as 1 μM. The main anion interferences for this new nitrite optical sensor are perchlorate, salicylate and thiocyanate. Chloride, the most common ion in physiological samples, causes very little absorbance change. Meanwhile, the optical nitrite sensor exhibits a fully reversible response to different concentrations of nitrite with response times typically < 1 min (see Figure 3.8).

3.4. Summary

In this chapter, a nitrite selective sensor with a low detection limit was developed. Co(III) porphyrin has been chosen as the ionophore. Coated wire type electrodes were employed in an attempt to achieve lower detection limits than the conventional type ISEs with inner filling solutions. It has been suggested that the membrane thickness of the CWEs can affect the performance of the electrodes in terms of the selectivity coefficients due to the thin aqueous layer formed between the nitrite sensing membrane and the electrode substrate. More lipophilic electrode substrates have been employed to eliminate this aqueous layer formation. With these lipophilic electrode materials (graphite paste made with mineral oil), the difference in the selectivity coefficients of electrodes possessing different membrane thicknesses is reduced although the electrodes no longer exhibit Nernstian responses. The

super-Nernstian behavior can be attributed to the unknown impurities from the mineral oil since adding little amounts of mineral oil into the membrane of a conventional type ISE with an internal solution also results in a slope value of ~ 80 mV/decade.

A methacrylate copolymer with covalently attached Co(III) porphyrin has been synthesized and characterized. Electrodes formulated with membrane containing the polymethacrylate material have dramatically longer operational lifetime than those containing the unattached Co(III)TPP. An optical sensor employing Co(III)TPP and chromoionophore I exhibited reasonably good selectivity toward nitrite with a detection limit of approximately 1 μM . The response is fast and reversible. Results are promising for future use of the sensor for measuring nitrite levels in physiological samples, by using a gas permeable membrane and acidification of the sample to further enhance selectivity.

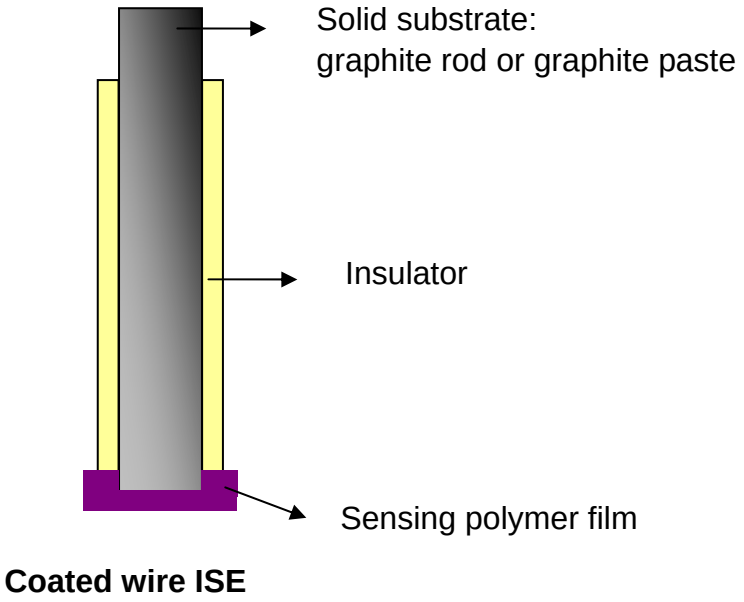

Figure 3.1. Schematic diagram of a coated wire type of electrode employing graphite rod or graphite paste as the solid substrate.

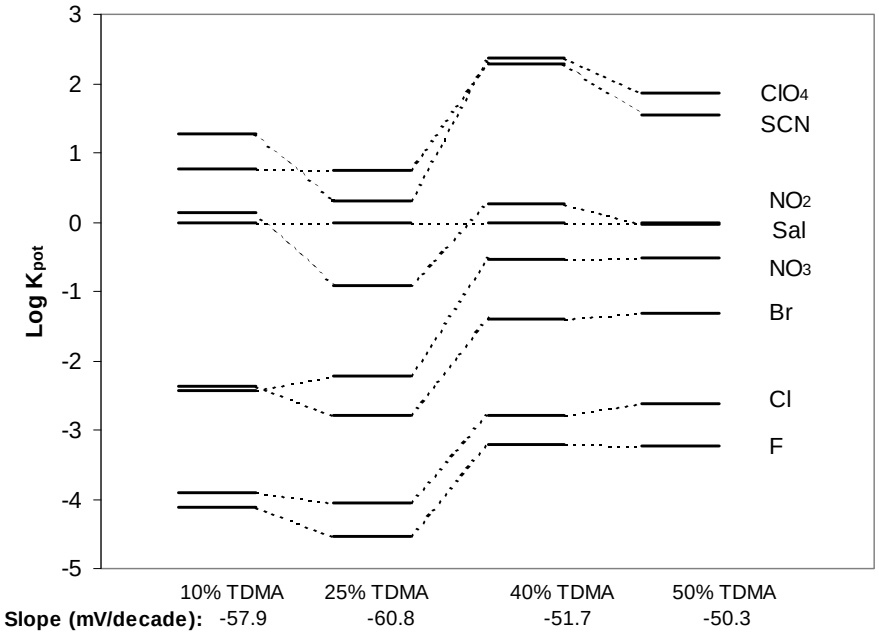

Figure 3.2. Logarithm of selectivity coefficients of NPOE/PVC (2:1) membranes doped with Co(III)TPP and different molar ratios of TDMA additive. The slope value of the nitrite calibration curve using each film composition is shown on the bottom.

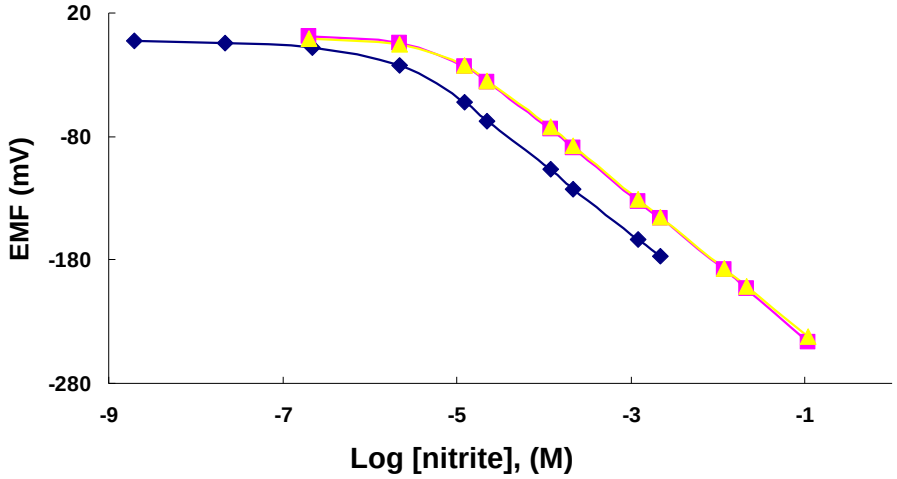

Figure 3.3. Nitrite calibration curves obtained by using CWEs with different membrane thickness, and by a conventional type of electrode. Membranes contain 33 wt% PVC, 66 wt% plasticizer, 1 wt% Co(III) TPP, and 25 mol% TDMA. (◆) CWE with three layer coatings; (■) CWE with ten layer coatings; (▲) conventional type ISE.

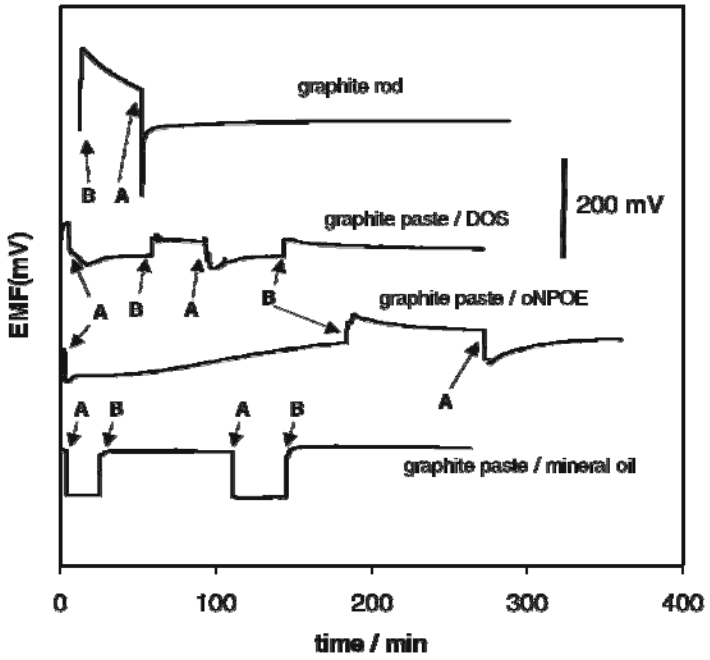

Figure 3.4. Test results to assess formation of an aqueous film between membrane and transducer. Membranes contain 33 wt% PVC, 66 wt% plasticizer, 1 wt% Co(III) TPP, and 10 mol% TDMA coated on different transducer types. Changes of sample: A: 0.1M $NaNO_2$;B: 0.1 M NaCl in MES buffer, pH 5.5.

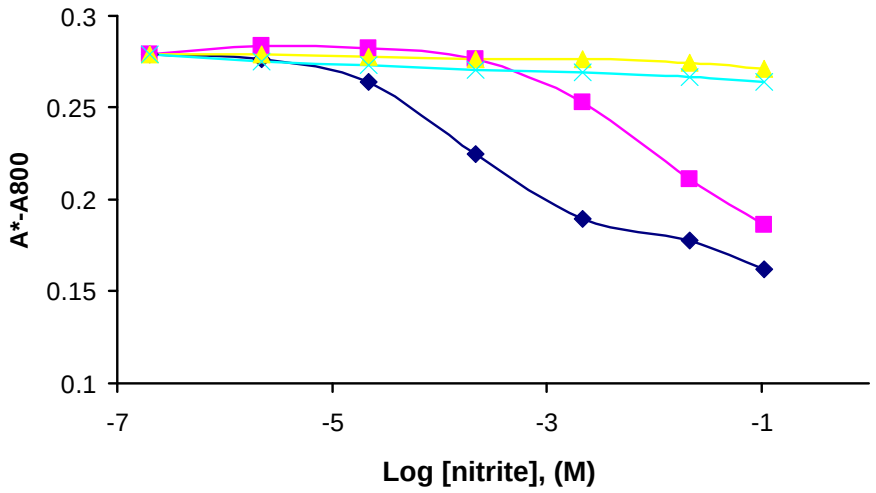

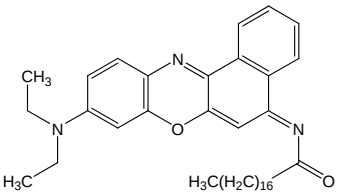

Chromoionophore I

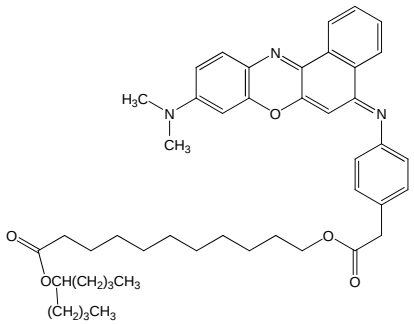

Chromoionophore II

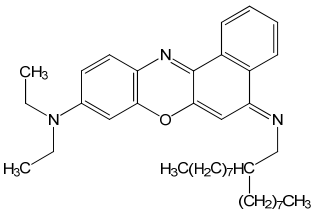

Chromoionophore III

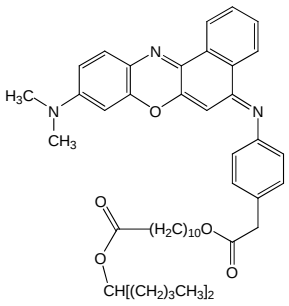

Chromoionophore VII

Figure 3.5. Absorbance change at wavelength corresponding to deprotonated band (background absorbance subtracted) of films containing Co(III)TPP and 100 mol% of different chromoionophores toward nitrite. λmax for I and III is A547; λmax for II and VII is A535. (◆) Chromoionophore I (■) Chromoionophore II; (▲) Chromoionophore III; (x) Chromoionophore VII.

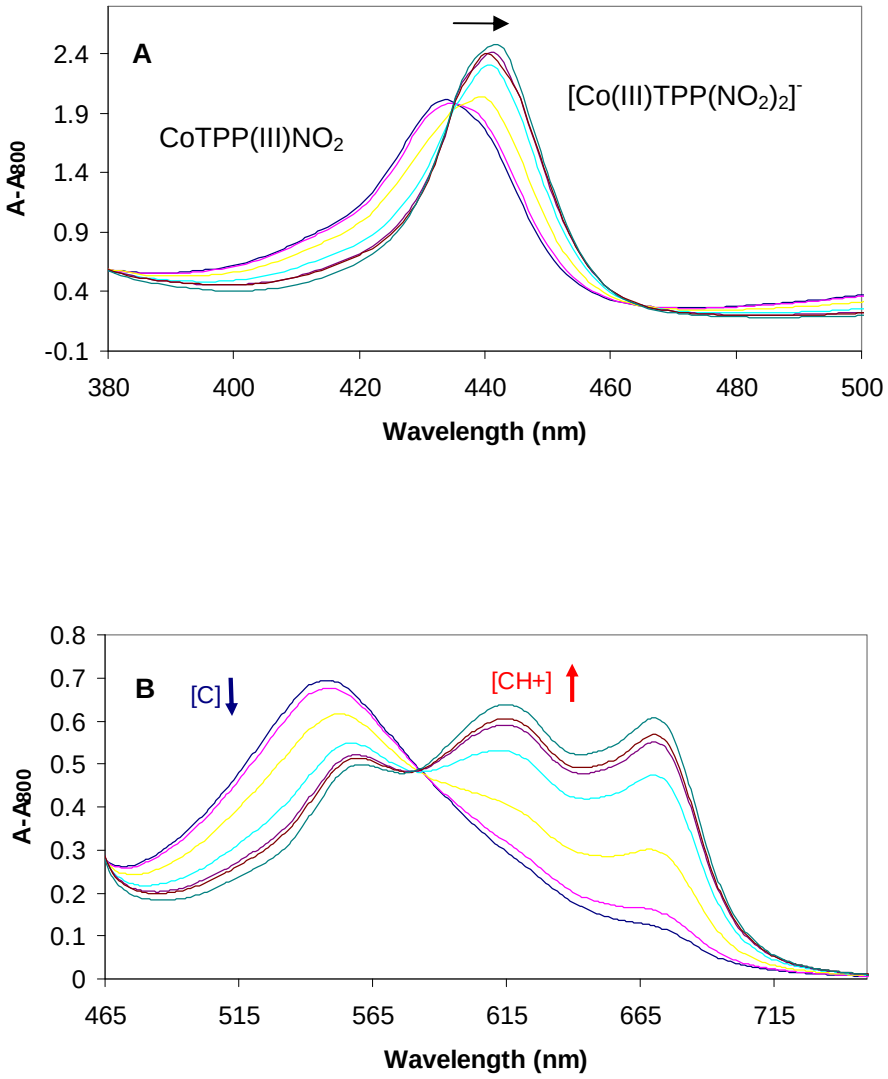

Figure 3.6. Absorption spectra measured in 50 mM MES buffer, pH 4.5, at varying nitrite concentrations (from 0.1μM to 0.1 M, increasing 10 fold each spectrum). (A) changes in Soret band; (B) changes in chromoionophore protonated/deprotonated bands.

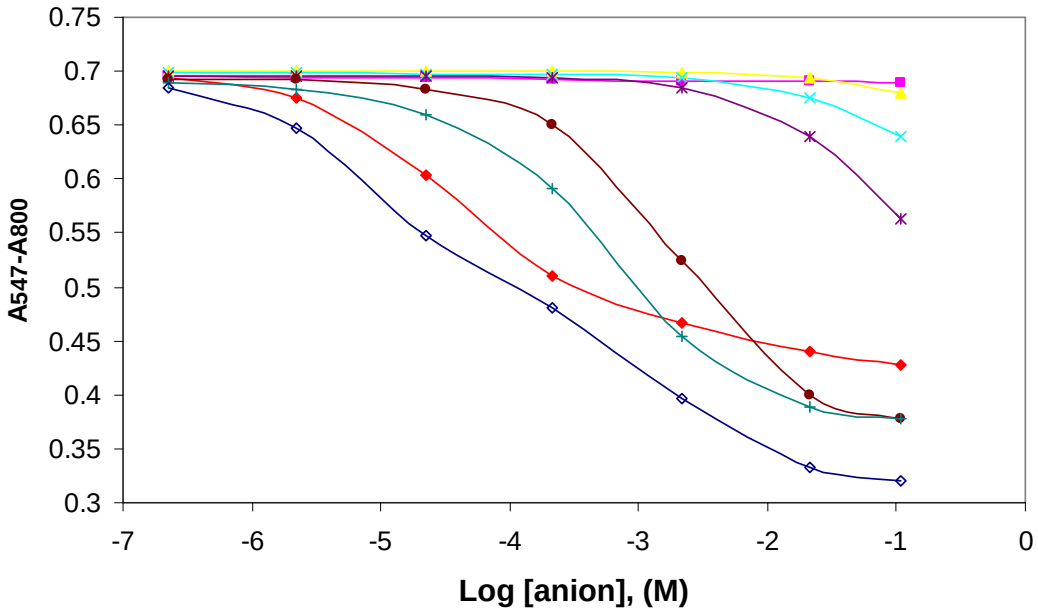

Figure 3.7. Optical response of PVC film containing Co(III)TPP and 100 mol% chromoionophore I toward different anions at pH 4.5 MES buffer. (◆) NO_2^- (■) F, (◇) SCN^-, (+) ClO_4^-, (×) Br^-, (*) NO_3^-, (▲) Cl^-, (●) Sal^-

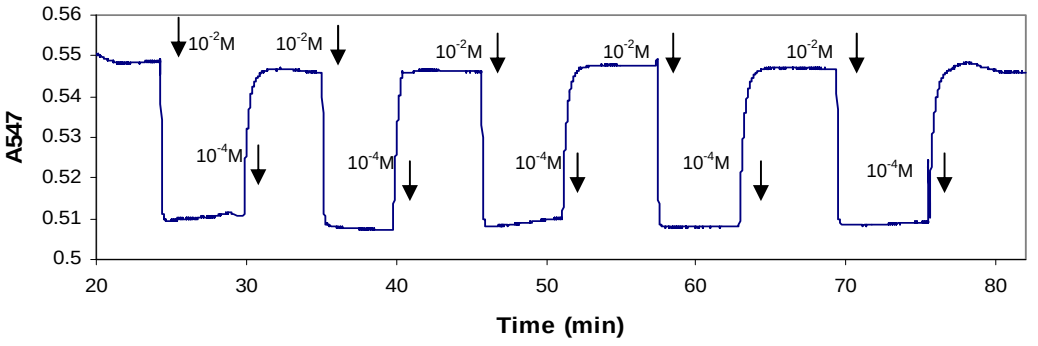

Figure 3.8. Optical response and recovery time trace measured when alternating flow solutions between 10^{-2} M and 10^{-4} M nitrite.

Table 3.1. Logarithm of selectivity coefficients of NPOE/PVC (2:1) membranes doped with Co(III)TPP and 25 mol% TDMA with different membrane thicknesses (n=3).

	Cl^-	NO_3^-	SCN^-	ClO_4^-	F^-	Br^-	Sal^-
3 layers	-4.1±0.3	-2.2±0.4	0.8±0.2	0.3±0.3	-4.5±0.1	-2.8±0.3	-0.9±0.2
10 layers	-3.8±0.1	-1.5±0.1	1.3±0.2	1.4±0.3	-3.7±0.1	-2.3±0.2	0.8±0.1

Table 3.2. Logarithm of selectivity coefficients of NPOE/PVC (2:1) membranes doped with Co(III)TPP and 25 mol% TDMA with different membrane thicknesses (n=3) using mineral oil graphite paste as the electrode substrate.

	Cl^-	NO_3^-	SCN^-	ClO_4^-	F^-	Br^-	Sal^-
3 layers	-3.7±0.2	-1.9±0.2	0.9±0.2	1.1±0.1	-4.1±0.2	-2.7±0.2	-0.4±0.2
10 layers	-4.1±0.1	-2.2±0.1	0.8±0.1	1.1±0.1	-4.8±0.2	-3.0±0.1	0.3±0.2

Table 3.3. Changes in slope value of nitrite calibration curve. Electrodes prepared with 33 wt% PVC, 66 wt% of NPOE, 1 wt% Co(III)TPP or the relative amount of methacrylate polymer with appended Co(III)TPP, and 25 mol% (relative to the ionophore) TDMA polymeric membranes. The internal solution is 0.01 M $NaNO_2$ and 0.01 M NaCl dissolved in 0.05 M MES buffer (pH = 4.8).

Co(III)TPP	Slope Value of Nitrite Calibration Curve (mV/decade)						
	Day1	Day4	Day7	Day11	Day14	Day21	Day 28
Free	-56.1	-51.4	-47.9	-33.6	-33.6	-33.8	
Covalently Attached	-55.8	-53.6	-54.1	-56.0	-55.6		-55.3

3.5. References

(1) Aydin, A.; Ercan, O.; Tascioglu, S. *Talanta* **2005**, *66*, 1181-1186.
(2) Cammack, R.; Joannou, C. L.; Cui, X. Y.; Martinez, C. T.; Maraj, S. R.; Hughes, M. N. *Biochim. Biophys. Acta-Bioenerg.* **1999**, *1411*, 475-488.
(3) Hord, N. G.; Tang, Y. P.; Bryan, N. S. *Am. J. Clin. Nutr.* **2009**, *90*, 1-10.
(4) Oh, B. K.; Meyerhoff, M. E. *Biomaterials* **2004**, *25*, 283-293.
(5) Milsom, A. B.; Hobbs, A. J.; Ahluwalia, A. *Nitric Oxide-Biol. Chem.* **2008**, *19*, S51-S52.
(6) Wallis, J. P. *Transfus. Med.* **2005**, *15*, 1-11.
(7) Guzik, T. J.; Korbut, R.; Adamek-Guzik, T. *J. Physiol. Pharmacol.* **2003**, *54*, 469-487.
(8) Cooke, J. P. *Atheroscler. Suppl* **2003**, *4*, 53-60.
(9) Norwitz, G.; Keliher, P. N. *Analyst* **1987**, *112*, 903-907.
(10) Misko, T. P.; Schilling, R. J.; Salvemini, D.; Moore, W. M.; Currie, M. G. *Anal. Biochem.* **1993**, *214*, 11-16.
(11) Badr, I. H. A.; Meyerhoff, M. E.; Hassan, S. S. M. *Anal. Chem.* **2002**, *67*, 2613-2618.
(12) Wroblewski, W.; Brzozka, Z.; Rudkevich, D. M.; Reinhoudt, D. N. *Sens. Actuator B-Chem.* **1996**, *37*, 151-155.
(13) Schulthess, P.; Ammann, D.; Simon, W.; Caderas, C.; Stepanek, R.; Krautler, B. *Helv. Chim. Acta* **1984**, *67*, 1026-1032.
(14) Schulthess, P.; Ammann, D.; Kraeutler, B.; Caderas, C.; Stepanek, R.; Simon, W. *Anal. Chem.* **2002**, *57*, 1397-1401.
(15) Stepanek, R.; Krautler, B.; Schulthess, P.; Lindemann, B.; Ammann, D.; Simon, W. *Anal. Chim. Acta* **1986**, *182*, 83-90.
(16) Li, J. Z.; Wu, X. C.; Yuan, R.; Lin, H. G.; Yu, R. Q. *Analyst* **1994**, *119*, 1363-1366.
(17) Shamsipur, M.; Javanbakht, M.; Hassaninejad, A. R.; Sharghi, H.; Ganjali, M. R.; Mousavi, M. F. *Electroanalysis* **2003**, *15*, 1251-1259.
(18) Pietrzak, M.; Meyerhoff, M. E. *Anal. Chem.* **2009**, *81*, 3637-3644.
(19) Caro, C. A.; Bedioui, F.; Zagal, J. H. *Electrochim. Acta* **2002**, *47*, 1489-1494.
(20) Martin, G. B.; Meyerhoff, M. E. *Anal. Chim. Acta* **1986**, *186*, 71-80.
(21) Malinowska, E.; Meyerhoff, M. E. *Anal. Chim. Acta* **1995**, *300*, 33-43.
(22) James, H.; Freiser, H.; Carmack, G. *Anal. Chem.* **1972**, *44*, 856-857.
(23) James, H. J.; Carmack, G. P.; Freiser, H. *Anal. Chem.* **1972**, *44*, 853-855.
(24) Buck, R. P.; Freiser, H. *Ion Selective Electrodes in Analytical Chemistry. vol. 1.*; Plenum: New York, 1978.
(25) Gorski, L.; Matusevich, A.; Pietrzak, M.; Wang, L.; Meyerhoff, M. E.; Malinowska, E. *J. Solid State Electrochem.* **2009**, *13*, 157-164.
(26) Badr, I. H. A. *Anal. Lett.* **2001**, *34*, 2019-2034.
(27) Adler, A. D.; Longo, F. R.; Kampas, F.; Kim, J. *J. Inorg. Nucl. Chem.* **1970**, *32*, 2443-2445.
(28) Sugimoto, H.; Ueda, N.; Mori, M. *Bull. Chem. Soc. Jpn.* **1981**, *54*, 3425-3432.

(29) Kamachi, M. A., H.; Nozakura, S. *J. Polym. Sci. Polym. Lett. Ed.* **1983**, *21*, 693.
(30) Coutant, D. E.; Clarke, S. A.; Francis, A. H.; Meyerhoff, M. E. *J. Chromatogr. A* **1998**, *824*, 147-157.
(31) Qin, Y.; Bakker, E. *Anal. Chem.* **2004**, *76*, 4379-4386.
(32) Gorski, L.; Malinowska, E. *Anal. Chim. Acta* **2005**, *540*, 159-165.
(33) Fibbioli, M.; Morf, W. E.; Badertscher, M.; de Rooij, N. F.; Pretsch, E. *Electroanalysis* **2000**, *12*, 1286-1292.
(34) Bakker, E.; Malinowska, E.; Schiller, R. D.; Meyerhoff, M. E. *Talanta* **1994**, *41*, 881-890.

CHAPTER 4

RAPID DETECTION AND QUANTIFICATION OF HIGH CHARGE DENSITY POLYANIONS CONTAMINANTS IN BIOMEDICAL HEPARIN PREPARATIONS USING POTENTIOMETRIC POLYANION SENSORS

4.1. Introduction

Heparin is a highly-sulfated glycosaminoglycan that is widely used as an injectable anticoagulant.[1-3] A variety of medical devices and diagnostic products may also contain or be coated with heparin. Recently, an acute, rapid onset of serious side effects indicative of an allergic type reaction (resulting in a large number of patient deaths) has been reported in connection with the use of certain lots of heparin. A specific contaminant, oversulfated chondroitin sulfate (OSCS), has been identified in given preparations that may have caused these adverse events.[4, 5] Due to the similarity in chemical structure and anticoagulant activity that OSCS possesses relative to heparin (see Figure 4.1), it is impossible for routine bioactivity assays[6] to detect the presence of the OSCS species. More advanced analytical methods including nuclear magnetic resonance (NMR)[5, 7] and capillary electrophoresis (CE)[8] have been suggested for the detection of the OSCS contaminant.

It has been demonstrated previously that large, reproducible EMF responses toward polyanionic species can be achieved if polymeric ISEs are formulated with lipophilic anion-exchangers, such as a tridodecylmethylammonium (TDMA) salt, in

plasticized poly(vinyl chloride) (PVC) membranes.[9-11] In the presence of relatively low concentrations of polyanions in the test solution, the surface of the polymer membrane becomes partially depleted of the small counter anion, and a gradient of the polyanion exists in aqueous layer adjacent to the polymer membrane and throughout the outermost layer of organic membrane (as an ion-pair with the TDMA species). Under such conditions, the phase boundary potential at the membrane/sample interface achieves a non-equilibrium pseudo steady-state value in proportion to the concentration of polyanion present in a background electrolyte solution.[11] This potentiometric response toward the polyion is super-Nernstian, and changes significantly over a relatively narrow range of low polyanion concentrations. However, if higher concentrations of polyanion are added to a background electrolyte solution, the outer surface of the polymeric membrane achieves a relatively rapid equilibrium phase boundary potential change toward the polyion, and this equilibrium potential change can be expressed by the following equation:[12] (see also, Chapter 1)

$$\Delta EMF = \frac{RT}{F}\ln\frac{a_{Cl}}{[R^-]([S_T]-[R^-])} - \frac{RT}{zF}\ln\left(\frac{za_{poly}}{[S_T]-[R^-]}\frac{k_{poly}}{(k_{Cl})^z}\beta\right)$$

(Eq. 4.1)

where ΔEMF represents the magnitude of the overall potential change after the polyanion is added, S_T denotes the total concentration of the lipophilic anion exchanger (TDMA) and $[R^-]$ is the added/endogenous anionic site concentration in the membrane; a_{Cl} and a_{poly} are the background chloride activity and polyanion (with charge z^-) activity in the sample solution, respectively; k_{Cl} and k_{poly} are the partition coefficient between membrane and aqueous phases of chloride and

polyanion, respectively; and β is the overall ion-pair formation constant in the membrane phase. Specifically, it has been shown previously[12] that the magnitude of the equilibrium EMF change in response to high polyanion concentrations is related to the charge density of the polyanion since a stronger cooperative ion-pair can be formed between the extracted polyanion with higher charge density and the TDMA exchanger species in the polymeric film (greater value for β in Eq. 4.1).[12] It should be noted that this equilibrium phase boundary potential change is essentially independent of polyion concentration, since when the outer surface of the ion-exchange membrane is at equilibrium, the classical Nernstian response to the polyion is observed, which given the very high charge for these species, yields very small EMF changes as function of polyion concentration (< 1 mV/decade for heparin).

Herein, we take advantage of the fundamental response principles of potentiometric polyanion sensors to demonstrate a simple and inexpensive method to detect of the presence OSCS contamination in heparin products as well as to quantitatively determine the weight percentage of the contaminant. Since OSCS has a greater charge density than heparin, a larger change in the equilibrium EMF response is observed when adequate levels of this contaminant is present compared to an untainted heparin preparation. At certain concentration range of OSCS, the measured potential first drops quickly to the EMF change typically observed for pure heparin (ca. -50 mV in background of phosphate buffered saline with 0.138 M chloride background), and then drifts down slowly toward the value observed for pure OSCS or the highly contaminated samples. We can take advantage of this kinetic response property to quantitatively determine the content of the contaminant if the

OSCS weight percentage in the total polyanion preparation is adjusted to be in a range (by dilution of the original heparin sample with pure heparin solution) which is low enough for the electrode not to achieve a rapid equilibrium phase boundary potential change at the membrane/sample interface. Under such conditions, the rate of EMF change of the membrane toward the equilibrium EMF response for the higher charge density OSCS species is proportional to the OSCS concentration. In this chapter, dextran sulfate (DS), another polysaccharide with higher charge density than porcine heparin (see Figure 4.1) was also used as a model contaminant species to test the broad applicability of the proposed method to detect a variety of high charge density polyanions in commercial porcine heparin preparations.

4.2. Experimental Section

4.2.1 Materials

Tridodedylmethylammonium chloride (TDMAC) was obtained from Aldrich (St. Louis, MO). Poly(vinyl chloride) (PVC), dioctylsebacate (DOS) and the cation-exchange resin Amberlite 200 were obtained from Fluka (St. Louis, MO). Distilled tetrahydrofuran (THF) and N,N-dimethylformamide (DMF) were purchased from Fisher Scientific (Pittsburgh, PA). DS, pure porcine heparin (171 units/mg), sodium salt of chondroitin sulfate (CS) and sulfur trioxide pyridine complex were obtained from Aldrich (St. Louis, MO). Phosphate-buffered saline (PBS, 138 mM sodium chloride, 2.7 mM potassium chloride, 10 mM sodium phosphate, pH 7.4), as well as all other solutions used in this work, were prepared in the laboratory from

Milli-Q grade deionized water (18.2 MΩ, Millipore Corp., Billerica, MA). Dialysis membranes (Spectra/Por 7, MWCO = 3.5 kD) were purchased from Spectrum Laboratories Inc. (Rancho Dominuez, CA). A commercial miniaturized Ag/AgCl electrode (BASi, West Lafayette, IN) was used as the reference electrode in the potentiometric measurements. The deuterium oxide used for NMR spectroscopy was obtained from Cambridge Isotope Laboratories, Inc. (Andover, MA).

4.2.2. Synthesis and Characterization of OSCS

OSCS was synthesized according to a previously reported procedure starting from the sodium salt of CS and sulfur troixde.[7] Chondroitin sulfate (108 mg) was converted into its tributylamine salt by passing through the strong cation-exchange column (Amberlite 200). The tributylamine salt was then dissolved in DMF (1 mL). An excess amount of sulfur trioxide pyridine complex was added. After 5 h of heating at 40 °C, the reaction was quenched by adding 2 mL of water. The fully sulfated OSCS was precipitated at 4 °C by addition of 35 mL of a cold ethanol solution saturated with sodium acetate. The product was collected by centrifugation and was re-dissolved in water, dialyzed, and lyophilized. Synthesis of partially sulfated OSCS is similar to the above procedure except the reaction with sulfur trioxide pyridine complex was carried out under 0 °C.

Sulfur contents of CS, porcine heparin and OSCS with different degree of sulfation were analyzed by elemental analyses performed by Atlantic Microlab (Norcross, GA). FTIR spectra were collected on a Perkin Elmer BX FT-IR system.

The bioactivity of fully and partially sulfated OSCS was analyzed by a

chromogenic assay as described by Teien et al.[13, 14] Anti-thrombin III (ATIII) (Haematologic Technologies Inc, Essex Junction,VT), factor Xa (FXa) (Haematologic Technologies Inc) and FXa-specific chromogenic substrate (S-2222) (Diapharma, West Chester, OH) were reconstituted from lyophilized powder with DI water. 132 μL heparin standards (171 units/mg) were incubated with 52.8 μL of 10 mM PBS buffer, 66 μL of bovine albumin fraction V solution (BSA Fraction V, Invitrogen, Grand Island, NY) and 66 μL ATIII in wells of a clear polystyrene 96-well flat bottom microplate (Fisher Scientific) at 37 °C for 2 min. After this initial period, the samples were further incubated with 13.2 μL of FXa (10 μg/mL) at 37 °C for 1 min. The 330 μL solution was divided evenly into three wells and each well was incubated with 70 μL PBS and 10 μL of 2 mg/mL S-2222 at 37 °C for 3 min. The reaction was terminated by the addition of 20 μL of acetic acid. Absorbance values at 405 nm were measured immediately using a Labsystems Multiskan RC 96-well microplate reader.

4.2.3. Fabrication of Polyanion Sensors and Potentiometric Measurements

The polyanion sensitive membrane employed in this work was formulated with 1.5 wt% tridodedylmethylammonium chloride (TDMAC), 66 wt% poly(vinyl chloride) (PVC) and 32.5 wt% dioctylsebacate (DOS) as reported previously.[10] Membrane components were dissolved in distilled THF at 100 mg per mL. To construct single-use disposable electrochemical sensors, sealed end glass capillary tubes (o.d. 0.8 – 1.1 mm) were inserted into short pieces of Tygon tubing (ca. 1 in. long, 1/16 in i.d., 1/8 in o.d.) with the sealed end protruding 3 - 4 mm beyond the end of the Tygon

tubing. The protruding capillary end was dip-coated with the membrane cocktail 12 times, leaving 15 min between each dip-coating to allow for adequate solvent evaporation. The membranes were allowed to dry overnight. The sensors were soaked in 10 mM PBS buffer for approximately 1 h before the glass capillaries were carefully removed. The Tygon tubing with the sensing membrane at the tip was then filled with the same PBS buffer, and a Ag/AgCl wire covered with heat shrink tubing on the top was inserted.

Ten mg/mL and 50 mg/mL DS solutions were used as initial test samples, and then further diluted with 10 mg/mL and 50 mg/mL solution of pure porcine heparin to obtain samples that have different DS contaminant content. An aliquot (400 μL) of these solutions was added to 3600 μL of PBS, (with the polyanion sensor and reference electrode in place within this well-stirred PBS solution) to yield a final polyanion concentration of 1 mg/mL and 5 mg/mL, respectively. ΔEMFs were obtained by subtracting the starting background cell potential in PBS alone from the potential value recorded 10 min after the injection of polyanion solutions. A 10 mg/mL solution (in PBS) containing the newly synthesized OSCS was mixed with pure porcine heparin to yield different levels of OSCS contaminated heparin samples and then tested with the polyanion sensors as above for DS contamination in heparin (except for 0.5 wt% OSCS in heparin at a final polyanion concentration of 1 mg/mL, the EMF change after 15 min was recorded). In addition, a 10 mg/mL reference sample of contaminated heparin known to have > 10 wt% OSCS was obtained from U.S. Pharmacopeia (USP) (Rockville, MD) and examined by the proposed method. It should be noted that the lower limit of detection for the proposed method is based on the ability to discriminate (based on EMF change) a given wt% of polyanion

contaminant in the presence of a large excess of heparin. To quantitatively determine the OSCS weight percentage in polyanion preparations, 10 mg/mL solution (in PBS) with OSCS wt% smaller than 1% was tested with the polyanion sensors as described above. The values of EMF change were integrated for 5 min after the injection of polyanion preparations. Integrations were performed by Origin Lab 7.5 (Northampton, MA)

4.2.4. NMR Spectroscopy

For quantification of OSCS, 30 mg/mL OSCS and heparin solutions in D_2O were constantly shaken for 1 h prior to the NMR measurements. Then the two solutions were mixed to give different wt% of OSCS. ^1H NMR spectra were recorded on a Varian 400 MHz spectrometer. For all the polyanion samples, 32 scans were collected over a spectral width of 6400 Hz. The acquisition time was 2.56 s, followed by a relaxation delay of 1 s. All the spectra were recorded at 315 K using a flip angle of 30° and the chemical shifts were reported to the solvent peak at 4.58 ppm (calculated by the equation $\delta = 7.83 - T/96.9$, where T is the absolute temperature in Kelvin[15]). The data were processed by MestReNova 5.3.2 (Mestrelab Research, Spain). Baseline corrections were mostly done automatically, and phasing was always performed manually.

4.3. Results and Discussion

4.3.1. Characterization of OSCS

The sulfur content of porcine heparin, CS and OSCS synthesized under different

conditions are shown in Table 4.1. It was found that the sulfur content increases once the sulfation reaction was carried out under a higher temperature and for a longer reaction time. We could also observe that the sulfur content of fully sulfated OSCS is very close to that of porcine heparin which suggests that the two compounds are hard to discriminate between.

Infrared (IR) spectra of CS and fully sulfated OSCS (see Figure 4.2) clearly indicate the conversion of hydroxyl groups to sulfate groups. The intensity at 1240 cm^{-1}, which is attributed to the stretching of S = O, is dramatically increased in the spectrum of fully sulfated OSCS. The intensity of the bands at 2900 and 1380 cm^{-1}, which are attributed to the stretching and/or deformation vibration of C-O-H bonds, are deceased after the sulfation reaction.

The anti-coagulant activity of the synthesized fully and partially sulfated OSCS was also evaluated by a factor Xa assay. Binding to heparin induces conformational change in the anti-thrombin that will facilitate its reaction with factor Xa. Factor Xa itself reacts with substrate and releases the chromophore; however, when factor Xa is bound with heparin and ATIII, this reaction is inhibited. Thus, the residual FXa activity, measured with the FXa-specific chromogenic substrate, is inversely proportional to the heparin concentration. It was determined that the synthesized fully sulfated OSCS has an activity of 36.6 unit/mg, and the partially sulfated OSCS has a much lower heparin activity of only 5.1 unit/mg. These values are similar to the values reported by others who have successfully synthesized fully OSCS from CS by using above sulfation method.[7]

4.3.2. Potentiometric Measurements on DS in Polyanion Preparations

As shown in Table 4.2, a large difference in the equilibrium EMF responses toward porcine heparin and DS is observed when the polyanion preparations with varying wt% were added to PBS. Based on results obtained from DS measurements (Table 4.2), a lower percentage of DS contaminant in the total polyanion preparation can be detected for 5 mg/mL final polyanion concentration than for the 1 mg/mL final polyanion concentration (Table 4.3). This implies that if a more concentrated contaminated heparin is used as the initial test sample, a lower weight percentage of the contaminant polyanion may be detected (i.e., an improved detection limit for contaminant wt% in the heparin).

4.3.3. Potentiometric Measurements on OSCS in Polyanion Preparations

As shown in Figure 4.3, large differences in the equilibrium EMF responses toward porcine heparin, DS, CS, OSCS, and USP contaminated heparin are observed when added to PBS, with each species at a final total concentration of 1 mg/mL. Pure OSCS or USP contaminated heparin yield EMF changes of ca. 25 mV more negative than pure porcine heparin, clearly suggesting that the polyanion sensors can be used as a screening tool to detect the presence of OSCS in biomedical heparin preparations.

Table 4.4 further summarizes the EMF responses toward polyanion mixtures with different ratios of OSCS to porcine heparin. The overall EMF response of the polyanion sensor is very rapid, usually within 30 s at relatively high OSCS contaminant content. For low OSCS content (< 1 wt%), the potential first drops quickly to the equilibrium EMF change typically observed for pure heparin, and then

drifts down slowly toward the value observed for the pure OSCS or the highly contaminated samples (see Figure 4.4). Indeed, when the contaminant polyanion level is lower, the amount of this species present is in a concentration range where the surface of the membrane does not achieve a full equilibrium EMF response quickly.

4.3.4. Quantitative Determination of OSCS Weight Percentage in Polyanion Preparations Using the New Electrochemical Method and NMR Method

Quantitative concentration data for the contaminant can be obtained when the total polyanion concentration in the final test solution is adjusted to be in a range where the contaminant concentration is low enough not to achieve a rapid equilibrium phase boundary potential change at the membrane/sample interface. Under these conditions the rate of EMF change of the polyanion sensor toward the equilibrium EMF response for the OSCS species is proportional to OSCS concentration.[16] The critical concentration of OSCS for the potential not to reach equilibrium rapidly has been found to be $\leq$ 1 wt%. As shown in Figure 4.5, when a series of standards containing synthesized OSCS mixed in different wt% with pure porcine heparin (with total polyanion concentration of 10 mg/mL), are injected (diluting the sample 1: 10 in the process) into a PBS electrolyte in which the polyanion sensor (and reference electrode) are placed, the EMF changes quickly to by ca. -50 mV (for pure heparin) and then drifts down slowly toward the -75 – 78 mV change observed for pure OSCS. If the values of ΔEMF are integrated for 5 min after the injection of polyanion sample preparations, the integrated signal, which is proportional to the rate of change over the 5 min interval, is linearly correlated with the weight percentage of OSCS in the polyanion standards (see Figure 4.6).

Table 4.5 summarizes the calculated value of OSCS wt% in several different

OSCS test sample solutions prepared with the synthesized OSCS and porcine heparin, after diluting these samples appropriately with pure heparin solutions to fall into the standard calibration range (see Figure 4.6). In addition, data is presented in this table for a commercial USP heparin preparation known to be contaminated with OSCS at a level ≥ 10 wt%. As shown in Table 4.5, the calculated OSCS wt% values found by the electrochemical method are very close to the OSCS wt% known for the three different OSCS synthetic sample solutions containing OSCS. The OSCS wt% in the USP contaminated heparin was found to be 21.3 % and 17.7 %, respectively, using different dilutions of the original sample, with the more diluted sample showing much larger standard deviation than the less diluted sample.

Previous studies have shown that NMR spectroscopy can be used to assess and quantify the OSCS impurities in heparin by means of the intensity of the N-acetyl proton resonance signal.[17, 18] Here, using the ratio of acetyl proton signal of OSCS at $\delta = 2.12$ ppm to that of heparin at $\delta = 2.02$ ppm (see Figure 4.7) enables the preparation of a calibration curve which can be used to determine the wt% OSCS in the given polyanion preparation (see Figure 4.8). As shown in Table 4.5, the results of OSCS wt% values determined by potentiometric polyanion sensors are in good agreement with the results obtained by NMR method for the same test samples. These results clearly indicate that the simple potentiometric polyanion sensor-based method described here can be applied to quantify OSCS or other high charge density polyanion contaminants in biomedical heparin preparations with reasonable accuracy.

4.4. Summary

A very simple methodology is introduced using disposable potentiometric

polyanion sensors to detect the presence of high charge density polyanion contaminants such as OSCS and DS in heparin preparations. The procedure could be used as an inexpensive screening method to assess raw materials or as a quality test control for finalized biomedical grade heparin products. The test samples can be used directly without complicated pretreatment, although pre-dialysis of the samples vs. PBS may be necessary in rare instances if there is chance that small lipophilic anions (e.g., perchlorate, thiocyanate) or organic anions (e.g., salicylate) could be present in the given sample preparation. The presence of such anions at high concentrations would also cause significant negative EMF response of the TDMA-based polymeric membrane owing to the favorable extraction thermodynamics of such anions into the organic membrane phase of the working electrode. However, in this work, and in all previous studies in which these same membrane electrodes have been examined for response to commercial heparin preparations, no such small anion interferences have been observed. A more quantitative test procedure for OSCS contaminant levels based on the dynamics of the observed EMF responses was also reported. The integrated area of ΔEMF values is linearly correlated with the weight percentage of OSCS in the polyanion preparations which enable the quantification of OSCS. The results obtained using the new potentiometric method are favorably comparable with those obtained using a more complicated NMR method based on the N-acetyl proton signal of heparin and OSCS species.

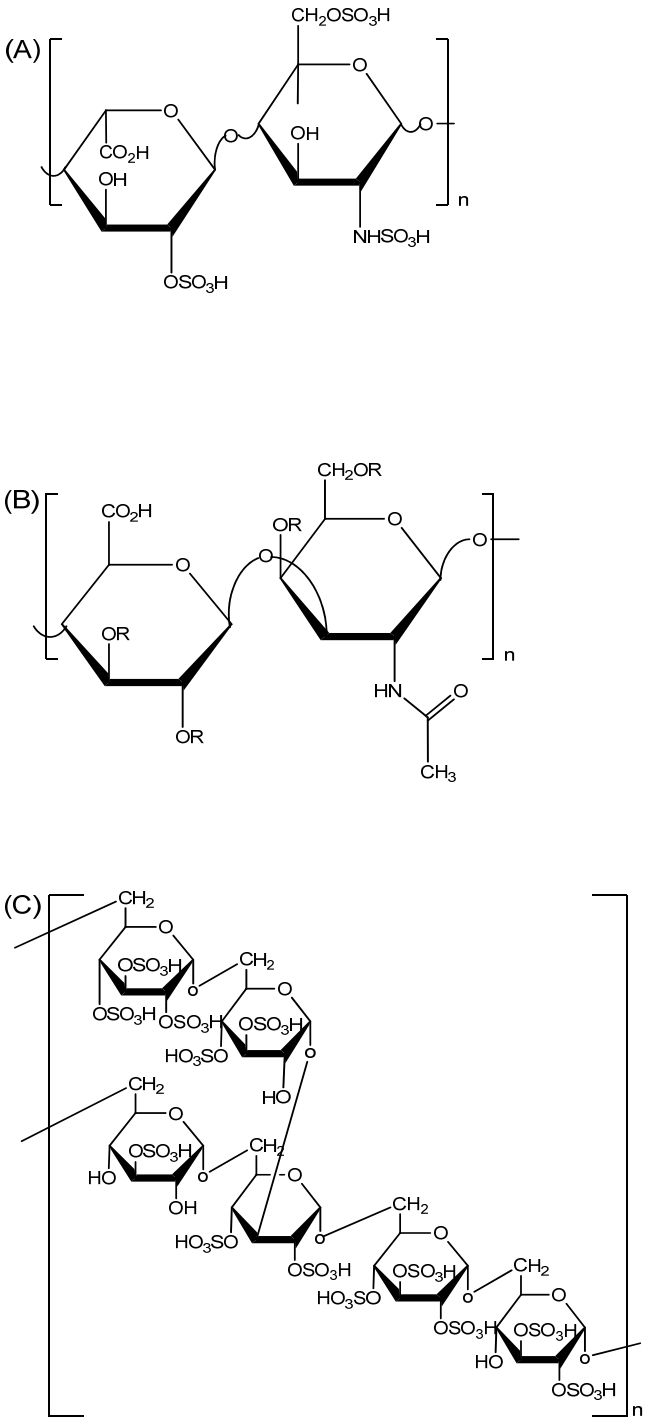

Figure 4.1. Chemical structures of heparin (A), OSCS (B) (R = SO_3H for fully sulfated OSCS, R = H or SO_3H for partially sulfated OSCS, R = H for CS), and DS (C)

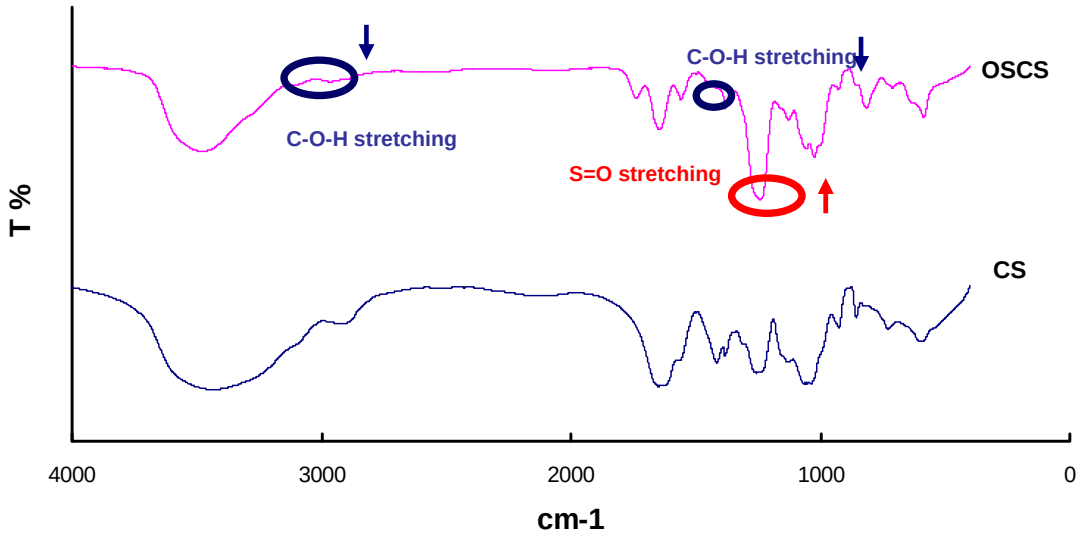

Figure 4.2. IR spectra of CS (A) and fully sulfated OSCS (B).

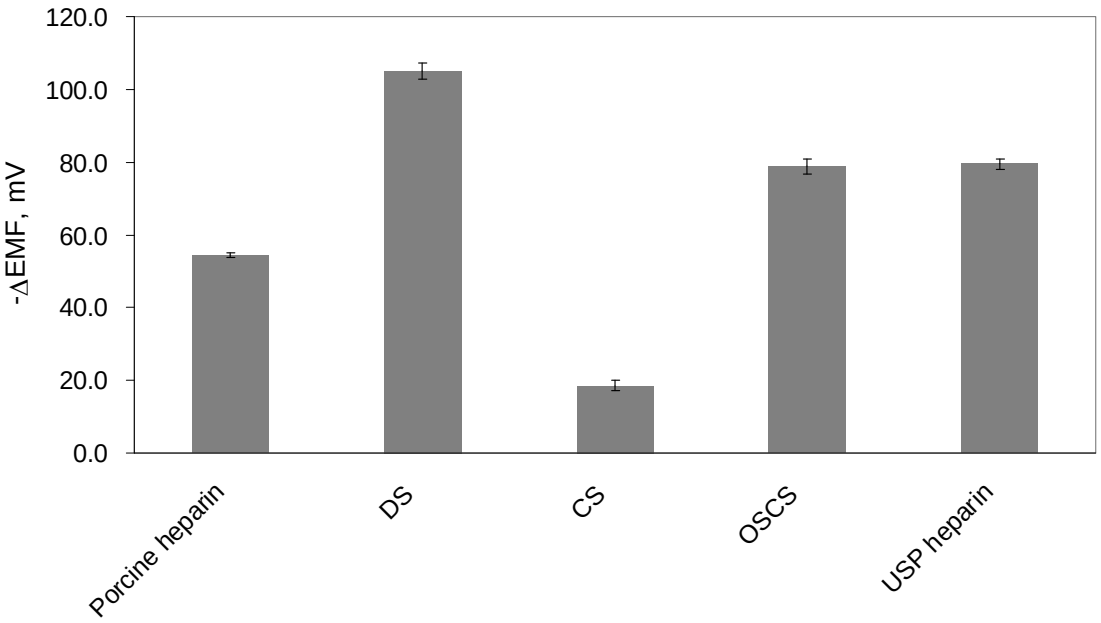

Figure 4.3. Equilibrium EMF response changes of PVC membranes doped with TDMAC toward various polyanion preparations at a final total polyanion concentration of 1 mg/mL. The standard deviations were calculated using data collected from 4 different tests with fresh sensors for each polyanion preparation reported.

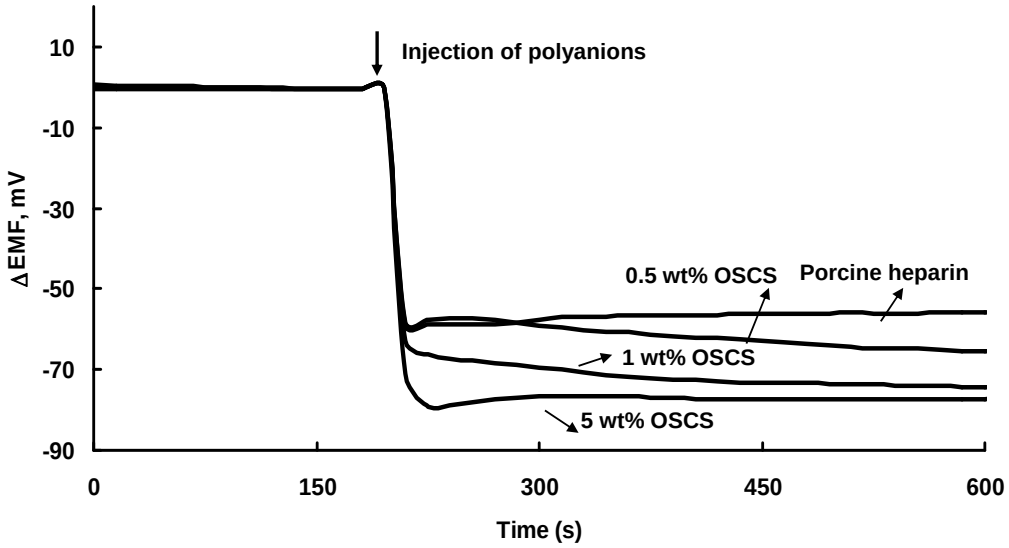

Figure 4.4. Response time trace of PVC membranes doped with TDMAC after injection of heparin/polyion preparations (at 1 mg/mL) possessing different degrees of OSCS contamination (5 wt%, 1 wt%, and 0.5 wt%). For comparison, the response to pure porcine heparin at a final polyanion concentration of 1 mg/mL is also shown.

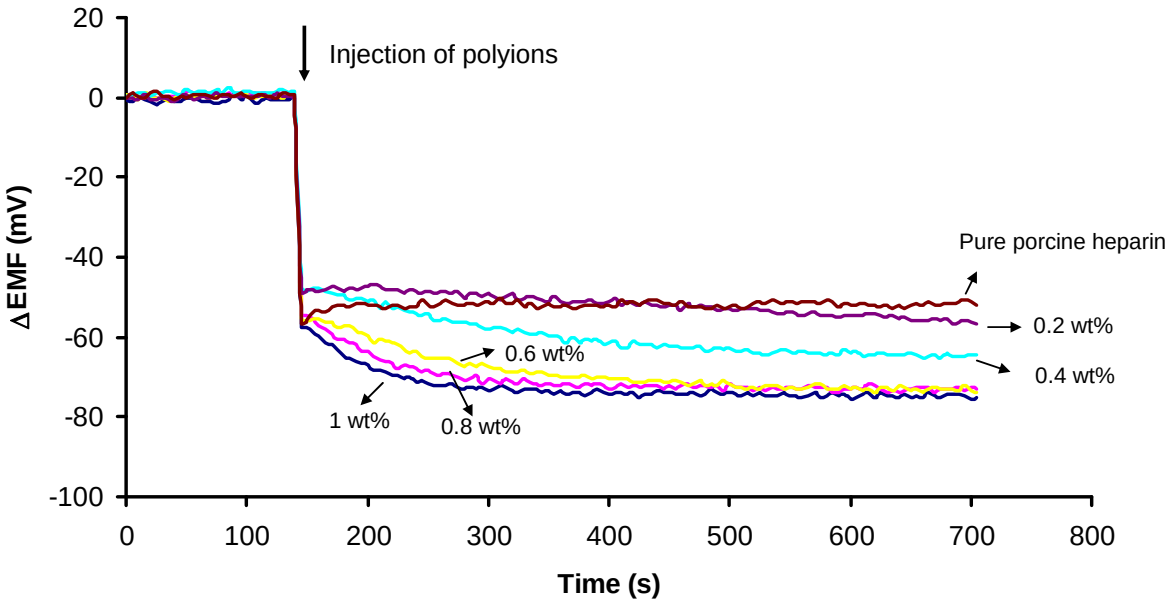

Figure 4.5. Response time trace of PVC membranes doped with TDMAC after injection of heparin/polyion preparations (at 1 mg/mL) possessing different degrees of OSCS contamination equal to or less than 1 wt%. For comparison, the response to pure porcine heparin at a final polyanion concentration of 1 mg/mL is also shown.

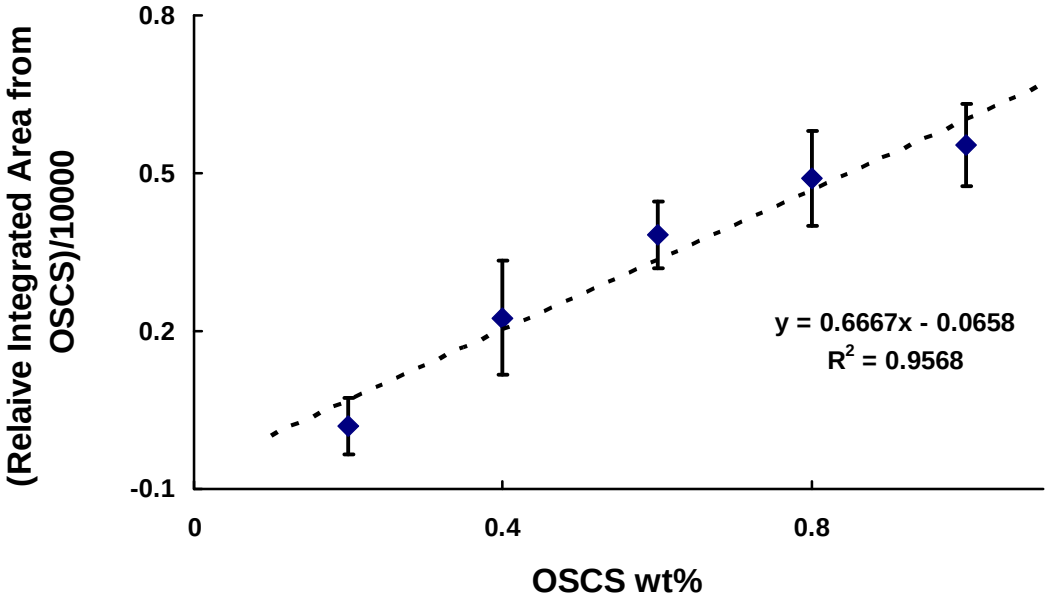

Figure 4.6. Calibration curve of the relative integrated area from OSCS for polyanion preparations with different OSCS wt%. The standard deviations were calculated using data collected from 6 electrodes for each concentration. Δ EMF was integrated for 5 min after the injection of polyanion preparation, and the relative integrated area from OSCS was calculated by subtracting the integrated area for the pure heparin response from the polyanion mixture response.

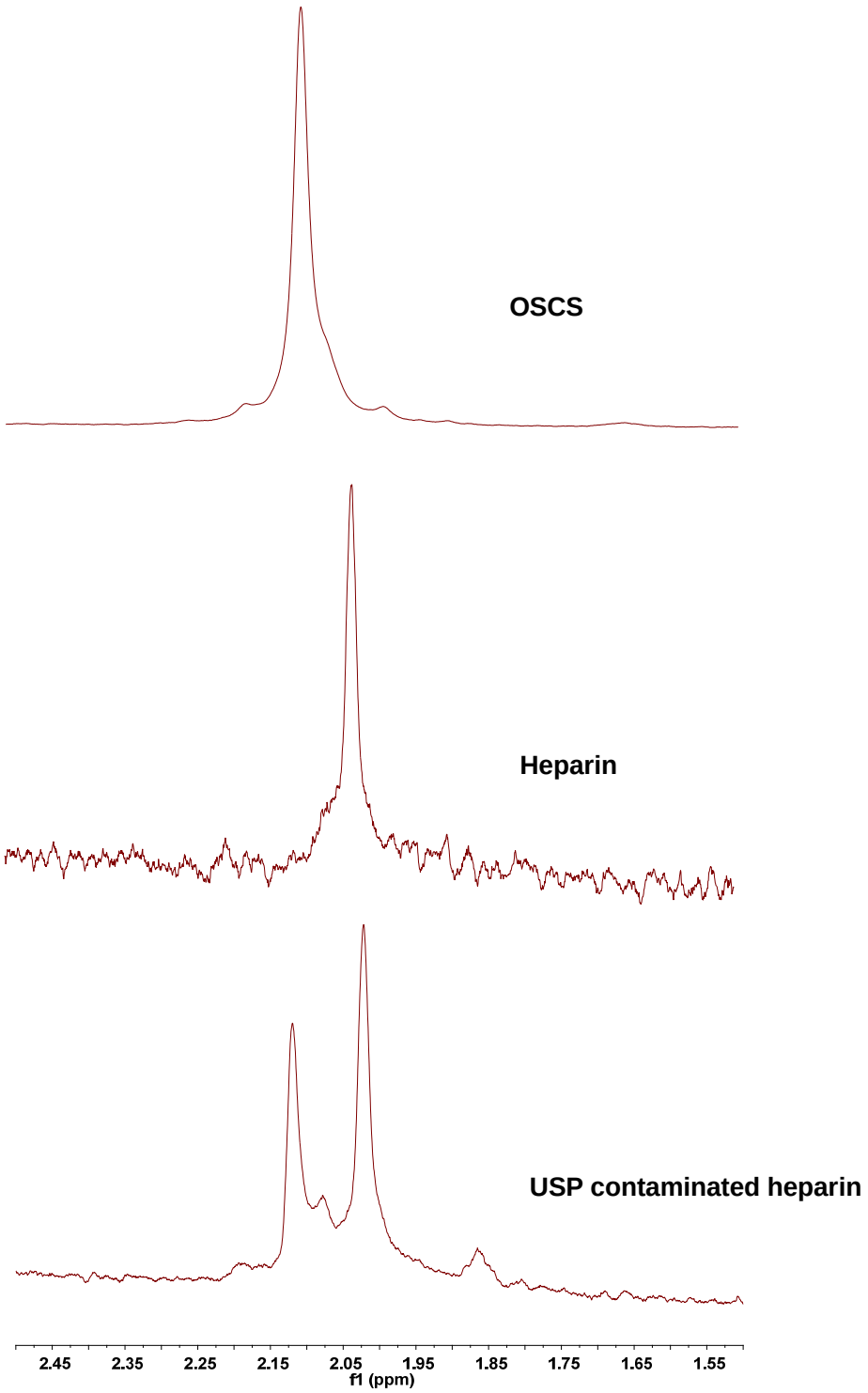

Figure 4.7. ^{1}H NMR spectra (400MHz) of the acetyl region of the OCSC, heparin and the USP contaminated heparin sample.

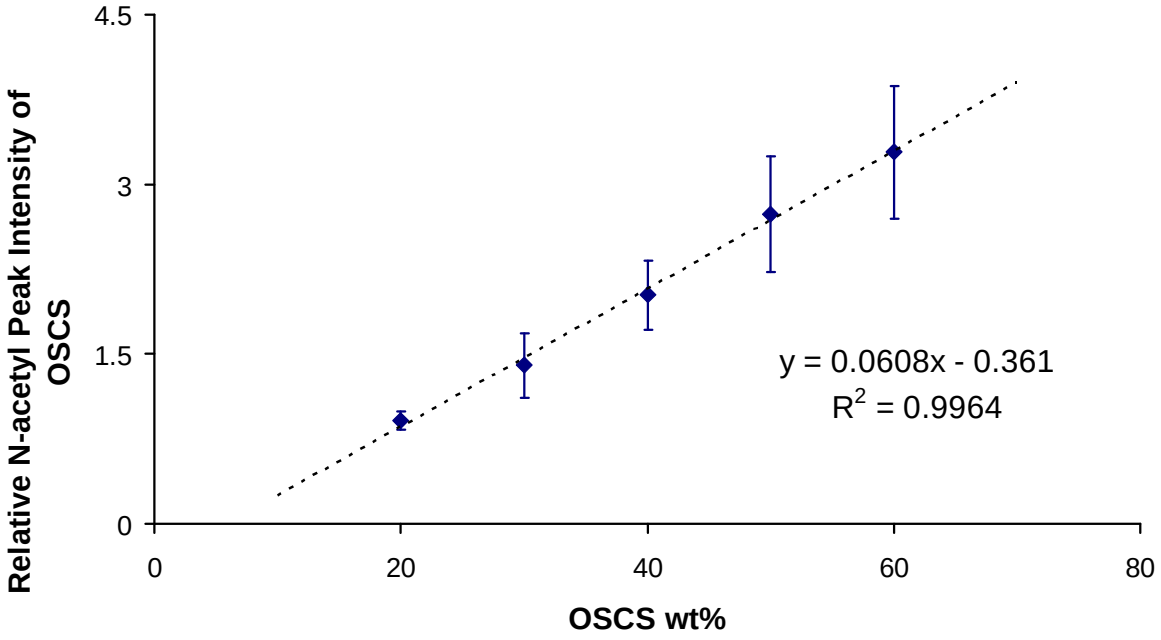

Figure 4.8. Calibration curve of the relative N-acetyl peak intensity of OSCS for polyanion preparations with different OSCS wt%. The standard deviations were calculated using data collected from 3 trails of measurements for each concentration. The relative N-acetyl peak intensity of OSCS was calculated by dividing the N-acetyl peak intensity of OSCS with the N-acetyl peak intensity of heparin.

Table 4.1. Sulfur contents of porcine heparin, CS and OSCS synthesized under different conditions.

Compounds	Porcine heparin	OSCS (40º C 3h)	OSCS (40º C 1h)	OSCS (0ºC 1h)	CS
Sulfur content (%)	10.44	10.12	9.28	7.71	4.56

Table 4.2. Potentiometric response of PVC membranes doped with TDMAC toward polyanion samples with different ratios of DS and porcine heparin.[a]

DS wt% in polyanion preparations	**Avg. ΔEMF (mV) [b]**	**SD (mV) [c]**
100	-105.0	2.1
20	-104.2	1.0
10	-102.6	0.6
1.0	-97.9	0.5

a. The final polyanion concentration is 1 mg/mL.
b. EMF values were recorded 10 min after the injection of polyanion solutions
c. The standard deviations were calculated using data collected from 4 sensors for each concentration.

Table 4.3. Potentiometric response of PVC membranes doped with TDMAC toward polyanion samples with different ratios of DS and porcine heparin.[a]

DS wt% in polyanion preparations	Avg. ΔEMF (mV) [b]	SD (mV) [c]
100	-107.2	1.2
20	-104.8	0.9
10	-104.5	1.5
1.0	-102.2	2.3
0.2	-101.5	0.8

a. The final polyanion concentration is 5 mg/mL.
b. EMF values were recorded 10 min after the injection of polyanion solutions
c. The standard deviations were calculated using data collected from 4 sensors for each concentration.

Table 4.4. Potentiometric response of PVC membranes doped with TDMAC toward polyanion samples with different ratios of OSCS and porcine heparin.[a]

OSCS wt% in polyanion preparations	Avg. ΔEMF (mV) [b]	SD (mV) [c]
100	-78.8	2.2
20	-78.8	1.3
10	-78.2	1.8
1.0	-74.7	1.5
0.75	-72.8	1.8
0.50	-72.7	1.1
0	-54.4	0.7

a. The final polyanion concentration is 1 mg/mL.
b. EMF values were recorded 10 min after the injection of polyanion solutions
c. The standard deviations were calculated using data collected from 4 sensors for each concentration.

Table 4.5. Calculated OSCS wt% based on the linear regression of integrated area of ΔEMF for 5 min after the injection of polyanion preparations and the N-acetyl signal of OSCS and heparin in polyanion preparations with difference OSCS wt%.[a]

Initial polyanion preparations	**Potentiometric Method**		**NMR Method**
	Dilution method[c]	**Calculated OSCS wt% in the initial sample[b]**	**30 mg/mL[d]**
10 wt% OSCS	5	8.7 ± 2.0	12.6 ± 0.2
20 wt% OSCS	3.5	19.2 ± 2.7	18.3 ± 1.1
30 wt% OSCS	3	28.5 ± 2.4	26.2 ± 1.3
USP contaminated heparin	2.5	21.3 ± 3.3	17.9 ± 1.1
	5	17.7 ± 1.5	

a. The final polyanion concentration for potentiometric method and NMR method are 1 mg/mL and 30 mg/mL respectively.

b. The confidence intervals (CIs) obtained in potentiometric method were calculated using data collected from 6 electrodes for each concentration.

c. wt% of the initial polyanion preparations in the final diluted sample by adding porcine heparin.

d. CIs obtained in NMR method were calculated using data collected from 3 trials of measurements.

4.5. References

(1) Capila, I.; Linhardt, R. J. *Angew. Chem. Int. Edn. Engl.* **2002**, *41*, 390-412.
(2) Lepor, N. E. *Rev. Cardiovasc. Med.* **2007**, *8*, S9-S17.
(3) Fischer, K. G. *Hemodial. Int.* **2007**, *11*, 178-189.
(4) Kishimoto, T. K.; Viswanathan, K.; Ganguly, T.; Elankumaran, S.; Smith, S.; Pelzer, K.; Lansing, J. C.; Sriranganathan, N.; Zhao, G. L.; Galcheva-Gargova, Z.; Al-Hakim, A.; Bailey, G. S.; Fraser, B.; Roy, S.; Rogers-Cotrone, T.; Buhse, L.; Whary, M.; Fox, J.; Nasr, M.; Dal Pan, G. J.; Shriver, Z.; Langer, R. S.; Venkataraman, G.; Austen, K. F.; Woodcock, J.; Sasisekharan, R. *N. Engl. J. Med.* **2008**, *358*, 2457-2467.
(5) Guerrini, M.; Beccati, D.; Shriver, Z.; Naggi, A.; Viswanathan, K.; Bisio, A.; Capila, I.; Lansing, J. C.; Guglieri, S.; Fraser, B.; Al-Hakim, A.; Gunay, N. S.; Zhang, Z. Q.; Robinson, L.; Buhse, L.; Nasr, M.; Woodcock, J.; Langer, R.; Venkataraman, G.; Linhardt, R. J.; Casu, B.; Torri, G.; Sasisekharan, R. *Nat. Biotechnol.* **2008**, *26*, 669-675.
(6) Klein, M. D.; Drongowski, R. A.; Linhardt, R. J.; Langer, R. S. *Anal. Biochem.* **1982**, *124*, 59-64.
(7) Maruyama, T.; Toida, T.; Imanari, T.; Yu, G. Y.; Linhardt, R. J. *Carbohydr. Res.* **1998**, *306*, 35-43.
(8) Volpi, N. *Carbohydr. Res.* **1993**, *247*, 263-278.
(9) Ma, S. C.; Yang, V. C.; Fu, B.; Meyerhoff, M. E. *Anal. Chem.* **1993**, *65*, 2078-2084.
(10) Fu, B.; Bakker, E.; Yun, J. H.; Yang, V. C.; Meyerhoff, M. E. *Anal. Chem.* **1994**, *66*, 2250-2259.
(11) Meyerhoff, M. E.; Fu, B.; Bakker, E.; Yun, J.-H.; Yang, V. C. *Anal. Chem.* **1996**, *68*, A168-A175.
(12) Fu, B.; Bakker, E.; Yang, V. C.; Meyerhoff, M. E. *Macromolecules* **1995**, *28*, 5834-5840.
(13) Teien, A. N.; Lie, M.; Abildgaard, U. *Thromb. Res.* **1976**, *8*, 413-416.
(14) Teien, A. N.; Lie, M. *Thromb. Res.* **1977**, *10*, 399-410.
(15) Jacobsen, N. E.; Wiley-Interscience: Hoboken, NJ, 2007.
(16) Wang, L.; Buchanan, S.; Meyerhoff, M. E. *Anal. Chem.* **2008**, *80*, 9845-9847.
(17) Sitkowski, J.; Bednarek, E.; Bocian, W.; Kozerski, L. *J. Med. Chem.* **2008**, *51*, 7663-7665.
(18) Beyer, T.; Diehl, B.; Randel, G.; Humpfer, E.; Schafer, H.; Spraul, M.; Schollmayer, C.; Holzgrabe, U. *J. Pharm. Biomed. Anal.* **2008**, *48*, 13-19.

CHAPTER 5

NITRIC OXIDE GAS SENSOR BASED ON POLYMERIC MEMBRANES DOPED WITH COBALT(III) PORPHYRIN

5.1. Introduction

Nitric oxide (NO) is a very important molecule. NO is an air pollutant emitted from cigarette smoke, automobile engines and power plants. More importantly, NO is a signaling molecule in animals and humans, and has been recognized to play significant roles in numerous physiological processes, including the regulation of vascular tone, inhibition of platelet aggregation, serving as a neurotransmitter, exhibiting cytotoxic effects, inhibiting thrombosis, and exhibiting anti-inflammatory properties.[1-3] Exhaled NO in breath can be detected by chemiluminescence and has been correlated with airway diseases, such as asthma.[4-6]

Potentiometric gas sensors based on internal glass pH electrodes are used frequently in various clinical and environmental analyse.[7, 8] To overcome the limitation of this design (i.e., slow response, long recovery times at low gas concentrations, poor selectivity over other acidic or basic gases), polymer membrane based potentiometric gas sensors using ion selective membranes as the internal probes were developed in this research group in early the 1980s.[9, 10] These electrodes respond to the equilibrium ionic forms of the analyte gases. This new design of gas sensors

offers many advantages over the traditional pH meter based gas sensor including improved detection limit and selectivity as well as the feasibility in miniaturization.

Metalloporphyrins have been used as ionophores in preparing anion-selective polymeric membrane based electrodes since the middle 1980s.[11] Binding between metalloporphyrins and gases such as oxygen, carbon monoxide, nitric oxide have also been reported.[12-15] van Eldik's group conducted a series of experiments and proposed a nitrite catalyzed reductive nitrosylation of water soluble Co(III) porphyrins.[14, 15] In this chapter, acetato-cobalt(III)-tetraphenylporphyrin (Co(III)TPP), which has been demonstrated to show strong affinity to nitrite[16-19] in the studies reported in Chapter 3 is used as a sensing element for the NO gas. When Co(III)TPP is incorporated in polymer membranes for this purpose, sub-Nernstian potentiometric response and a lower detection limit toward NO gas is observed compared to nitrite. Therefore, the goal of this work is to understand the mechanism of the response in the hope that such potentiometric sensitivity for NO gas by Co(III) porphyrin-doped polymer membrane could be analytically useful.

5.2. Experimental Section

5.2.1. Material

4-Hydroxybenzaldehyde, benzaldehyde, pyrrole and cobalt(II) acetate tetrahydrate were all purchased from Aldrich (Milwaukee, WI) to synthesize the acetato-cobalt(III)-tetraphenylporphyrin (Co(III)TPP) according to previous

procudures.[20, 21] Tridodecylmethylammonium chloride (TDMA), o-nitrophenyl octyl ether (NPOE), and high molecular weight poly(vinyl chloride)(PVC) were purchased from Fluka (Milwaukee, WI). Sulfanilamide was obtained from Acros (New Jersey, NJ). N-(1-naphthyl)ethylenediamine dihydrochloride (NED) and all salts were obtained from Aldrich, and aqueous solutions of them were prepared by dissolving the appropriate sodium salts in Millipore purified water (18MΩ cm). All solvents, including ethanol, acetone, tetrahydrofuran (THF), and N,N-dimethylformamide (DMF) were obtained from Fisher Scientific (Pittsburgh, PA). Pure nitric oxide (NO) gas, 45 ppm NO gas, and argon gas were delivered from Metro Welding Supply Corporation (Detroit, MI).

5.2.2. ISE Membrane Formulation and EMF Measurements

The ISE membranes used for potentiometric measurements consisted of 1 wt% Co(III)TPP ionophore and 25 mol% TDMA (relative to Co(III)TPP), 66 wt% NPOE plasticizer, and 33 wt% PVC. All components (total mass 200 mg) were dissolved in 2 - 3 mL of freshly distilled THF and the cocktails were poured into a 25 mm-id glass ring affixed to a glass microscope slide. The solvent was allowed to evaporate overnight, yielding a transparent brown film. Disks with 8 mm diameter were cut from the parent membrane and mounted in electrode bodies (Oesch Sensor Technology, Sargans, Switzerland). An internal filling solution composed of 0.01 M NaCl and 0.01 M $NaNO_2$ was used. These same solutions were also employed as conditioning solutions for the ISEs prior to potentiometric measurements. The sample

buffer employed in this study was 0.05 M or 0.25 M 4-morpholinoethanesulfonic acid (MES), adjusted to pH = 4.8 with sodium hydroxide. All the buffer solutions and the salt solutions were deoxygenated before use to slow NO oxidation. NO saturated solutions were prepared by purging pure NO gas through deoxygenated buffer solutions.

5.2.3. Fabrication of NO Gas Electrodes with Gas Permeable Membrane

The NO gas electrode was constructed as shown in Figure 1.9. The internal sensor was a conventional electrode as described in previously section (Section 5.2.2).

The electrode body was inserted into a slightly larger glass tube which had been filled with buffer solutions. The end of the glass tube was sealed by a polytetrafluoroethylene (PTFE) gas permeable membrane (GPM) which was held in place by parafilm. When the internal sensor was pressed carefully into the glass tube, a thin film of the internal buffer formed between the GPM and the polymer membrane. Finally, a second Ag/AgCl electrode (BASi, West Lafayette, IN) was placed in the glass tube.

5.2.4. Optical Measurements

The optical sensing films contained the same components as the films employed in electrochemical measurements. All the components (total mass 200 mg) were dissolved in distilled THF to give a 2 mL cocktail. Then the films were made by a

spin-coating device (model SCS-G3-8 obtained from Cookson Electronics; Providence, RI) on a square-shaped quartz plate of 35 mm in length. The rotation speed was 1000 rpm, and 150 μL of the polymer film cocktail was injected onto the rotating glass plate each time to spin for 20 sec. The films were dried in air for at least 1 h before use and were prepared freshly. The flow cell setup and the experimental procedure were the same as described in Chapter 2. The UV/visible spectra of the films were recorded in the range between 360 nm to 800 nm when equilibrium with NO gas was reached. To correct for the background absorbance, the absorbance measured at 800 nm was subtracted from the absorbance values at the wavelengths of interest. When conducting the gas phase reaction, a chamber with two inlets and one outlet was used. Nitrogen gas was continuously flowed through one inlet, pure NO (or 45 ppm NO gas) was flowed through the other inlet. UV/visible spectra were taken before and after the flow of NO gas.

For spectrophotometric determination of nitrite, a Griess assay was performed.[22] The sulfanilamide-(N-(1-naphthyl)ethylenediamine dihydrochloride (NED)) reagent was prepared by dissolving 0.25 g of sulfanilamide in 75 mL of 1 M hydrochloric acid at room temperature, 3 mL of 0.20 wt% NED solution was then added, and the solution was diluted to 100 mL. One mL of nitrite solutions with different concentrations were mixed with 1 mL of the sulfanilamide-NED reagent. The absorbance was measured after 15 min at 542 nm.

5.2.5. Electron Spin Resonance (ESR) Spectroscopy

Co(III)TPP was dissolved in ethanol to a concentration of 10^{-4} M. The solution was bubbled with argon gas and then pure NO gas. After this treatment, argon gas was flowed again to remove the extra dissolved NO gas. The solutions were transferred to ESR tubes. The ESR spectra were recorded at 120 K on a Bruker EMX spectrometer (Billerica, MA) equipped with a liquid nitrogen cryostat. A microwave power of 20 mW, a modulation amplitude of 0.5 mT and a modulation frequency of 100 kHz were used. To correct for the background, a blank spectra was subtracted from all of the recorded spectrum.

5.3. Results and Discussion

5.3.1. Potentiometric and Optical Response Characteristics of ISEs Formulated Co(III)TPP

It was reported in Chapter 3 that ISEs formulated Co(III)TPP can be used to measure nitrite with a detection limit around 10^{-5} M (see Figure 5.1). However, when we used the same electrode to measure NO in NO saturated solution, a much lower detection limit (about one or two order of magnitude lower) was observed (see Figure 5.1).

Compared with the Nernstian response toward nitrite, Figure 5.1 shows that the response toward low concentration of NO is sub-Nernstian and at higher NO concentration the response becomes super-Nernstian. The change in the slope and the detection limit are not consistent with the conventional selective binding reaction

between NO and Co(III)TPP, and may suggest alternative mechanisms including redox reaction during the process.[23]

We further used UV/visible absorption spectroscopy to probe optical response of the sensing membranes upon the addition of NO saturated solution. Figure 5.2 shows the UV/visible spectra of a polymer film prepared using the same composition as the membrane employed in the potentiometric measurements reported in Figure 5.1. The film was initially equilibrated in 0.25 M MES buffer (pH = 4.8), and the Soret absorbance band was observed at 413 nm. After the film was equilibrated with solutions containing increasing concentrations of nitrite by using a flow cell system to pump the solution over the film, the absorbance at 413 nm decreases with a concomitant appearance and increase of a new band at 440 nm (see Figure 5.2 (A)). Previous studies have attributed such a bathochromic shift in the Soret band to the change of the axial ligands of Co(III)TPP from single nitrite ligand to two nitrite ligands. When the same film was equilibrated with solutions containing increasing concentrations of NO, the absorbance at 413 nm decreases also with a concomitant appearance and increase of a broad band at a higher wavelength of 440 nm (see Figure 5.2 (B)). The bands at the higher wavelength start to appear at 10^{-5} M for nitrite addition; however, a much lower concentration of NO (ca. 10^{-7} M) can shift the Soret band of Co(III)TPP. The better sensitivity of the optical sensor toward NO is consistent with our previous observation via potentiometric measurements.

Optical responses of the sensing membranes toward NO gas were also examined by flowing NO gas directly onto a film prepared using the same composition as the

membrane employed in the previous potentiometric and optical measurements (see Figure 5.3). To avoid the oxidation of NO by the oxygen in the environment, nitrogen gas was flowed continuously together with the NO gas. Similarly, we observe that by blowing pure NO gas for 5 min, the Soret band of the Co(III)TPP was shifted from 413 nm to 435 nm, which is 5 nm different from the band shift for flowing nitrite solution (413 nm to 440 nm) to the film. By equilibrating with a lower concentration of NO gas (45 ppm), the shift of the Soret band of Co(III)TPP is not as obvious, however, a change of the Soret band shape is apparent. A much broader band replaces the previous narrow peak before exposure to NO gas.

Based on the above observations from potentiometric and optical measurements, it was found that both NO saturated solution and NO gas could react with the Co(III)TPP. The sensitivity of Co(III)TPP toward NO is better than that toward nitrite. Therefore some redox reaction between NO and Co(III)TPP appears to be responsible for the low detection limit.

5.3.2. Potentiometric Response Characteristics of ISEs Formulated Co(III)TPP in a Gas Permeable Membrane Configuration

The NO saturated solutions used in the electrochemical and optical measurements were prepared by bubbling NO through deoxygenated buffer solutions. The NO concentration of such solutions is known to be 1.8 mM at 25°C.[24] However, several groups have reported that nitrite and/or nitrous acid (HNO_2) are common impurities in the aqueous NO solutions.[25, 26] These impurities come from higher

nitrogen oxides present in the NO gas and/or from traces of oxygen present or adsorbed in the instruments. To estimate the nitrite impurities in the NO saturated solution, argon gas was used to purge the NO saturated solution to exclude the dissolved NO. Then a Griess assay was employed to determine that the nitrite content in the NO stock solution is 5.8 ± 0.2 mM. However, even considering such interference from nitrite, the ISEs would not show response at 10^{-7} M nitrite concentration; therefore, the better sensitivity of the electrodes for the NO exposed solutions appear to come from NO gas instead of nitrite impurities in NO stock solution.

To prevent the even small amount of nitrite from contacting the electrode's membrane, a configuration employing gas permeable membrane was used (see Figure 1.9). NO in the sample solution diffuses across the gas permeable membrane until the partial pressure of NO gas is equal on both side of the membrane. Figure 5.4 shows a comparison of response curves obtained for this type configuration vs. a regular ISE without gas permeable membrane. It can be observed that adding a gas permeable membrane did not change the potentiometric response dramatically and a similar low detection limit toward NO gas was still observed. Therefore, it is concluded that the better sensitivity of the Co(III)TPP electrode toward NO is not due to the nitrite impurities in the NO stock solution, but stems from the interaction between Co(III)TPP and NO gas.

5.3.3. ESR Spectroscopy Study on the Oxidation State of Cobalt Porphyrins after Reaction with NO

ESR spectroscopy is a technique used to study chemical species that have one or more unpaired electrons, such as organic and inorganic free radicals, or inorganic complexes possessing a transition metal ion. It has been found that many planar Co(II) complexes are paramagnetic and can be studied by ESR.[27, 28] Trying to mimic the membrane environment, ethanol was chosen as the solvent since its dielectric constant (ε_r = 24.3) is very close to that of the plasticizer of the membrane (NPOE, ε_r = 21).

Figure 5.5 shows the ESR spectrum of Co(III)TPP ethanol solution exposed to pure NO gas for 10 min, and then with argon gas for 20 min to remove the dissolved NO gas. The spectrum is different from the silent ESR spectrum of Co(III)TPP ethanol solution, and indicates the formation of Co(II)TPP.[28] We also examined the electrode's membrane after the potentiometric measurements toward NO by dissolving the membrane in acetone (ε_r = 20.7) and taking ESR spectrum of the solution. As shown in Figure 5.6, the ESR spectrum also indicates a redox reaction that reduces Co(III)TPP to Co(II)TPP compared with the ESR spectrum of the same membrane without contacting NO.

5.3.5. Possible Sensing Mechanism of ISEs Formulated Co(III)TPP Toward Nitric Oxide (NO)

Based on the ESR spectra and the observation that the Co(III)TPP based membrane electrodes show sub-Nernstian response and low detection limit toward

NO,[23] a redox reaction mechanism is proposed that may explain the very low detection limit toward NO. Figure 5.7 illustrates the processes that occur within membranes containing Co(III)TPP when in contact with an NO solution. During pre-conditioning, nitrite from the conditioning solution is extracted into the membrane and binds with Co(III)TPP. A portion of Co(III)TPP binds with two nitrite as axial ligands, and forms an ion pair with the TDMA cation doped to the polymer membrane. The rest of Co(III)TPP bind only one nitrite as axial ligand and form a neutral complex. After the membranes are exposed to NO solutions, NO gas diffuses into the membrane and reduces Co(III)TPP to Co(II)TPP. In this way, the previous complex with one nitrite axial ligand has one negative charge and will form an ion pair with the TDMA in the polymer membrane. The previous complex with two nitrite axial ligands has two negative charges. Therefore, more negative charges are created at the surface of the membrane compared with the initial polymer film. The increasing generated anionic sites at the membrane interface could explain the observation that Co(III)TPP electrodes show negative potentiometric response at a much lower concentration of NO gas that nitrite anions.

5.4. Summary

It has been shown in this chapter that electrodes containing Co(III)TPP exhibit a very low detection limit toward NO gas and yield sub Nernstian potentiometric response to this gaseous species. We propose a redox reaction instead of a selective binding reaction when Co(III)TPP contacts NO solutions. The redox reaction

mechanism is supported by the ESR data, as the Co(III)TPP ethanol solution and Co(III)TPP containing membranes both show ESR signal after being exposed to NO gas. Therefore, based on the above observations, it may be possible to utilize Co(III)TPP containing films to electrochemically and optically detect NO gas in breath. The redox reaction mechanism observed here for polymer membranes doped with Co(III)TPP is somewhat analogues to the response of membranes doped with dithiocarbamate complexes of Hg(II) toward sulfite.[23] In that early work, it was shown that potentiometric response to sulfite was due to a redox reaction between sulfite and the Hg(II) complex at the membrane/sample interface.

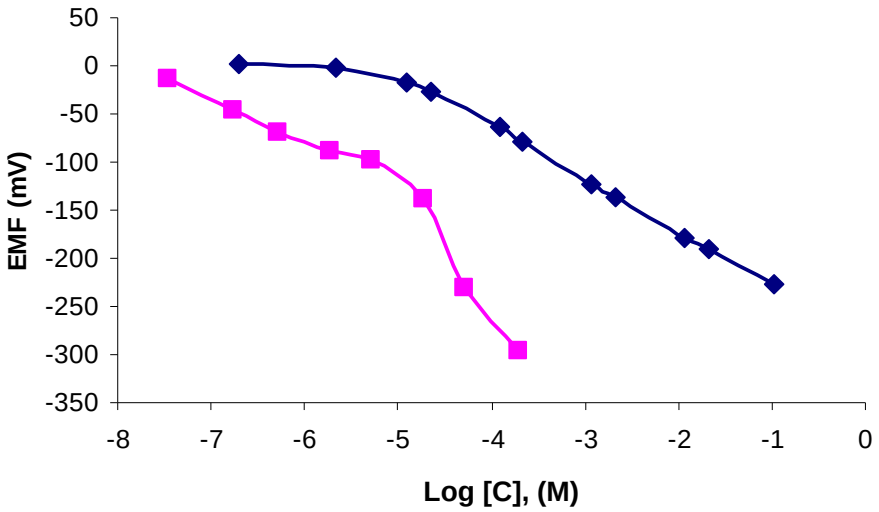

Figure 5.1. Potentiometric response for electrodes containing 1 wt% Co(III)TPP and 25 mol% TDMA (relative to Co(III) porphyrin) in PVC/NPOE matrix; (■) NO_3^- (◆) nitrite. Response obtained in pH = 4.8 MES buffer. Internal solution: 0.01 M NaCl/$NaNO_2$ in pH = 4.8 MES buffer.

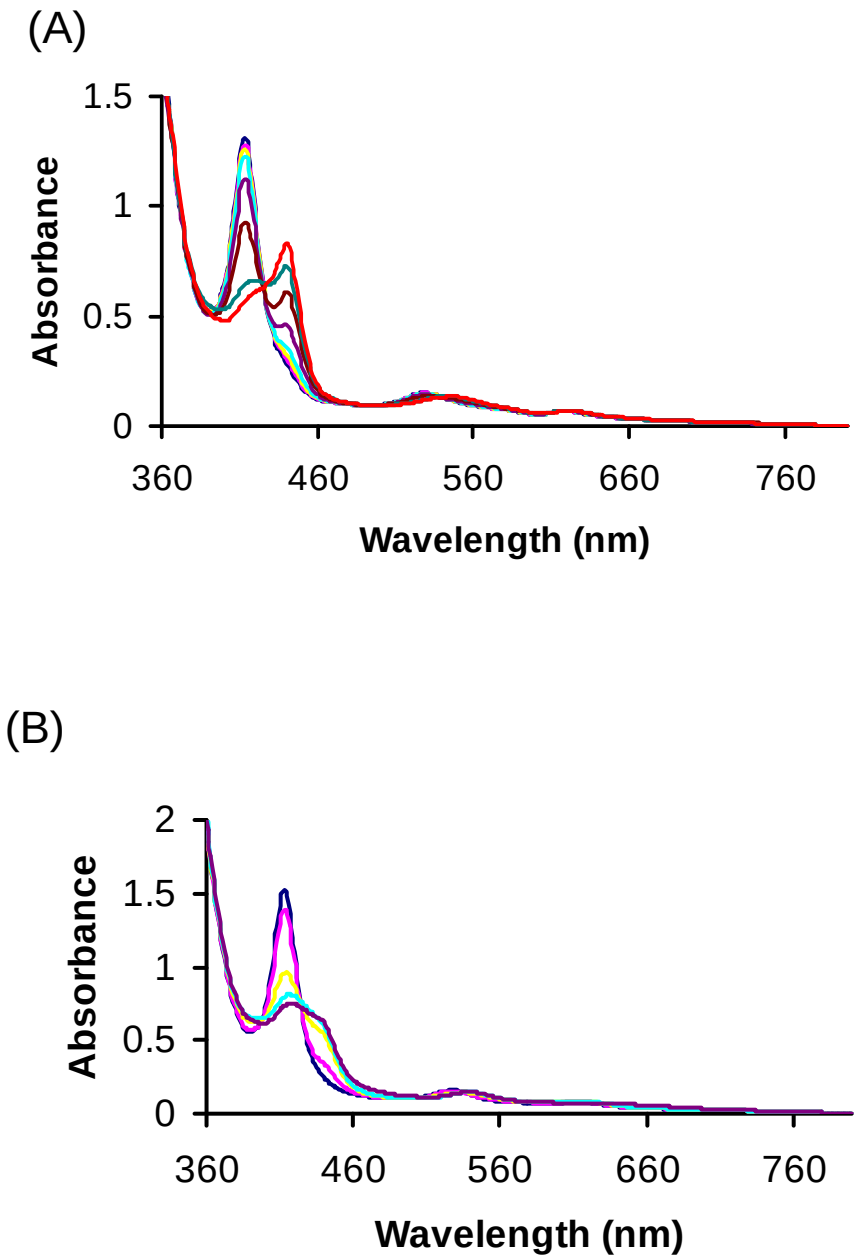

Figure 5.2. UV/visible spectra of a membrane containing Co(III)TPP and 25 mol% TDMA (relative to Co(III)TPP) upon increasing the bathing concentration of nitrite (A), NO saturated solution (B). Initial spectrum equilibrated in MES buffer, pH = 4.8. Concentration of nitrite increased from zero to 0.1M, increasing 10 fold each spectrum. Concentration of NO increased from zero to 0.2 mM, increasing 10 fold each spectrum.

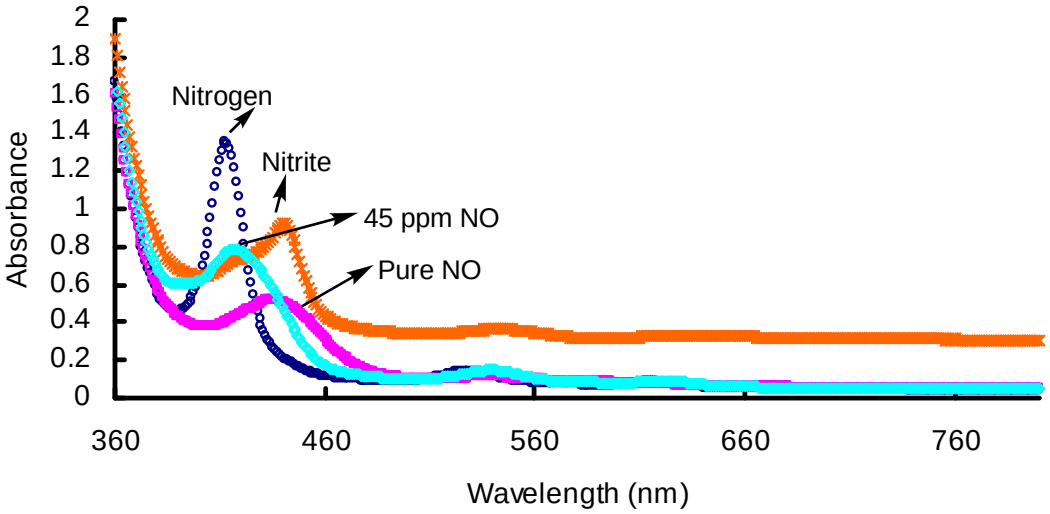

Figure 5.3. UV/visible spectra of a membrane containing Co(III)TPP and 25 mol% TDMA (relative to Co(III)TPP) upon increasing concentration of (○) nitrogen, (□) pure NO gas, (◊) 45 ppm NO gas, (*) 20 mM nitrite solution in 0.25 M MES buffer (pH = 4.8). The pure NO gas and 45 ppm NO gas was blown for 5 min before the spectra were taken.

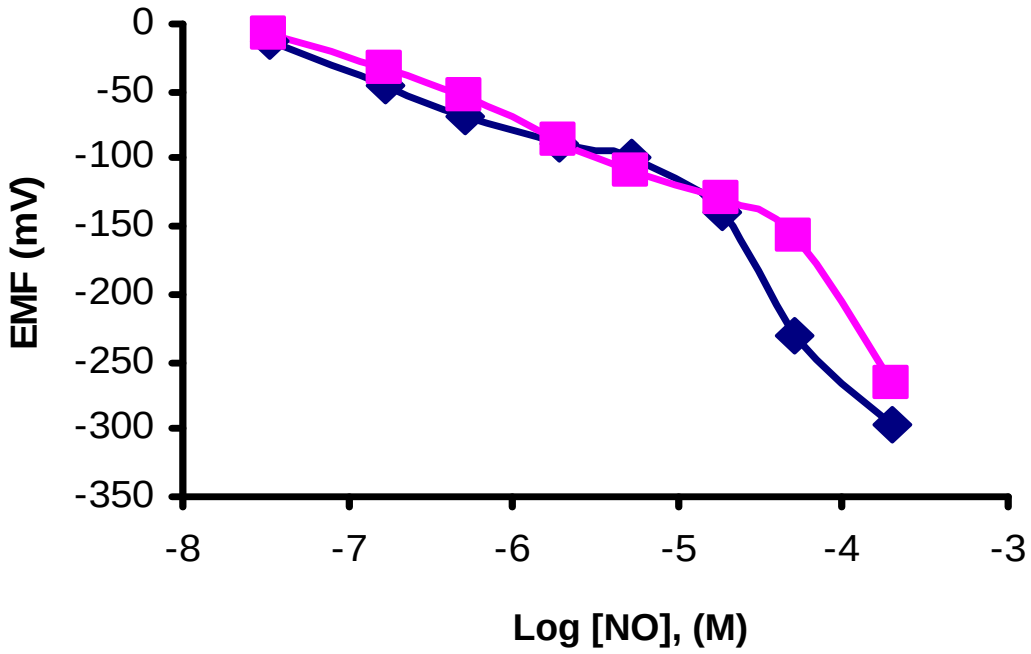

Figure 5.4. Potentiometric response for electrodes containing 1 wt% Co(III)TPP and 25 mol% TDMA (relative to Co(III) porphyrin) in PVC/NPOE matrix; (◆) regular ISE, (■) ISE with a gas permeable membrane configuration. Response obtained in pH = 4.8 MES buffer. Internal solution: 0.01 M NaCl/$NaNO_2$ in pH = 4.8 MES buffer.

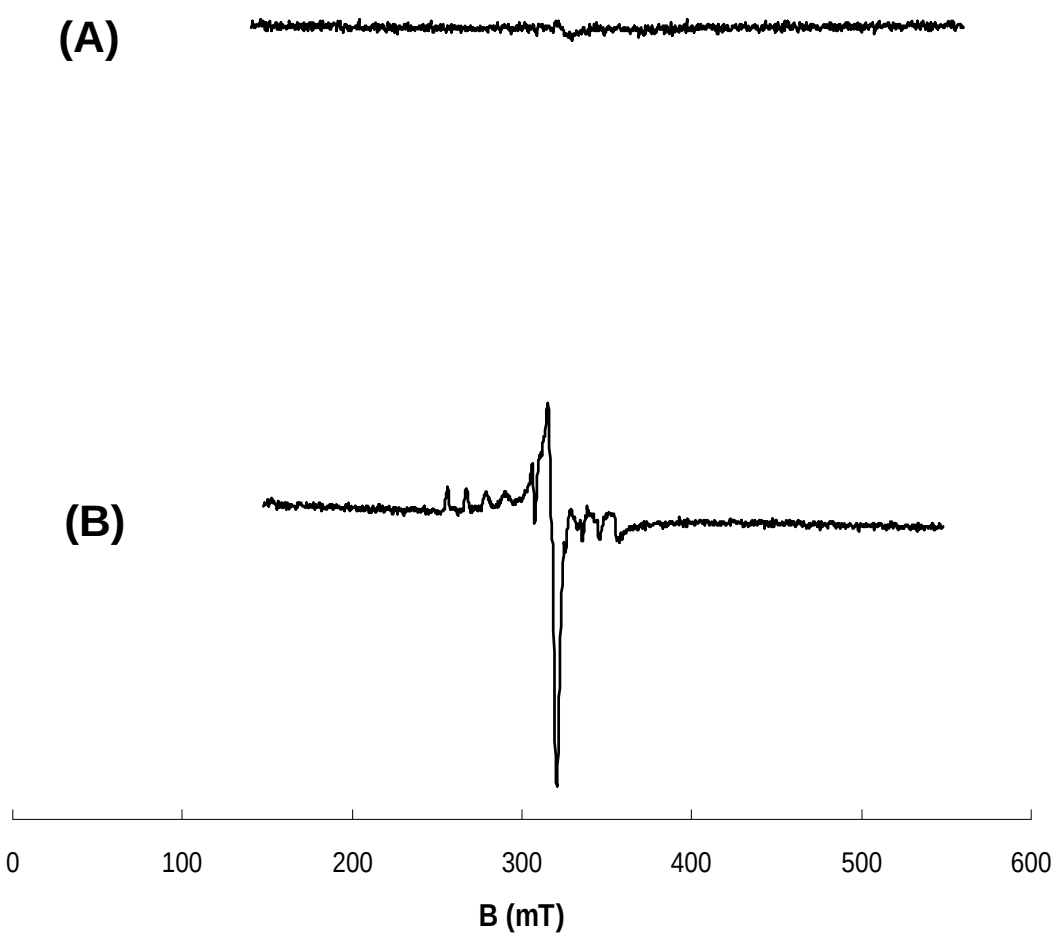

Figure 5.5. ESR spectrum of a deoxygenated solution containing Co(III)TPP in ethanol before (A) and after (B) exposing to NO solution for 10 min. (B) was taken after purging argon gas for 20 min to remove the dissolved NO gas. A blank spectrum of the system was subtracted for both (A) and (B).

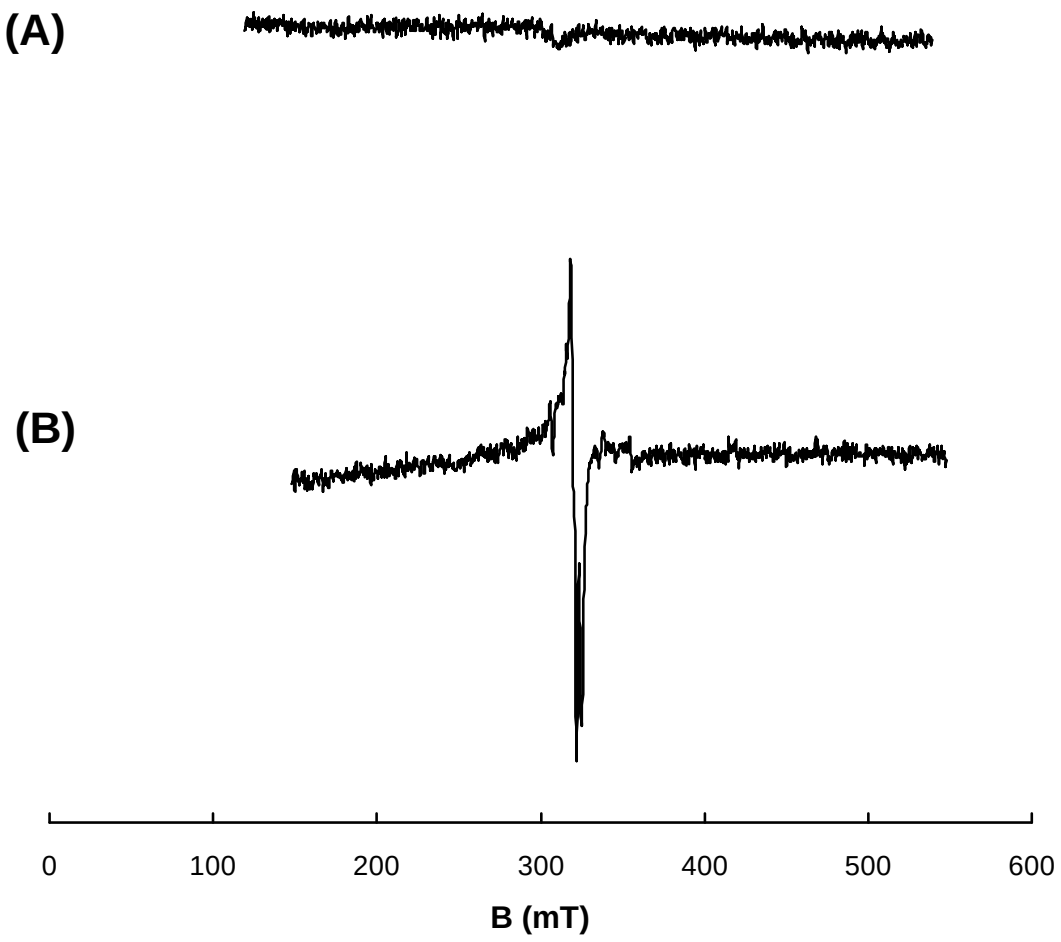

Figure 5.6. ESR spectrum of a membrane containing 1 wt% Co(III)TPP and 25 mol% TDMA (relative to Co(III) porphyrin) in PVC/NPOE matrix before (A) and after (B) contact NO solution. The solvent used was acetone. A blank spectrum of the system was subtracted for (A); a blank spectrum of a blank polymer membrane without Co(III)TPP was subtracted for (B)

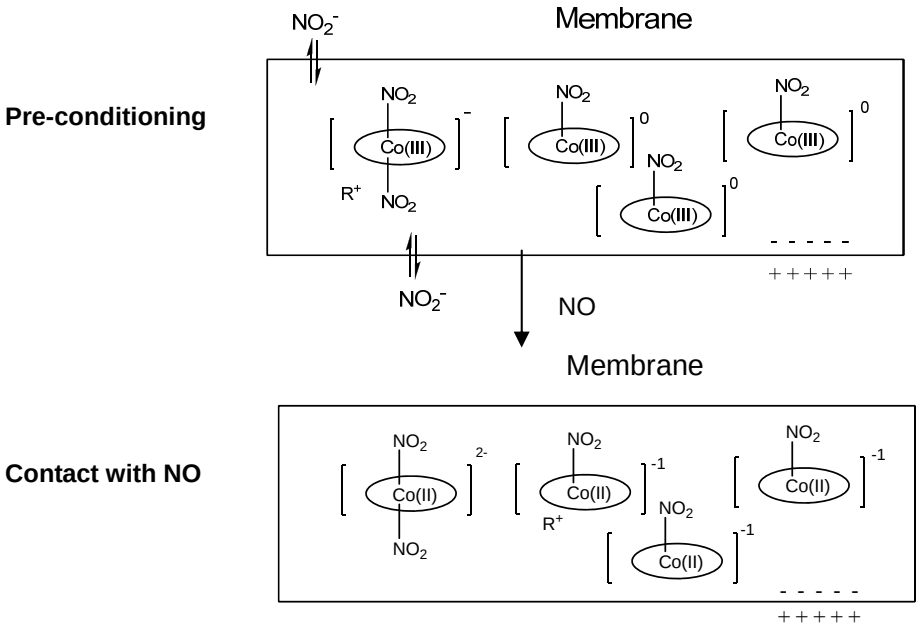

Figure 5.7. Proposed reaction mechanism of electrodes containing1 wt% Co(III)TPP and 25 mol% TDMA (relative to Co(III) porphyrin) in PVC/NPOE matrix upon contacting with NO stock solution.

5.5. References

(1) Wallis, J. P. *Transfus. Med.* **2005**, *15*, 1-11.
(2) Guzik, T. J.; Korbut, R.; Adamek-Guzik, T. *J. Physiol. Pharmacol.* **2003**, *54*, 469-487.
(3) Cooke, J. P. *Atheroscler. Suppl* **2003**, *4*, 53-60.
(4) Gustafsson, L. E. *Eur. Resp. J.* **1998**, *11*, 49S-52S.
(5) Yates, D. H. *Immunol. Cell Biol.* **2001**, *79*, 178-190.
(6) Turner, S. *Mini-Rev. Med. Chem.* **2007**, *7*, 539-542.
(7) Severinghaus, J. W.; Bradley, A. F. *J. Appl. Physiol.* **1958**, *13*, 515-520.
(8) Meyerhoff, M. E.; Fraticelli, Y. M. *Anal. Chem.* **1982**, *54*, R27-R44.
(9) Meyerhoff, M. E. *Anal. Chem.* **1980**, *52*, 1532-1534.
(10) Meyerhoff, M. E.; Robins, R. H. *Anal. Chem.* **1980**, *52*, 2383-2387.
(11) Chang, Q.; Meyerhoff, M. E. *Anal. Chim. Acta* **1986**, *186*, 81-90.
(12) Jones, R. D.; Budge, J. R.; Ellis, P. E.; Linard, J. E.; Summerville, D. A.; Basolo, F. *J. Organomet. Chem.* **1979**, *181*, 151-158.
(13) Franke, A.; Roncaroli, F.; van Eldik, R. *Eur. J. Inorg. Chem.* **2007**, 773-798.
(14) Roncaroli, F.; van Eldik, R. *J. Am. Chem. Soc.* **2006**, *128*, 8042-8053.
(15) Roncaroli, F.; Shubina, T. E.; Clark, T.; van Eldik, R. *Inorg. Chem.* **2006**, *45*, 7869-7876.
(16) Ammann, D.; Huser, M.; Krautler, B.; Rusterholz, B.; Schulthess, P.; Lindemann, B.; Halder, E.; Simon, W. *Helv. Chim. Acta* **1986**, *69*, 849-854.
(17) Huser, M.; Morf, W. E.; Fluri, K.; Seiler, K.; Schulthess, P.; Simon, W. *Helv. Chim. Acta* **1990**, *73*, 1481-1496.
(18) Li, X. Z.; Harrison, D. J. *Anal. Chem.* **1991**, *63*, 2168-2174.
(19) Shamsipur, M.; Javanbakht, M.; Hassaninejad, A. R.; Sharghi, H.; Ganjali, M. R.; Mousavi, M. F. *Electroanalysis* **2003**, *15*, 1251-1259.
(20) Adler, A. D.; Longo, F. R.; Kampas, F.; Kim, J. *J. Inorg. Nucl. Chem.* **1970**, *32*, 2443-2445.
(21) Sugimoto, H.; Ueda, N.; Mori, M. *Bull. Chem. Soc. Jpn.* **1981**, *54*, 3425-3432.
(22) Norwitz, G.; Keliher, P. N. *Analyst* **1987**, *112*, 903-907.
(23) Badr, I. H. A.; Meyerhoff, M. E.; Hassan, S. S. M. *Anal. Chim. Acta* **1995**, *310*, 211-221.
(24) Roncaroli, F.; Olabe, J. A.; van Eldik, R. *Inorg. Chem.* **2002**, *41*, 5417-5425.
(25) Wolak, M.; Stochel, G.; Hamza, M.; van Eldik, R. *Inorg. Chem.* **2000**, *39*, 2018-+.
(26) Fernandez, B. O.; Lorkovic, I. M.; Ford, P. C. *Inorg. Chem.* **2004**, *43*, 5393-5402.
(27) Smith, T. D.; Pilbrow, J. R. *Coord. Chem. Rev.* **1981**, *39*, 295-383.
(28) Van Doorslaer, S.; Schweiger, A. *Phys. Chem. Chem. Phys.* **2001**, *3*, 159-166.

CHAPTER 6

CONCLUSIONS AND FUTURE DIRECTIONS

6.1. Summary of the Dissertation Research

This dissertation research was mainly focused on the development of anion and polyanion selective electrodes or optodes based on polymeric membranes. Efforts were made in optimizing the sensing system, studying the mechanism, as well as implementing new applications of the sensors. The research employed both synthetic work, including synthesis of metalloporphyrins, modification of polymers and polyanions, and analytical methods in potentiometric and optical measurements.

As for anions, sensors were developed toward the detection of two very common anions, fluoride and nitrite, using Al(III) and Co(III) porphyrins as the ion sensing reagents, respectively.

Dimer-monomer equilibrium has been reported for metalloporphyrin species doped within polymeric membranes.[1] This equilibrium can be utilized when designing optical sensors,[2-4] however, it brings various disadvantages in electrochemical potentiometric measurements.[1] Chapter 2 verified the formation of dimeric structures of Al(III) porphyrins when in contact with fluoride ions using a synthesized protoporphyrin diester derivative. Efforts aimed at eliminating the dimer formation

by covalently attaching the Al(III) porphyrin onto a polymethacrylate backbone[5] were also described. Although employing this new material in the polymer membrane cannot completely eliminate the dimer formation, the use of the macromolecular ionophore provided a relatively longer lifetime for the fluoride electrodes.

Chapter 3 focused on the optimization of a nitrite selective electrode. Co(III) porphyrins have been reported previously as nitrite selective ionophores.[6, 7] The main aim of this chapter was to achieve a lower detection limit rather than to obtain absolute selectivity of the sensor since interference anions (e.g., perchlorate, salicylate and thiocyanate) can be enhanced by various methods.[8] For example, using appropriate membranes to prevent these ionic interferences from reaching the sensor when sample nitrite can be first converted to NO_x (g) via acidification of the sample, and then passing through a gas permeable membrane. For this purpose, a coated wire electrode (CWE) system was chosen and was optimized for nitrite detection by varying the amount of lipophilic additive and thickness of the membrane. The CWEs exhibited lower detection limits than the conventional ion selective electrodes (ISEs) with inner filling solution. However, the selectivity coefficients of CWEs with varying membrane thicknesses were different, and the lifetime of the CWEs was shorter than conventional nitrite ISEs with inner filling solutions. Both of these observations result from the thin water layer formed between the ion sensing membrane and the solid substrate.[9] A more lipophilic substrate material was employed to eliminate the water layer formation. Co(III) porphyrin was also covalently attached to a polymethacrylate backbone similar to Chapter 2, and the lifetime of the

electrode was dramatically increased to over one month compared to the several days' lifetime for the unattached porphyrins. An optical sensor employing Co(III) porphyrin and a chromoionophore was also designed, which shows a detection limit of ca. 1 μM, and seems very promising for measuring nitrite levels in physiological samples.

In Chapter 4, a new application of a previously reported polyanion sensor based on a polymer membrane[10] was described. The polyanion sensor was used to measure a high charge density polyanion contaminant, oversulfated chondroitin sulfate (OSCS), in biomedical heparin preparations. Compared with the current US Food and Drug Administration (FDA) suggested methods, nuclear magnetic resonance (NMR)[11, 12] and capillary electrophoresis (CE)[13], the potentiometric sensors are smaller, easier to construct, disposable and have a rapid response. The detection limit can be as low as 0.2 wt% OSCS, and can be even lower if a more concentrated initial test sample is used. Quantitative analysis of the OSCS content was also achieved based on the dynamics of the polyanion sensors. By carefully adjusting the OSCS content in the polyanion preparations to less than 1 wt%, the integrated area of the potential is proportional to the OSCS wt%. The OSCS wt% determined by the potentiometric method was found to be in good agreement with the value determined by the NMR method based on the intensity of the N-acetyl proton signal of OSCS and heparin.

6.2. Future Directions

6.2.1. Application of the Fluoride Sensor

One of the most attractive applications of fluoride sensors based on thin polymeric films is their potential in giving valuable results in biomedical related analyses. As reported previously, a good fluoride sensor can be used to detect glucose, cholesterol and a host of other clinically relevant species by employing a coupled enzyme reaction.[14-16] The sensing process is based on the peroxidase-catalyzed rupture of the covalent C-F bond in certain organo-fluoro compounds in the presence of hydrogen peroxide (H_2O_2)[17] and the measurement of liberated fluoride by a fluoride sensor. The liberated fluoride may be used as a marker for the quantification of peroxidase or its substrate H_2O_2. In addition, by coupling this reaction with other oxidase enzymatic reactions, we should be able to measure either the enzymes or their respective substrates (Reaction 6.1). Among the organo-fluoro compounds, fluorine in the para-position to a powerful electron-donating substituent, such as OH or NH_2, gives the most effective C-F bond rupture. 4-Fluoroaniline, 4-fluorophenol, 2,3,5,6-tetrafluorophenol, penta-fluorophenol, and 3-fluoro-DL-tyrosine appear to be suitable for analytical use since they yield not only good linearity between reaction rate and analyte concentration, but also high rates to achieve adequate analytical sensitivity.

$$\text{Substrate} + O_2 \xrightarrow{\text{Oxidase}} \text{Products} + H_2O_2$$

$$H_2O_2 + \text{Fluoroaromatic compounds} \xrightarrow{\text{Peroxidase}} F^- + H_2O + \text{Product(s)}$$

(Reaction 6.1)

Moreover, the polymer membrane based fluoride sensors can also be used for the direct measurement of organophosphate nerve agents, such as sarin, soman, and VX (see Figure 6.1), by detecting the fluoride ions released during organophosphorus hydrolase (OPH)[18] or copper complex [19]catalyzed hydrolysis (see Reaction 6.2). Actually, a recent collaborating project with Dr. Simonian at Auburn University has proved that diisopropyl fluorophosphate (DFP) (see Figure 6.1), a structural analogue to nerve gas agents, can be quantified by the optical fluoride sensor using OPH to catalyze the DFP hydrolysis.

$$\text{Organofluorophosphates} + H_2O \xrightarrow{\text{OPH/Cu-Complex}} \text{Products} + F^- \quad \text{(Reaction 6.2)}$$

6.2.2. Detection of Other High Charge Density Polyanions Using Potentiometric Polyanion Sensors

Based on the work in Chapter 4, the polyanion sensors can be used to discriminate other high charge density polyanions (see Figure 6.2). For example, chondroitin sulfate (CS), which was used as a starting material to synthesize OSCS, is an ingredient commonly found in dietary supplements used as an alternative medicine to treat osteoarthritis. It is approved and regulated as a symptomatic slow-acting drug for osteoarthritis in Europe and some other countries. However, here in the US, CS is regulated as a dietary supplement by the Food and Drug Administration. As a result, there are no mandatory standards for formulation of the CS supplements and no

guarantee that the products are correctly labeled. Adebowale et al. reported in 2000 that among the 32 chondroitin supplements they analyzed, only 5 were labeled correctly, and more than half contained less than 40% of the labeled amount.[20] Commercial CS comes from porcine or bovine trachea, chicken keel and shark tissues. Different sources result in CS with different structures in terms of the degree of sulfation. The shark source of CS has a higher degree of sulfation than the trachea source of CS.[21] The current method for the identification of CS uses an enzyme to hydrolyze the chondroitin and to break them into individual unsaturated disaccharides, and then measures them by high performance liquid chromatography (HPLC) with ultraviolet detection.[22]

Based on our previous study in discriminating OSCS from heparin based on the different charge density of the polyanions, we believe that the potentiometric method may also be feasible in discriminating if a CS sample is from shark tissues or from tracheal or even some other adulterant. Quantification of the CS from a shark source may also be achieved by diluting the sample with constant concentration of lower charge density polyanion species, as describe in Chapter 4. As shown in Table 6.1, the preliminary results show that CS from different sources gives different potential changes (samples received from Dr. Lauder's lab in Lancaster University, UK). Particularly, CS from shark sources show greater potential changes than CS from porcine and bovine, and the common adulterant of CS shows almost no potential change. We could also observe that reducing the background chloride concentration could further increase the maximum potential change of the CS samples as explained

by the theory of polyanion sensors, as described in Chapter 1.[23] Therefore, further studies in this area are worth pursuing.

6.2.3. Nitric Oxide Gas Sensors Based on Other Metalloporphyrins and Coated Wire Type of ISEs

As described in Chapter 5, nitric oxide (NO) plays a significant role in physiological processes. Since the first attempt to identify endogenous NO present in the exhaled air of animals and humans in 1991,[24] numerous studies have been conducted to discover an increase in the exhaled NO levels in asthmatics as compared to healthy subjects.[25-27] In Chapter 5, we demonstrated that a Co(III) porphyrin based system would potentially be used for NO sensing, both optically and electrochemically. Such an NO sensor system can be extended to other metalloporphyrins. For example, iron(III) porphyrin has been reported to form a nitrosyl complex with NO, along with a redox reaction where Fe(III) was reduced to Fe(II) and NO was oxidized to NO^+.[28] Rodium(III) porphyrin, reported as a selective nitrite ionophore recently by this lab[29],may also interact with NO and can be utilized as a sensing reagent. The concentration of NO in human breath falls in the ppb level,[30] which is lower than our current achievable detection limit, and thus, preconcentration of the sample would be necessary. The preconcentration can be achieved by adsorption onto a sorbent trap, coated fibers (solid phase microextraction (SPME)),[31, 32] or by direct cryofocussation.[32, 33]

It has been described in Chapter 3 that using a coated wire type electrode results

in a lower detection limit. We can also employ these all solid state electrodes in designing NO gas sensors, which can not only lower the detection limit, but also are easy to be miniaturized.

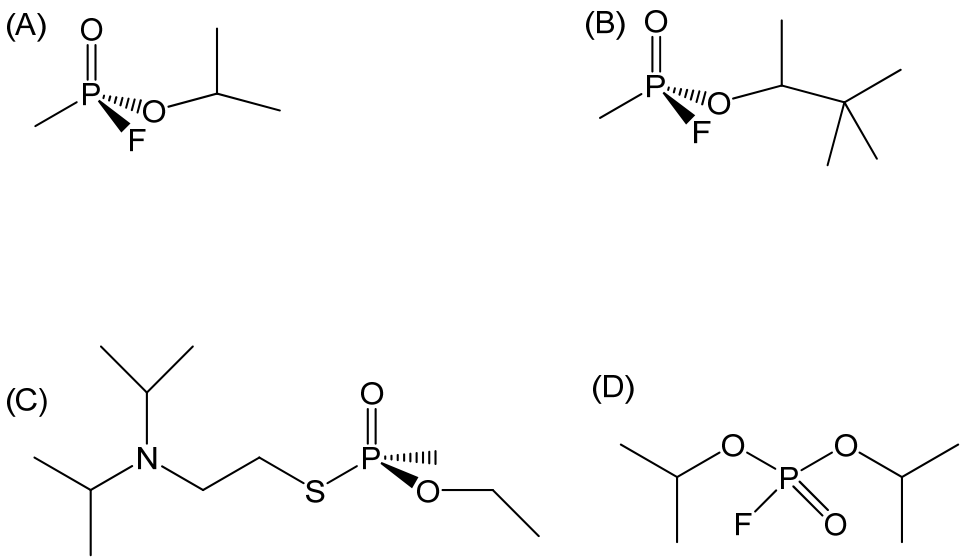

Figure 6.1. Chemical structures of Sarin (A), Soman (B), VX (C), and DFP (D).

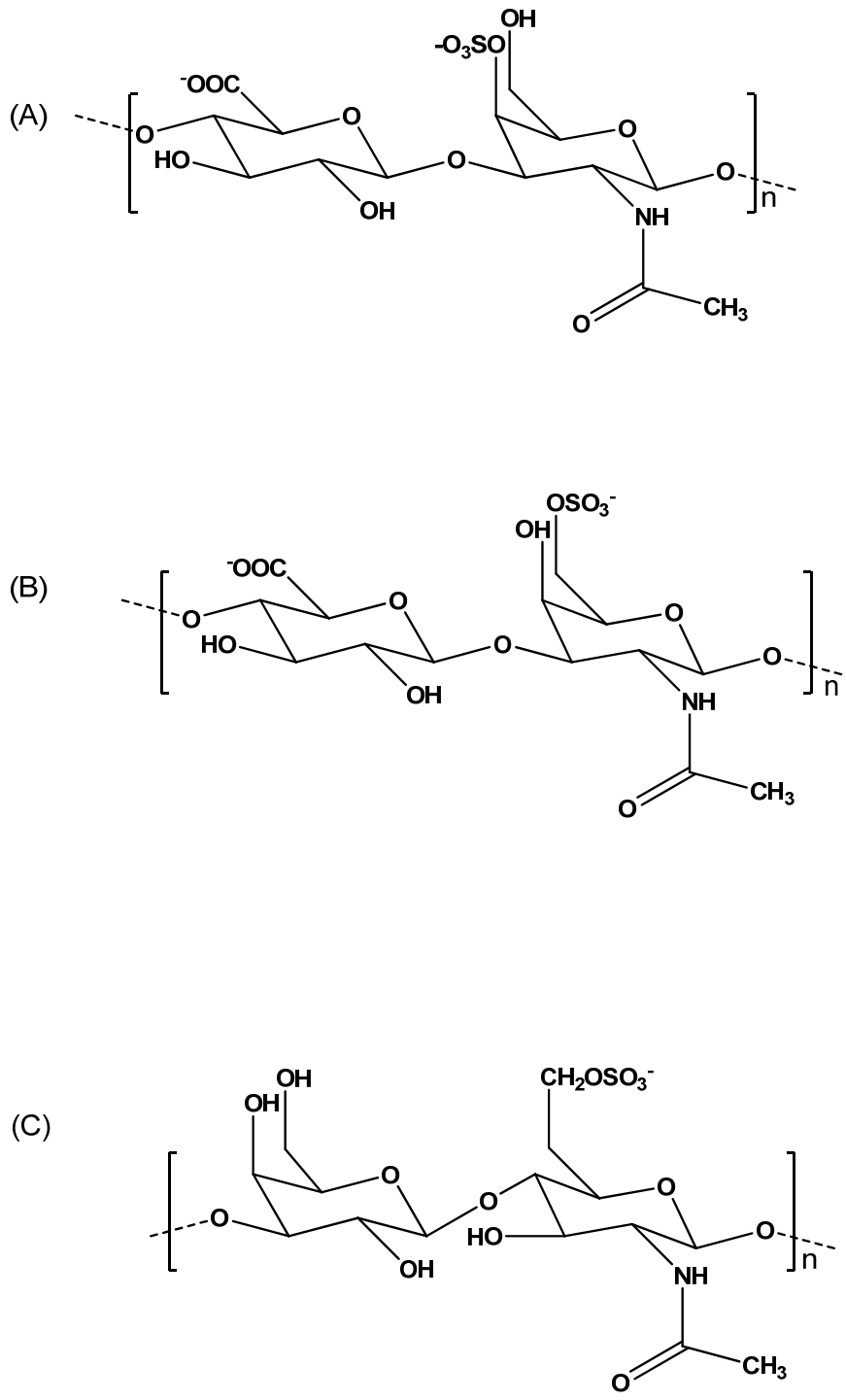

Figure 6.2. Chemical structures of Chondroitin-4-sulfate (from bovine trachea) (A), Chondroitin-6-sulfate (from shark cartilage) (B), and Keratan Sulphate (C).

Table 6.1. Potentiometric responses of PVC membranes doped with TDMAC toward polyanion samples with 16 CS samples in buffers with different chloride backgrounds with a final polyanion concentration of 250 μg/ml.

Sample	Description	In PBS (140 mM Cl^-, 10 mM phosphate)		10 mM Cl^-, 10 mM phosphate	
		Ave. ΔEMF(mV)	SD (mV), n=3	Ave. ΔEMF(mV)	SD (mV), n=3
1	Porcine tracheal CS	-14.3	0.6	-67.2	1.9
2	Porcine tracheal CS	-13.4	1.0	-62.1	1.3
3	Porcine tracheal CS	-14.0	1.9	-66.7	2.1
4	Porcine tracheal CS	-15.7	0.4	-63.9	4.8
5	Shark CS	-23.6	0.9	-79.0	0.7
6	Shark CS	-21.2	1.3	-74.8	1.5
7	Shark CS	-16.4	0.4	-75.3	2.1
8	Bovine Tracheal CS	-15.6	1.9	-70.6	3.0
9	Bovine Tracheal CS	-13.3	1.3	-75.1	3.5
10	Bovine Tracheal CS	-15.3	1.2	-72.6	1.5
11	Bovine Tracheal CS	-23.6	0.9	-77.0	2.0
12	Chicken Sternal CS	-6.0	1.3	-62.9	2.0
13	Chicken Sternal CS	-12.1	0.4	-66.0	1.0
14	Chicken Sternal CS	-13.3	1.2	-66.3	3.1
15	Common Adulterant	0.6	0.8	-0.2	3.1
16	Shark Keratan Sulphate	-24.6	0.7		
17	Tracheal KS	-5.9	1.1		

TDMA: tridodedylmethylammonium chloride
PBS: phosphate-buffered saline

6.3. References

(1) Steinle, E. D.; Amemiya, S.; Buhlmann, P.; Meyerhoff, M. E. *Anal. Chem.* **2000**, *72*, 5766-5773.
(2) Badr, I. H. A.; Meyerhoff, M. E. *J. Am. Chem. Soc.* **2005**, *127*, 5318-5319.
(3) Badr, I. H. A.; Meyerhoff, M. E. *Anal. Chem.* **2005**, *77*, 6719-6728.
(4) Qin, W.; Parzuchowski, P.; Zhang, W.; Meyerhoff, M. E. *Anal. Chem.* **2003**, *75*, 332-340.
(5) Qin, Y.; Bakker, E. *Anal. Chem.* **2004**, *76*, 4379-4386.
(6) Malinowska, E.; Meyerhoff, M. E. *Anal. Chim. Acta* **1995**, *300*, 33-43.
(7) Shamsipur, M.; Javanbakht, M.; Hassaninejad, A. R.; Sharghi, H.; Ganjali, M. R.; Mousavi, M. F. *Electroanalysis* **2003**, *15*, 1251-1259.
(8) Martin, G. B.; Meyerhoff, M. E. *Anal. Chim. Acta* **1986**, *186*, 71-80.
(9) Buck, R. P.; Freiser, H. *Ion Selective Electrodes in Analytical Chemistry. vol. 1.*; Plenum: New York, 1978.
(10) Fu, B.; Bakker, E.; Yun, J. H.; Yang, V. C.; Meyerhoff, M. E. *Anal. Chem.* **1994**, *66*, 2250-2259.
(11) Guerrini, M.; Beccati, D.; Shriver, Z.; Naggi, A.; Viswanathan, K.; Bisio, A.; Capila, I.; Lansing, J. C.; Guglieri, S.; Fraser, B.; Al-Hakim, A.; Gunay, N. S.; Zhang, Z. Q.; Robinson, L.; Buhse, L.; Nasr, M.; Woodcock, J.; Langer, R.; Venkataraman, G.; Linhardt, R. J.; Casu, B.; Torri, G.; Sasisekharan, R. *Nat. Biotechnol.* **2008**, *26*, 669-675.
(12) Maruyama, T.; Toida, T.; Imanari, T.; Yu, G. Y.; Linhardt, R. J. *Carbohydr. Res.* **1998**, *306*, 35-43.
(13) Volpi, N. *Carbohydr. Res.* **1993**, *247*, 263-278.
(14) Siddiqi, I. W. *Clin. Chem.* **1982**, *28*, 1962-1067.
(15) Matuszewski, W.; Trojanowicz, M.; Meyerhoff, M. E. *Electroanalysis* **1990**, *2*, 525-531.
(16) Abd-Rabboh, H. S. M.; Meyerhoff, M. E. *Talanta* **2007**, *72*, 1129-1133.
(17) Hughes, G. M. K.; Saunders, B. C. *Chem. Ind.* **1954**, 1265-1265.
(18) Mulchandani, A.; Pan, S. T.; Chen, W. *Biotechnol. Prog.* **1999**, *15*, 130-134.
(19) Hammond, P. S.; Forster, J. S. *J. Appl. Polym. Sci.* **1991**, *43*, 1925-1931.
(20) Adebowale, A. O.; Cox, D. S.; Liang, Z.; Eddington, N. D. *J Am Nutr Assoc* **2000**, *3*, 37-44.
(21) Lauder, R. *Int. J. Exp. Pathol.* **2004**, *85*, A70-A70.
(22) Ji, D.; Roman, M.; Zhou, J.; Hildreth, J. *J. AOAC Int.* **2007**, *90*, 659-669.
(23) Fu, B.; Bakker, E.; Yang, V. C.; Meyerhoff, M. E. *Macromolecules* **1995**, *28*, 5834-5840.
(24) Gustafsson, L. E.; Leone, A. M.; Persson, M. G.; Wiklund, N. P.; Moncada, S. *Biochem. Biophys. Res. Commun.* **1991**, *181*, 852-857.
(25) Yates, D. H. *Immunol. Cell Biol.* **2001**, *79*, 178-190.
(26) Gustafsson, L. E. *Eur. Resp. J.* **1998**, *11*, 49S-52S.
(27) Turner, S. *Mini-Rev. Med. Chem.* **2007**, *7*, 539-542.
(28) Theodoridis, A.; Maigut, J.; Puchta, R.; Kudrik, E. V.; van Eldik, R. *Inorg.*

Chem. **2008**, *47*, 2994-3013.
(29) Pietrzak, M.; Meyerhoff, M. E. *Anal. Chem.* **2009**, *81*, 3637-3644.
(30) Miekisch, W.; Schubert, J. K.; Noeldge-Schomburg, G. F. E. *Clin. Chim. Acta* **2004**, *347*, 25-39.
(31) Grote, C.; Pawliszyn, J. *Anal. Chem.* **1997**, *69*, 587-596.
(32) Miekisch, W.; Schubert, J. K.; Vagts, D. A.; Geiger, K. *Clin. Chem.* **2001**, *47*, 1053-1060.
(33) Knutson, M. D.; Viteri, F. E. *Anal. Biochem.* **1996**, *242*, 129-135.